DESIGN AND ANALYSIS OF THREE PHASE INDUCTION DIELECTRIC HEATING (IDH) USING TRAVELLING WAVE PHENOMENA WITH SPACE VECTOR MODULATION

By

YAGNESH B. SHUKLA

DEPARTMENT OF ELECTRICAL ENGINEERING

FACULTY OF TECHNOLOGY & ENGINEERING

M. S. UNIVERSITY OF BARODA

SEPTEMBER, 2011

DESIGN AND ANALYSIS OF THREE PHASE INDUCTION DIELECTRIC HEATING (IDH) USING TRAVELLING WAVE PHENOMENA WITH SPACE VECTOR MODULATION

A Thesis submitted for the Award of the

Degree of

Doctor of PHILOSOPHY

in

Electrical Engineering

By

YAGNESH B. SHUKLA

DEPARTMENT OF ELECTRICAL ENGINEERING

FACULTY OF TECHNOLOGY & ENGINEERING

M. S. UNIVERSITY OF BARODA

SEPTEMBER, 2011

Certificate

This is to certify that the thesis entitled **DESIGN AND ANALYSIS OF THREE PHASE INDUCTION DIELECTRIC HEATING (IDH) USING TRAVELLING WAVE PHENOMENA WITH SPACE VECTOR MODULATION** submitted by ***Yagnesh B. Shukla*** in fulfillment of the degree of **DOCTOR OF PHILOSOPHY** in Electrical Engineering Department, Faculty of Technology & Engineering, The M. S. University of Baroda, Vadodara is a bonafide record of investigations carried out by him in the Department of Electrical Engineering, Faculty of Technology & Engineering, M. S. University of Baroda, Vadodara under my guidance and supervision. In my opinion the standards fulfilling the requirements of the Ph.D. Degree as prescribed in the regulations of the University has been attained.

(Prof. S. K. Joshi)
Professor
Department of Electrical Engineering
Faculty of Technology & Engineering,
The Maharaja Sayajirao University of Baroda,
Vadodara 390 001

September, 2011

Head
Electrical Engineering Dept.
Faculty of Tech. & Engg.

Dean
Faculty of Tech. & Engg.

Declaration

I, Mr. Yagnesh B. Shukla hereby declare that the work reported in this thesis entitled DESIGN AND ANALYSIS OF THREE PHASE INDUCTION DIELECTRIC HEATING (IDH) USING TRAVELLING WAVE PHENOMENA WITH SPACE VECTOR MODULATION submitted for the award of the degree of DOCTOR OF PHILOSOPHY in Electrical Engineering Department, Faculty of Technology & Engineering, The M. S. University of Baroda, Vadodara is original and has been carried out in the Department of Electrical Engineering, Faculty of Technology & Engineering, M. S. University of Baroda, Vadodara. I further declare that this thesis is not substantially the same as one, which has already been submitted in part or in full for the award of any degree or academic qualification of this University or any other Institution or examining body in India or abroad.

(*Yagnesh B. Shukla*)

September, 2011.

SYNOPSIS

Name of Student: Yagnesh Bhupatray Shukla Roll No.: 316
Degree for which submitted: Ph.D. Department: Electrical Engineering

Thesis Title: **DESIGN AND ANALYSIS OF THREE PHASE INDUCTION DIELECTRIC HEATING (IDH) USING TRAVELLING WAVE PHENOMENA WITH SPACE VECTOR MODULATION**

Name of thesis supervisor: Professor S. K. Joshi

Electric heating can be accurately applied at the precise point needed in a process, at high concentration of power per unit area or volume. Electric heating apparatus can be built in any required size and can be located anywhere within a plant. Electric heating processes are generally clean, quiet and do not emit much by-product heat to the surroundings. Electrical heating equipment has high speed response, lending it to rapid-cycling and mass-production equipment.

Design of heating system starts with assessment of the temperature required, the amount of heat required and the feasible modes of transferring heat energy. In addition to conduction, convection and radiation, electrical heating methods can use electric and magnetic fields to heat the material.

Methods of electric heating include resistance heating, induction heating, and dielectric heating. In some processes (for example, arc welding), electric current is directly applied to the workpiece. In other processes, heat is produced within the workpiece by induction or dielectric losses. The heat can be produced and, transferred to the work-piece by conduction, convection or radiation.

Induction heaters produce heat by means of a periodically varying electromagnetic field within the body of a nominally conducting material [2]. This method of heating is sometimes called eddy-current heating and is used to achieve temperatures below the melting point of metal [5]. Induction heating is used to temper steel, to heat metals for forging, to heat the metal elements inside glass bulbs and to make glass-to-metal joints [8], [9], [10].

Dielectric heaters use currents of high frequency which generate heat by dielectric hysteresis (loss) within the body of a nominally nonconducting material. These heaters are used to warm to a moderate temperature, certain materials that have low thermal conducting properties; for example, to soften plastics, to dry textiles and to work with other materials like rubber and wood [4], [6].

The present technique used for induction heating is to heat the object by single phase coil through converter inverter technique. Where there is more loss of power conversion, poor power factor, poor efficiency and increase cost and space.

3-phase linear induction heating system is very rarely and lately introduced [3], [53], [99]. It works on the principle of linear induction motor using travelling wave technique to flat surface heat up [53]. In this method, power can be fed at any frequency and accordingly the electronic system device is selected as discussed [99]. It has been mainly used for surface heating and gluing of two dissimilar metals.

Therefore, the motivation behind the work presented in this thesis are:

(i) To develop three phase control circuit for three phase induction dielectric heating system.

(ii) To develop the induction dielectric heating system which is applicable for both conducting and non-conducting material to heat up.

(iii) To explore a new method to determine the material characteristics and performance.

(iv) To study the effectiveness of optimal adjustment of control circuit, switching losses and IDH output in temperature stability.

(v) To develop high efficiency heating system for conducting and non-conducting.

(vi) To explore a new concept to preserve food (lemon) using IDH. It is also useful for industrial and commercial application like drying, forging, surface hardening etc.

A brief description of the research work reported in the thesis is given below:

Chapter 1 introduces the electric heating application and problem, which presents a brief state-of-art survey of research work carried out in the areas of induction heating and dielectric heating. The various modulation techniques have been presented for switching devices used for heating to material. The latest development on three phase linear induction heating application and problem has been reviewed and lays down the motivation behind the research work carried out.

In chapter 2, a symmetrical space vector modulation pattern has been proposed, to reduce Total Harmonic Distortion (THD) without increasing the switching losses. The design and implementations of a 3 phase PWM inverter for 3 phase IDH to control temperature using space vector modulation (SVM) has been carried out.

Chapter 3 presents the mathematical model for steady state IDH process for conducting & non-conducting material and its numerical solution using Matlab and finite element method (FEM).

Chapter 4 describes the three phase MOSFET based inverter for non-conducting material sample as dehydration of food (lemon) application. The operating frequency has been adjusted by the micro controller to maintain constant leading phase angle when parameters of IDH load are varied. The output power can be controlled by setting frequency. The load voltage is controlled to protect the MOSFETs.

Chapter 5 deals with experimental verification of three phase IDH, which converts main frequency AC power into three phase high frequency AC power. The control system presented here control the output temperature of the load and responds accordingly by adjusting the driving frequency of the three phase inverter, to keep the IDH load at resonance throughout the heating cycle.

Chapter 6 summarizes the main finding and significant contributions of the thesis and provides a few suggestions for further scope of research work in this area.

References

[1] E.R. Laithwaite, *Linear induction motors*, The Institution of Electrical Engineers, pp. 461-470, Dec.1957.

[2] E. Davies, *Induction heaters*, British Patent No. 1 513 242, Issued June 1978.

[3] Dughiero F., Lupi S., Nemkov V., Siega P., *Traveling wave Inductors for the continuous Induction heating of metal strips*, Electro Technical Conference, Proceedings., 7th Mediterranean, Vol.3, pp.1154-1157, April 1994.

[4] A. C. Metaxes, *Foundations of Electroheat*, Chichester, U.K., Wiley, 1996

[5] P. Dorland. and J. D. Van Diyck, *On the influence of coil design and electromagnetic configuration on the efficiency of an induction melting furnace*, IEEE transactions on Industry applications, Vol.36, No.4, pp.946-957, 2000.

[6] Christopher J. Cottee and Stephen R. Duncan, *Design of Matching Circuit Controllers for Radio Frequency Heating*, IEEE Transaction on Control System Technology, Vol.11, No.1,pp.91-100, Jan.2003.

[7] Tomita H., Sekine T., Obata S., *Induction heating using traveling magnetic field and three-phase high frequency inverter*, Power Electronics and Applications , 2005 European Conference,6 pp-P.6, Aug.2006.

[8] Nabil A. Ahmed, *Three phase high frequency AC conversion circuit with dual mode PWM/PDM control strategy for high power IH application*, Proc. of world academy of science, Engineering & Technology Vol.35,pp.723-729, Nov. 2008.

[9] Wang Youhua, Wang Junhnua, Li Jiangui, Li Haohuna, *Analysis of Induction Heating Eddy Current Distribution Based On 3D FEM*,Computational Technologies in Electrical and Electronics Engineering, 2008. SIBIRCON 2008. IEEE Region 8 International Conference,pp.238-241 July 2008.

[10] Ahmed N.A, *High-Frequency Soft-Switching AC Conversion Circuit With Dual-Mode PWM/PDM Control Strategy for High-Power IH Applications*, Industrial Electronics, IEEE Transactions, Vol.58, Issue:4,pp.1440-1448, March 2011.

Dedicated

to

my wife Bhavini,

my Parents

and

my adorable Children

ACKNOWLEDGEMENTS

I, with great privilege and deep sense of gratitude, heartly thank my thesis guide, Dr. S K Joshi, who has constantly guided me throughout the tenure of research. His positive and painstaking efforts, constructive suggestions and his readiness to help at any time even after office hours has resulted in research. I am also thankful to Prof. S K Shah, Head of Electrical Engineering Department, Faculty of Technology & Engineering, for his inspiration and support.

I would like to convey my sincere thanks to Board of Management, Sardar Vallabhbhai Patel Institute of Technology (SVIT)-Vasad for giving me a golden opportunity to pursue my doctoral program. I am also thank Shri. B C Patel, Chariman-SVIT, Principal of SVIT and Head of E & C Department, SVIT. I thank Prof. C D Kotwal, Head of Electrical Engineering Department, SVIT, for his valuable guidance and suggestions on various occasions. I thank Mr. T S Patel and Mr. P G Patel, Lab Technician, SVIT, for kindness cooperation. There are usually upsetting occasions during research work. On such occasions Dr. M D joshi, Ex Director of SVIT, Prof H B Dave, Ex R & D Director of SVIT and Dr. S K Vij, MCA Director of SVIT, to induced a sense of positive attitude.

I heartly thank to Prof. B K Shukla having industrial expertise for supporting me to incorporate design aspects in my research. I can not forget to thank M/S Mirali Agro Product, Anand and M/S Farcon Engineering, V.V.Nagar, for allowing me to validate the developed and fabricated model.

I respectfully thank to my parents and my parents-in-law for their blessing, encouragement and belief in myself. The continuous support of my wife Bhavini, my daughter Khushi and my son Rudra had been very valuable. Their understanding and happily agreeing to devoting the time which truly belonged to them on my research work rather than with them.

Finally, I thank all those who had helped me directly or indirectly and whose names would have been inadvertently missed above.

Yagnesh B. Shukla

Contents

List of Figures

List of Tables

Chapter 1

INTRODUCTION

1.1 General

Electric heating can be accurately applied at the precise point needed in a process, at high concentration of power per unit area or volume. Electric heating apparatus can be built in any required size and can be located anywhere within a plant. Electric heating processes are generally clean, quiet and do not emit much by-product heat to the surroundings. Electrical heating equipments have high speed response, lending it to rapid-cycling and mass-production equipment.

Design of heating system starts with assessment of the temperature required, the amount of heat required and the feasible modes of transferring heat energy. In addition to conduction, convection and radiation, electrical heating methods utilize electric and magnetic fields to heat the material.

Methods of electric heating include resistance heating, induction heating and dielectric heating. In some processes (for example, arc welding), electric current is directly applied to the work-piece. In other processes, heat is produced within the work-piece by induction or dielectric losses. The heat can be produced and transferred to the work-piece by conduction, convection or radiation.

Induction heaters produce heat by means of a periodically varying electromagnetic field within the body of a nominal conducting material [12]. This method of heating is sometimes called eddy-current heating and is used to achieve temperatures below the melting point of metal [77]. Induction heating is used to temper steel, to heat metals for forging, to heat the metal elements inside glass bulbs and to make glass-to-metal

joints [109], [110], [117].

Dielectric heaters use high frequency currents, which generate heat by dielectric hysteresis (loss) within the body of a nominal non-conducting material. These heaters are used to warm up to moderate temperature of certain materials, that have low thermal conducting properties; for example, to soften plastics, to dry textiles and to work with other materials like rubber and wood [61], [82].

Figure 1.1 shows a schematic classification of electroheat processes [61], according to the voltage frequency used, from DC ($0Hz$) to frequencies up to $10^{12}Hz$.

1.2 State of The Art

Out of many heating methods, a few of them related to electric heating have been described in this section. These includes

- Resistance Heating (RH)
- Induction Heating (IH)
- Dielectric Heating (DH)
- Multiphase Induction heating (MIH)

Resistance heating:

Electric resistance furnaces offer a safe, efficient, reliable and clean method for heat treating, melting and heating prior to forming and brazing metals [102]. Electric furnaces are also easy to control and operate over a wide temperature range. In addition to heating metals, they are used for melting glass, sintering ceramics and curing coatings [61], [65]. The number of applications continues to grow as technological developments broaden the operating temperature range of electric furnaces and the demand for automatic process control increases [56].

Resistance heating is based on the principle of converting electric energy into thermal energy [102]. The thermal energy is then transferred to the part by convection, radiation and/or conduction [61]. There are two types of resistance heating, Indirect resistance heating is described in [56] and discusses the technical and economic factors to consider while deciding whether the process could benefit a particular application or product. Direct resistance heating and encased resistance heaters are discussed in [26]. Direct resistance heating works only for electrically conductive work-pieces; while any material, either solid or liquid can be heated with an encased resistance heater [26], [61]. Encased

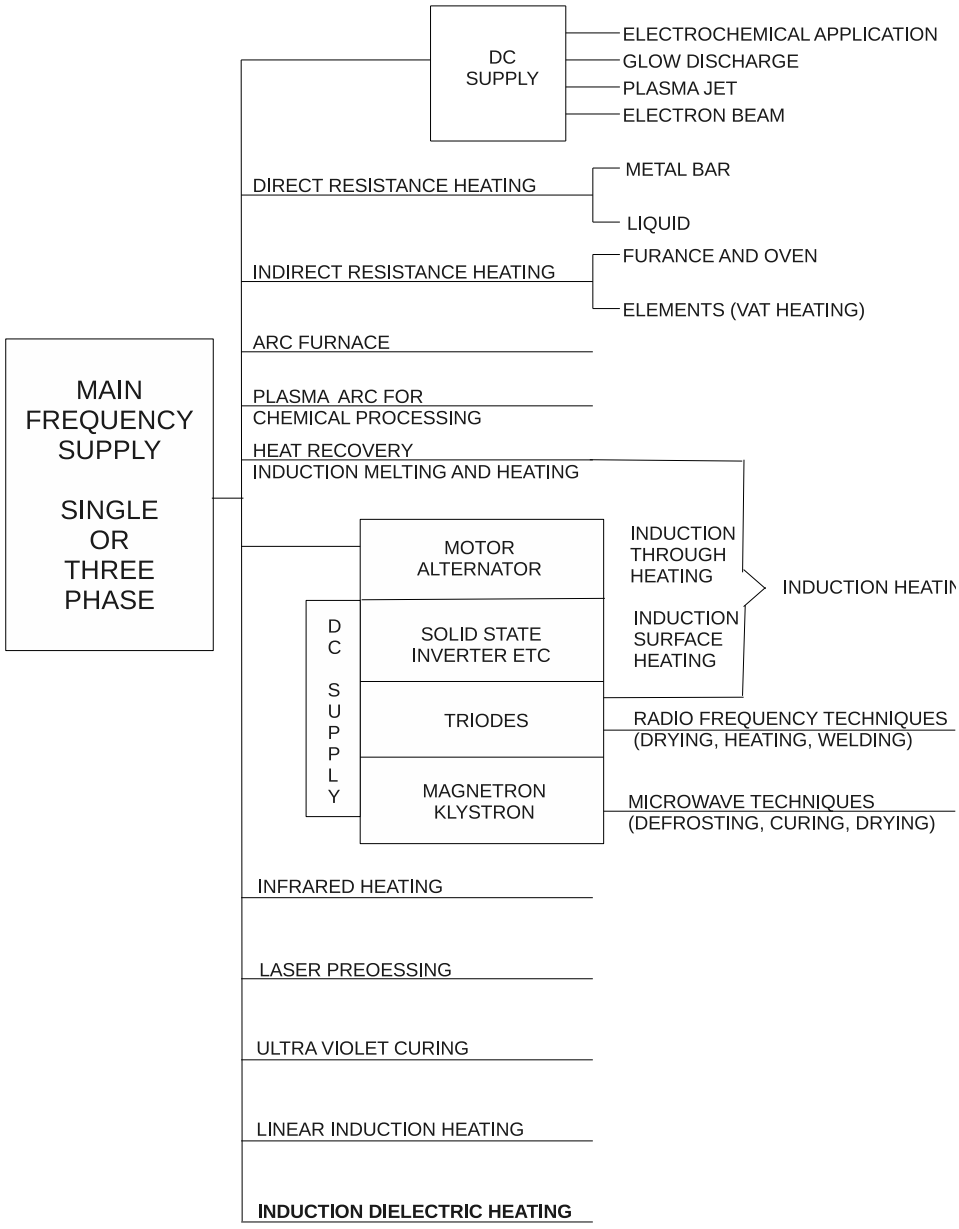

Figure 1.1: Classification of Some Electroheat Processes in Industry

resistance heaters, available in a wide range shapes, sizes and electrical rating are generally used when reliable, long-term heating at low to medium temperature is required [26], [102].

Induction heating:

Induction heating has been used to heat electrically conductive materials [36], [41]. Industrial application of the technology include metal melting and heat treating, crystal growing, semiconductor wafer production, high speed sealing and packaging, preheating for forging operations, brazing, food cooking and curing of organic coating [13], [29], [36], [40], [41], [63], [88], [98], [103], [116].

Induction heating is the process of heating an electrically conducting material (usually a metal) by electromagnetic induction, where eddy currents are generated within the work-piece and resistance leads to Joule heating (I^2R) of the material in the form of temporal and spatial volumetric heating [36], [40], [61]. Induction heating provides a number of advantages such as; quick heating, high production rates, ease of automation, control, safe and clean working [6], [29], [36], [86], [103].

The energy transferred from an induction heating unit to an object can be controlled by various methods like varying DC link voltage or duty ratio of the high frequency inverter [37], [39], [50], [60], [72], [90], [97], [116]. The most common method is by varying the operating frequency of the inverter [1], [8], [17], [38], [49].

A large number of topologies have been developed in this area, among them current fed and voltage fed inverters are most commonly used [114], [116]. Important advantage of voltage source inverter is their various control methods such as Pulse Frequency Modulation [74] and Pulse Amplitude Modulation to control output power [101], [107]. The current source inverter has limited control methods. But, it is less affected by input voltage ripple and has short circuit protection capability [39], [71], [116].

If frequency is too low, then an eddy current cancellation within the billet can occur, resulting in poor coil efficiency [4], [77], [116]. When the frequency is too high, the skin effect will be highly pronounced, leading to a current concentration in a fine surface layer compared to the diameter of the billet [4]. In this case, a long heating time will be required in order to provide sufficient heating of the billets core [11]. Prolonged heat time corresponds to a longer heating line, which in turn, increases surface heat losses due to thermal radiation and convection. The choice of frequency is always a reasonable compromise [21], [81]. These methods use single phase supply system.

Dielectric heating:

Electromagnetic fields are used for dielectric heating in industrial processes and domestic applications since the early 1960s. Plastics, food, pharmaceutical, textile and wood industries are well established sectors in which operations such as welding, heating, tempering, defrosting, drying, baking, etc., are carried out using radio-frequency (RF) or microwave (MW) heating applicators [27], [31], [43], [61], [93], [105].

Dielectric heating for industry employs two different types of power system each covering a band of frequencies, radio (RF) and Microwaves (MW) frequencies [31], [33], [82]. The difference between microwave and radio frequency heating is that the operating frequency of the microwave radiation is in the range 433 MHz and 40 GHz, which is much higher than the dimensions of the objects being heated are usually much bigger than the wavelength of the microwave heating and it is necessary to move the object to ensure even heating [33]. In both techniques, the material that is heated is exposed to an electromagnetic field that is continuously reversing direction (alternating) at a very high frequency [82].

Dielectric heaters use high frequency currents, which generate heat by dielectric hysteresis (loss) within the body of a nominally non-conducting material. These heaters are used to warm up to moderate temperature, certain materials that have low thermal conducting properties; for example, to soften plastics, to dry textiles and to work with other materials like rubber and wood [2], [27].

The advantages of dielectric heating equipment are high rate of heating, uniform heating of materials having a low thermal conductivity and the feasibility of local and selective heating [105].

Microwave heating takes place due to the polarization effect of electromagnetic radiation at frequencies between 300 MHz and 300 GHz [22], [66]. Microwave heating has also found applications in the food industry, including tempering of frozen foods for further processing, pre-cooking of bacon for institutional use and final drying of pasta products [66]. In those applications, microwave heating demonstrates significant advantages over conventional methods in reducing process time and improving food quality [5], [7]. But in general, applications of microwave heating in industrial food processing are much less common than home applications. Reasons for this difference include a lack of basic information on the dielectric properties of foods and their relationship to microwave heating characteristics and the historically high cost of equipment and electricity [100], [105].

The way in which a material will be heated by microwaves depends on its shape, size, dielectric constant and the nature of the microwave equipment used [66], [95], [100].

Multiphase Induction heating:

The induction heating of metal strips is widely applied in the metal industry and different types of inductors are used according to the process requirements. Two different types of inductors, namely Transverse Flux (TF) inductors and Travelling Wave (TW) inductors are considered. While Transverse Flux Induction Heating (TFIH) systems have been studied for many years, Travelling wave induction heating (TWIH) inductors are not yet fully appreciated with respect to their main advantages and possible industrial applications [15], [59], [68], [73], [87], [91].

The main attractive characteristics of TF inductors are: 1) a high electrical efficiency, including the heating of strips of low resistivity materials; 2) the possibility of using low frequencies (in particular 50 Hz); 3) more useful "open" inductor geometry [73].

Travelling Wave Induction Heating (TWIH), as one of the multiphase induction heating systems, has particular features which make them attractive for application to some heating and melting processes in industry [15], [48]. Among the advantages, which can be mentioned are the possibility to heat quite uniformly thin strips or regions of a body without moving the inductor above its surface [73], [118], to reduce the vibrations of inductor and load due to the electrodynamics forces and also the noise provoked by them, to obtain nearly balanced distributions of power and temperature [15].

TWIH introduces three-phase induction heating, using the typical three-phase windings and parametric analysis to assess the key parameters (transfer of electricity to the work-piece, efficiency, power factor, etc) and the distribution of electricity [15], [78]. Compared with the single-phase induction heating of Transverse Flux Induction Heating inductors [73], three-phase induction heating not only has the same advantages, but also owns the ability to produce more uniform temperature distributions and reduces industrial noise with low vibration. Especially in the conditions that electromagnetic force increases significantly and heating parameters change with the rise of temperature, the advantage is very important [57].

A fundamental problem in the TWIH design is the prediction of the electromagnetic forces acting on inductor and work-piece, which can give rise to drag forces and vibrations and noise dangerous for the induction heating system itself and for the workers near the system [53], [57], [118].

Transverse Flux and Travelling Wave induction heating methods present some drawbacks because of the intrinsic uneven distribution of the heat distribution inside the workload. In both cases a high concentration of power density is localized at the edge of the work-piece with their consequent possibility of mechanical deformation of the strip during the heating process [73], [118].

Because of advances in solid state power devices and microprocessors [19], [20], [23], [24], switching power converters are used in more and more modern three phase induction load to convert and deliver the required energy to the object [10], [18], [25], [35], [44], [45], [67], [69]. The energy that a switching power converter delivers to an induction load is controlled by modulation techniques.

Modulation Techniques:

The fundamental of the modulation techniques have been well established in [9], [10], [14], [18], [25], [32]. The maximum voltage transfer ratio has been found to be $\sqrt{3}/2$ for sinusoidal input and output waveforms [8], and can be obtained by adding third harmonic voltage components to the desired ac output voltage [32].

Pulse Width Modulated (PWM) signals applied to the gates of the power devices. PWM signals are pulse trains with fixed frequency and magnitude and variable pulse width. There is one pulse of fixed magnitude in every PWM period. However, the width of the pulses changes from pulse to pulse according to a modulating signal. When a PWM signal is applied to the gate of power devices, it causes the turn on and turns off intervals of the power devices to change from one PWM period to another PWM period according to the same modulating signal. The frequency of a PWM signal must be much higher than that of the modulating signal, the fundamental frequency, such that the energy delivered to the load depends mostly on the modulating signal [64].

The basic PWM techniques are:

- Single Pulse Width Modulation
- Multi Pulse Width Modulation
- Sinusoidal Pulse Width Modulation (SPWM)

But when the technology progresses some advanced modulation techniques are also proposed by the different researcher like:

- Trapezoidal Modulation

- Staircase Modulation
- Stepped Modulation
- Harmonic Injection Modulation
- Delta Modulation
- Space vector Modulation (SVM)
- Random PWM

The pulse width modulation (PWM) DC-AC converter has well known for more than three decades. Due to limitations imposed by conventional PWM technique (e.g. over modulation, high switching loss and reduced fundamental component), the SVM technique has gained a lot of importance over PWM technique [92]. Space Vector Modulation became a standard for the switching power converters. The theory of Space Vector Modulation is already well established [30], [34], [35], [46], [47], [52], [80], [84]. Diverse implementation methods were tried and some dedicated hardware pieces were developed based on this principle. The initial use of Space Vector Modulation at three-phase voltage-source inverters has been expanded by application to novel three-phase topologies as AC/DC Voltage Source Converter, AC/DC or DC/AC Current Source Converters, Resonant Three-Phase Converters, Inverter, Multilevel Converters, AC/AC Matrix Converters and so on [47], [58], [75], [79], [85], [89], [96], [107], [111], [113].

The SVM has been concept to compute the duty cycle of the switches. It is simply the digital implementation of PWM modulators [62], [79], [111], [113]. An aptitude for easy digital implementation and wide linear modulation range for output line-to-line voltages are the notable features of space vector modulation as following:

- Immediate comprehension of the required commutation processes.
- Wide linear modulation range.
- Less switching loss.
- Less total harmonic distortion (THD) in the spectrum of switching waveform.
- Easy implementation and less computation time.

- No synchronization requirement with input voltage waveforms.
- Simplified control algorithm.
- Full utilization of the DC bus voltage.

1.3 Motivation

The present technique used for induction heating is to heat the object by single phase coil through converter inverter technique. Where there is more loss of power conversion, poor power factor, poor efficiency and increase cost and space.

3-phase linear induction heating system is very rarely and lately introduced [3], [53], [99]. It works on the principle of linear induction motor using travelling wave technique to flat surface heat up [53]. In this method, power can be fed at any frequency and accordingly the electronic system device is selected as discussed [99]. It has been mainly used for surface heating and gluing of two dissimilar metals.

Hence, the motivation behind the resarch work reported in this thesis was

(i) To develop three phase control circuit for three phase induction dielectric heating system.

(ii) To develop the induction dielectric heating system which is applicable for both conducting and non-conducting material to heat up.

(iii) To explore a new method to determine the material characteristics and performance.

(iv) To study the effectiveness of optimal adjustment of control circuit, switching losses and IDH output in temperature stability.

(v) To develop high efficiency heating system for conducting and non-conducting.

(vi) To explore a new concept to preserve food (lemon) using IDH. It is also useful for industrial and commercial application like drying, forging, surface hardening etc.

1.4 Thesis Organization

The present Chapter 1 introduces the electric heating application and problem, which presents a brief state-of-art survey of research work carried out in the areas of induction

heating and dielectric heating. The various modulation techniques have been presented for switching devices used for heating to material. The latest development on three phase linear induction heating application and problem has been reviewed and lays down the motivation behind the research work carried out.

In chapter 2, a symmetrical space vector modulation pattern has been proposed, to reduce Total Harmonic Distortion (THD) without increasing the switching losses. The design and implementations of a 3 phase PWM inverter for 3 phase IDH to control temperature using space vector modulation (SVM) has been carried out.

Chapter 3 presents the mathematical model for steady state IDH process for conducting & non-conducting material and its numerical solution using Matlab and finite element method (FEM).

Chapter 4 describes the three phase MOSFET based inverter for non-conducting material sample as dehydration of food (lemon) application. The operating frequency has been adjusted by the micro controller to maintain constant leading phase angle when parameters of IDH load are varied. The output power can be controlled by setting frequency. The load voltage is controlled to protect the MOSFETs.

Chapter 5 deals with experimental verification of three phase IDH, which converts main frequency AC power into three phase high frequency AC power. The control system presented here control the output temperature of the load and responds accordingly by adjusting the driving frequency of the three phase inverter, to keep the IDH load at resonance throughout the heating cycle.

Chapter 6 summarizes the main finding and significant contributions of the thesis and provides a few suggestions for further scope of research work in this area.

Chapter 2

DESIGN AND IMPLEMENTATION OF A 3 PHASE PWM FOR 3 PHASE IDH

2.1 Introduction

The overall performance and the cost of the heating system will be one of the important issues to be considered during the design process for the next generation of Induction Dielectric Heating (IDH) applications. The power conversion circuit (Three phase Pulse Width Modulation (PWM) inverter) of IDH applications must achieve high efficiency, low harmonic distortion, high reliability and low electromagnetic interference (EMI) noise. Three phase PWM inverters are becoming more and more popular in present day induction heating system [92], [107], [109].

Sinusoidal Pulse Width Modulation (SPWM) has been used to control the three phase inverter output voltage [8]. To maintain a good performance of the drive the operation has been restricted between 0 to 78 % of the value that would be reached by square wave operation [30], [64], [92].

Since the concept of PWM inverter was introduced, the various modulation strategies have been developed [30], [47], [51], [75], [76], [79], [80], [83], [92], [104], [107], [113], and analyzed. The space vector modulation (SVM) [25], [96] offers significant flexibility to optimize switching waveforms. It has been well suited for digital implementation.

For the IDH application, full utilization of the DC bus voltage is extremely important

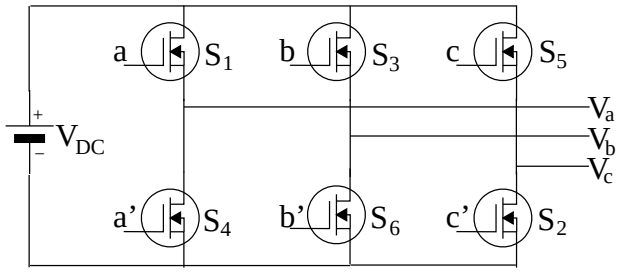

Figure 2.1: 3 Phase PWM Inverter Circuit for IDH

to achieve the maximum temperature under all conditions. The current ripple in three phase pulse width modulation inverter under steady state operation can be minimized using SVM compared to any other PWM methods for voltage control mode.

A symmetrical space vector modulation pattern has been proposed in this chapter, to reduce Total Harmonic Distortion (THD) without increasing the switching losses [42]. The design and implementation of a 3 phase PWM inverter for 3 phase IDH to control temperature using space vector modulation (SVM) has been described.

2.2 Principle of Space Vector Modulation

The circuit model of a typical three-phase voltage source PWM inverter is shown in Figure 2.1. S_1 to S_6 are the six power switches that shape the output voltage, which are controlled by the switching variables a, $a^{'}$, b, $b^{'}$ and c, $c^{'}$. When an upper MOSFET is switched on, i.e., when a, b, or c is 1, the corresponding lower MOSFET is switched off, i.e., the corresponding $a^{'}$, $b^{'}$, or $c^{'}$ is 0. Therefore, the on and off states of the upper MOSFET S_1, S_3 and S_5 can be used to determine the output voltage [85].

The relationship between the switching variable vector $[a, b, c]^t$ and the line-to-line voltage vector $[V_{ab}, V_{bc}, V_{ca}]^t$ are given by equation 2.1 in the following:

$$\begin{bmatrix} V_{ab} \\ V_{bc} \\ V_{ca} \end{bmatrix} = V_{DC} \begin{bmatrix} 1 & -1 & 0 \\ 0 & 1 & -1 \\ -1 & 0 & -1 \end{bmatrix} \begin{bmatrix} a \\ b \\ c \end{bmatrix} \tag{2.1}$$

Also, the relationship between the switching variable vector $[a, b, c]^t$ and the phase voltage

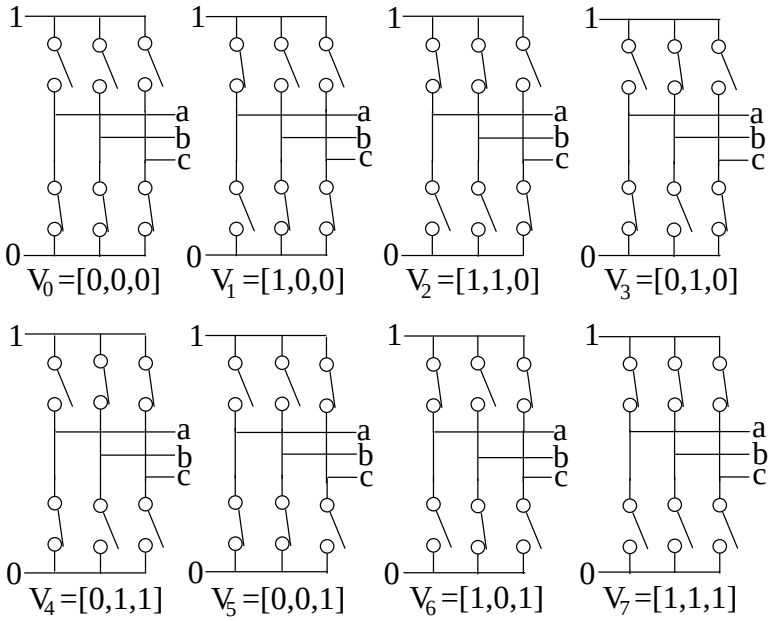

Figure 2.2: Eight Inverter Voltage Vectors

vector $[V_{an}, V_{bn}, V_{cn}]^t$ can be expressed as below.

$$\begin{bmatrix} V_{an} \\ V_{bn} \\ V_{cn} \end{bmatrix} = \frac{V_{DC}}{3} \begin{bmatrix} 2 & -1 & -1 \\ -1 & 2 & -1 \\ -1 & -1 & 2 \end{bmatrix} \begin{bmatrix} a \\ b \\ c \end{bmatrix} \tag{2.2}$$

As illustrated in Figure 2.1, there are eight possible combinations of on and off patterns for the three upper power switches. The on and off states of the lower power devices are opposite to the upper one and so are easily determined once the states of the upper power MOSFET's are determined. According to equation 2.1 and equation 2.2, the eight switching vectors, output line to neutral voltage (phase voltage) and output line-to-line voltages in terms of DC-link V_{DC}, are given in Table 2.1 and Figure 2.2 show the eight inverter voltage vectors [75] (V_0 to V_7).

Space Vector Modulation (SVM) refers to a special switching sequence of the upper three power MOSFETs of a three-phase inverter. The source voltage has been utilized most efficiently by the space vector modulation (SVM) compared to sinusoidal pulse width modulation [75] as shown in Figure 2.3.

Table 2.1: Switching Vectors, Phase Voltages and Output Line to Line Voltage

Voltage Vectors	Switching Vector						Line to line voltage			Vector
	a	b	c	a'	b'	c'	V_{ab}	V_{bc}	V_{ca}	
$V_0(000)$	OFF	OFF	OFF	ON	ON	ON	0	0	0	Zero
$V_1(100)$	ON	OFF	OFF	OFF	ON	ON	V_{DC}	0	-V_{DC}	Active
$V_2(110)$	ON	ON	OFF	OFF	OFF	ON	0	V_{DC}	-V_{DC}	Active
$V_3(010)$	OFF	ON	OFF	ON	OFF	ON	-V_{DC}	V_{DC}	0	Active
$V_4(011)$	OFF	ON	ON	ON	OFF	OFF	-V_{DC}	0	V_{DC}	Active
$V_5(001)$	OFF	OFF	ON	ON	ON	OFF	0	-V_{DC}	V_{DC}	Active
$V_6(101)$	ON	OFF	ON	OFF	ON	OFF	V_{DC}	-V_{DC}	0	Active
$V_7(111)$	ON	ON	ON	OFF	OFF	OFF	0	0	0	Zero

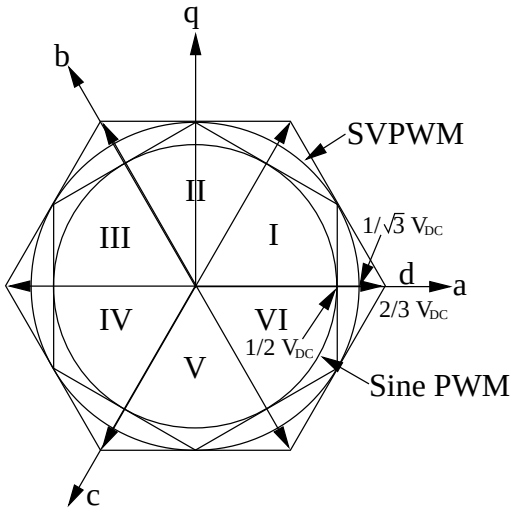

Figure 2.3: Locus of Maximum Linear Control Voltage in Sine PWM and SVPWM

In the vector space, according to the equivalence principle, the following operating rules are obtained:

$$\begin{aligned} V_1 &= -V_4 \\ V_2 &= -V_5 \\ V_3 &= -V_6 \\ V_0 &= V_7 = 0 \\ V_1 + V_3 + V_5 &= 0 \end{aligned} \tag{2.3}$$

In one sampling interval, the output voltage vector V_t can be written as

$$V_t = \frac{t_0}{T_s}V_0 + \frac{t_1}{T_s}V_1 + ... + \frac{t_7}{T_s}V_7 \tag{2.4}$$

Where

$t_0, t_1, ...t_7$ are the turn-on time of the vectors $V_0, V_1, ...V_7$;
$t_0, t_1, ...t_7 > 0$,

$$\sum_{i=0}^{7} t_i = T_s$$

Where

T_s = Sampling time.

According to equation 2.3 and equation 2.4, there are infinite ways of decomposition of V into V_1, V_2, ... V_6. However, in order to reduce the number of switching actions and make full use of active turn-on time for space vectors, the vector V is commonly split into the two nearest adjacent voltage vectors and zero vectors V_0 and V_7 in an arbitrary sector. For example, in sector I, in one sampling interval, vector V can be expressed as

$$V = \frac{T_1}{T_s}V_1 + \frac{T_2}{T_s}V_2 + \frac{T_0}{T_s}V_0 + \frac{T_7}{T_s}V_7 \tag{2.5}$$

Where

$T_s - T_1 - T_2 = T_0 + T_7 \geq 0$, $T_0 \geq 0$ and $T_7 \geq 0$

Let the length of V be mV_{DC}, then

$$\frac{m}{sin\frac{2\pi}{3}} = \frac{T_1}{T_s}\frac{1}{sin(\frac{\pi}{3} - \alpha)} = \frac{T_2}{T_s}\frac{1}{sin\alpha} \tag{2.6}$$

Where

m = Modulation index

Table 2.2: Space Vector Modulation Algorithm

Sector I $(0 \leq \omega t \leq \pi/3)$	Sector II $(\pi/3 \leq \omega t \leq 2\pi/3)$
$T_1 = \frac{\sqrt{3}}{2} T_c m \cos(\omega t + \pi/6)$ $T_2 = \frac{\sqrt{3}}{2} T_c m \cos(\omega t + 3\pi/2)$ $T_0 + T_7 = T_c - T_1 - T_2$	$T_2 = \frac{\sqrt{3}}{2} T_c m \cos(\omega t + 11\pi/6)$ $T_3 = \frac{\sqrt{3}}{2} T_c m \cos(\omega t + 7\pi/6)$ $T_0 + T_7 = T_c - T_2 - T_3$
Sector III $(2\pi/3 \leq \omega t \leq \pi)$	Sector IV $(\pi \leq \omega t \leq 4\pi/3)$
$T_3 = \frac{\sqrt{3}}{2} T_c m \cos(\omega t + 3\pi/2)$ $T_4 = \frac{\sqrt{3}}{2} T_c m \cos(\omega t + 5\pi/6)$ $T_0 + T_7 = T_c - T_3 - T_4$	$T_4 = \frac{\sqrt{3}}{2} T_c m \cos(\omega t + 7\pi/6)$ $T_5 = \frac{\sqrt{3}}{2} T_c m \cos(\omega t + \pi/2)$ $T_0 + T_7 = T_c - T_4 - T_5$
Sector V $(4\pi/3 \leq \omega t \leq 5\pi/3)$	Sector VI $(5\pi/3 \leq \omega t \leq 2\pi)$
$T_5 = \frac{\sqrt{3}}{2} T_c m \cos(\omega t + 5\pi/6)$ $T_6 = \frac{\sqrt{3}}{2} T_c m \cos(\omega t + \pi/6)$ $T_0 + T_7 = T_c - T_5 - T_6$	$T_6 = \frac{\sqrt{3}}{2} T_c m \cos(\omega t + \pi/2)$ $T_1 = \frac{\sqrt{3}}{2} T_c m \cos(\omega t + 11\pi/6)$ $T_0 + T_7 = T_c - T_6 - T_1$

Thus,

$$\begin{aligned} \frac{T_1}{T_s} &= \frac{2}{\sqrt{3}} m sin(\frac{\pi}{3} - \omega t) = \frac{2}{\sqrt{3}} m cos(\frac{\pi}{6} + \omega t) \\ \frac{T_2}{T_s} &= \frac{2}{\sqrt{3}} m sin\omega t = \frac{2}{\sqrt{3}} m cos(\frac{3\pi}{2} + \omega t) \\ T_0 + T_7 &= T_s - T_1 - T_2 \end{aligned} \tag{2.7}$$

Where

$$2n\pi \leq \omega t = \alpha \leq 2n\pi + \pi/3.$$

The length and angle of V determined by vectors $V_1, V_2, ...V_6$ are called as active vectors and V_0, V_7 are called zero (space) vectors. The decomposition of voltage V in different sectors has been presented in Table 2.2. Equation 2.5 and equation 2.6 have been commonly used for formulation of the space vector modulation. It has been shown that the turn on times $T_i (i = 1, ...6)$ for active vectors are identical in different space vector modulation [92], [104], [107], [113]. The different distribution of T_0 and T_7 for zero vectors yields different space vector modulation.

There are not separate modulation signals in each of the three space vector modulation technique [54]. Instead, a voltage vector is processed as a whole [25]. For space vector

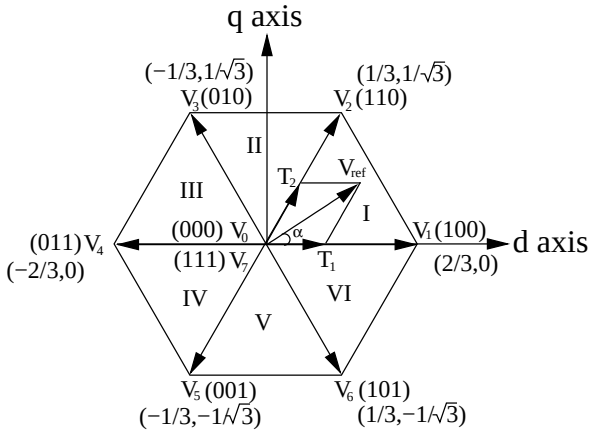

Figure 2.4: The Relationship of abc and Stationary dq Reference Frame

modulation, the boundary condition for sector I is:

$$\begin{aligned} T_s &= T_1 + T_2 \\ T_0 &= T_7 = 0 \end{aligned} \tag{2.8}$$

From equation 2.6 to equation 2.8;

$$\frac{m}{1} = \frac{sin\frac{\pi}{3}}{sin(\frac{2\pi}{3} - \alpha)} \tag{2.9}$$

The boundary of the linear modulation range is the hexagon [54], [67] as shown in Figure 2.3. The linear modulation range is located within the hexagon. If the voltage vector V exceeds the hexagon, as calculated from equation 2.7, then $T_1 + T_2 > T_s$ and it is unrealizable. Thus, for the over modulation region space vector modulation is outside the hexagon. In six step mode, the switching sequence is $V_1 - V_2 - V_3 - V_4 - V_5 - V_6$ [54]. Furthermore, it should be pointed out that the trajectory of voltage vector V should be circular while maintaining sinusoidal output line-to-line voltages. From Figure 2.4, it has been seen that for linear modulation range, the length of vector mV_{DC} should be $V = (\sqrt{3}/2)V_{DC}$, the trajectory of V becomes the inscribed circle of the hexagon and the maximum amplitude of sinusoidal line-to-line voltages is the source voltage V_{DC}.

Moreover, for space vector modulation, there is a degree of freedom in the choice of zero vectors in one switching cycle, i.e., whether V_0 and V_7 or both.

For continuous space vector schemes, in the linear modulation range, both V_0 and V_7 are used in one cycle, that is, $T_7 \geq 0$ and $T_0 \geq 0$.

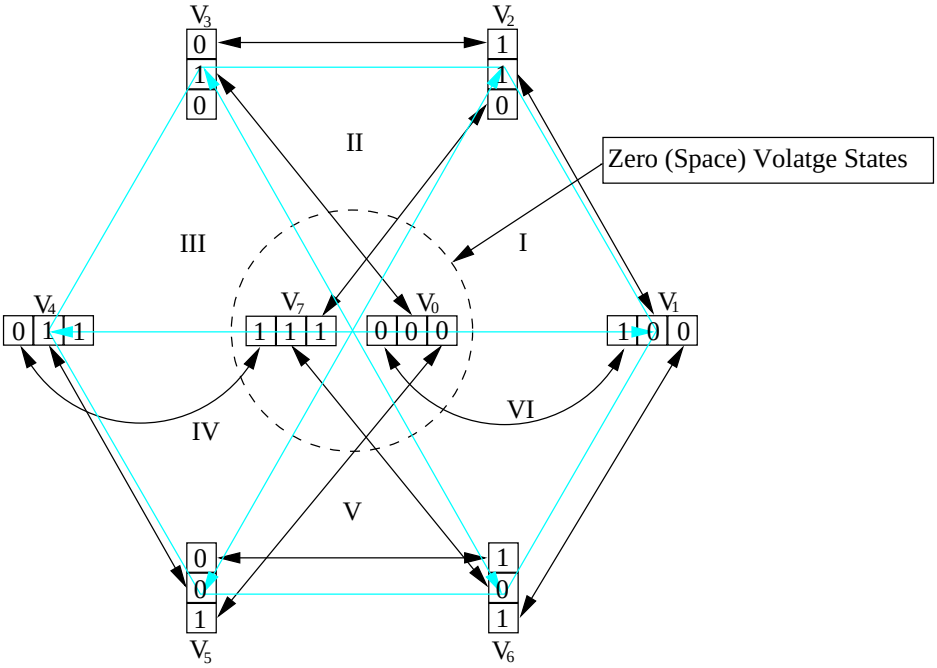

Figure 2.5: Transitions Between Different Switching States

For discontinuous space vector schemes, in the linear modulation range, only V_0 or only V_7 is used in one cycle, that is $T_7 = 0$ and $T_0 = 0$.

2.3 SVM Technique for Three Phase Inverter

Figure 2.1 shows a typical three phase inverter. There are eight possible states: six active vectors and two zero vectors, as shown in Table 2.1 and Figure 2.2. Each inverter switching vectors specifics as the space vector for the output voltage of inverter. The six active switching space vector are evenly distributed 60^o intervals with length of $\sqrt{3}V_{DC}/2$ and from a hexagon. Also two zero space vectors are located at a center of hexagon in the complex plane, as shown in Figure 2.5.

Eight space vectors depending on the switching condition can be represented as complex vector can be given as,

$$\begin{aligned} V_k &= \frac{2}{3}V_{DC}e^{j(k-1)\frac{\pi}{3}}, \qquad k = 1, 2, - - --, 6 \\ &= 0, \qquad k = 0, 7 \end{aligned} \tag{2.10}$$

When the location of V_{ref} has been fixed, for example, in sector I of Figure 2.4 the integral

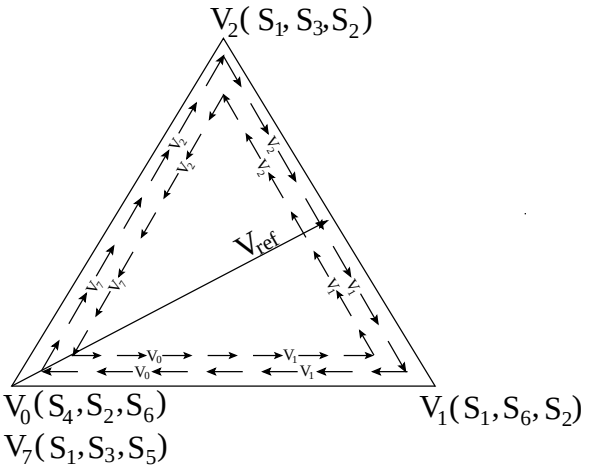

Figure 2.6: Optimal Vector Commutation for Sector I

equation for V_{ref} over a single space vector modulation cycle give.

$$\int_0^{T_s} V_{ref}dt = \int_0^{T_1} V_1 dt + \int_{T_1}^{T_1+T_2} V_2 dt + \int_{T_1+T_2}^{T_s} V_0 dt \tag{2.11}$$

T_1 and T_2 are the switching time spent on the output voltage vectors V_1 and V_2 respectively. The representation of V_{ref} by V_1 and V_2 and switching sequences has been shown in Figure 2.6

2.3.1 Six space vectors of three phase inverter

Assuming the three phase induction dielectric heating by using the proposed technique operates ideally. Balanced set of output voltage v_A, v_B, v_C and a set of output currents i_A, i_B, i_C for the three phase PWM inverter has been expressed by

$$\begin{aligned} v_A &= \frac{V_{DC}}{2} m sin\omega t = V_o sin\omega t \\ v_B &= V_o sin(\omega t - 120) \\ v_C &= V_o sin(\omega t - 240) \end{aligned} \tag{2.12}$$

Where

$-1 < m < 1$

$$\begin{aligned} i_A &= I_o sin(\omega t - \phi) \\ i_B &= I_o sin(\omega t - \phi - 120) \\ i_C &= I_o sin(\omega t - \phi - 240) \end{aligned} \tag{2.13}$$

Where
V_o = Maximum amplitude of the output voltage in $Volt$
I_o = Maximum amplitude of the output current in Amp
Determined by modulation index m.

There are six switching vectors in three phase inverter when the switches S_1, S_2, S_3, S_4, S_5 and S_6 are turn on and off, as shown in Figure 2.2. Based on the six possible combination of the six individual switches signified by its switching states labelled as $[S_1, S_2, S_3]$, the six space voltage vectors can be produced in the complex plane, as shown in Figure 2.4 and Figure 2.5. Six space vectors are evenly distributed 60^o interval with length of $\sqrt{3}V_{DC}/2$. However, two zero vectors as (1,1,1) and (0,0,0) are available in three phase inverter. Accordingly, the maximum trajectory locus has been the form of an exact square wave with corner points defined by the realizable space voltage vector $(V_1, V_2, V_3, V_4, V_5, V_6)$. In the Figure 2.4, each '1' represents an output line attached to the positive DC link, whereas '0' denotes connection to the negative DC link of source.

If the balanced three phase sinusoidal waveforms are required, the reference voltage vector should be controlled in a circular manner.

2.3.2 Determination of switching times in the proposed SVM

The realization method for SVM technique of three phase inverter has been proposed with zero space vectors. To determine the switching times for the reference vector V_{ref} by adjusting six voltage space vectors.

The V_{ref} in sector I has four voltage space vectors V_1, V_2, V_0 and V_7 which are adjacent to the V_{ref}. The T_1 and T_2 are the switching time spent on the V_1 and V_2, respectively. The T_1 and T_2 do not satisfy the constant switching interval T_s except for the reference vector reaching to the maximum voltage. The remainder of the switching interval should be utilized in the main sector and diagonal sector because of zero space vectors in three phase inverter. Accordingly, the new reference vectors replacing the role of zero space vectors should be set again. For example, sector I sets as the main sector and sector IV sets as the diagonal sector in Figure 2.5.

The amount of the switching times T_1, T_2, T_0 and T_7 should be equal to switching interval T_s.

$$T_s = T_1 + T_2 + T_0 + T_7 \tag{2.14}$$

Where

$T_0 \quad = \quad T_7 = T_o/2$

The T_1 and T_2 is the remainder time spent on the V_1 and V_2 in the sector I and also the same time spent on the V_4 and V_5 in the sector IV, respectively. ΔV is defined as the difference between desired voltage vectors for V from V_{ref} in the Figure 2.4. The ΔV is divided into halves on the main sector I, $\Delta V/2$. Then, it is added to V_{ref} and the new reference vector $(V_{ref} + \Delta V/2)$ has been formed again in main sector. Let $(V_{ref} + \Delta V/2)$ called "the re-formed reference vector".

On the contrary, the vector $(-\Delta V/2)$ to restrain the reference vector in main sector I should be inserted in the diagonal sector IV. Let $(-\Delta V/2)$ called "the restraint reference vector". Its direction is opposite to V_{ref} and its $(\Delta V/2)$ in the re-formed reference vector $(V_{ref} + \Delta V/2)$ of the main sector I.

The T_1, T_2, T_0 and T_7, can be calculated as the following process. Absolute value of maximum space vector to the square locus at $\omega t = \alpha$ is given by

$$|V_{max}| \quad = \quad |V_{ref} + \Delta V| = \frac{\sqrt{3}V_{DC}}{2}\frac{1}{sin\alpha + cos\alpha} \tag{2.15}$$

Where

$\alpha \ (0^o < \alpha < 60^o) \quad = \quad$ Phase angle in Deg

From equation 2.15, the absolute value of a reference vector difference ΔV is given by

$$|\Delta V| \quad = \quad \frac{\sqrt{3}V_{DC}}{2}\frac{1}{sin\alpha + cos\alpha} - |V_{ref}| \tag{2.16}$$

Absolute value of the re-formed reference vector $(V_{ref} + \Delta V/2)$ in a main sector is given by

$$|V_{ref} + \frac{\Delta V}{2}| \quad = \quad \frac{\sqrt{3}V_{DC}}{4}\frac{1}{sin\alpha + cos\alpha} + |\frac{V_{ref}}{2}| \tag{2.17}$$

Absolute value of a restraint reference vector $-\Delta V/2$ in the diagonal sector is given by

$$|-\frac{\Delta V}{2}| \quad = \quad \frac{\sqrt{3}V_{DC}}{4}\frac{1}{sin\alpha + cos\alpha} - |\frac{V_{ref}}{2}| \tag{2.18}$$

When the re-formed reference vector $(V_{ref} + \Delta V/2)$, for instance, is located in the main sector I, the integral for $(V_{ref} + \Delta V/2)$ can be divided into the integral for the V_1 and V_2.

$$\int_0^{T_1+T_2}\left(V_{ref} + \frac{\Delta V}{2}\right)dt \quad = \quad \int_0^{T_1} V_1 dt + \int_{T_1}^{T_1+T_2} V_2 dt \tag{2.19}$$

Similarly, the integral equation for $-\Delta V/2$ in the diagonal sector IV can be divided into the integral for the V_4 and V_5

$$\int_{T_4+T_5}^{T_s} \frac{-\Delta v}{2} dt = \int_{T_4+T_5}^{T_4+T_5+T_0} V_4 dt + \int_{T_4+T_5+T_0}^{T_s} V_5 dt \tag{2.20}$$

Assuming the V_{ref} is constant and the switching frequency is high during a switching period T_s, equation 2.19 is arranged by

$$T_1 + T_2 \left(V_{ref} + \frac{\Delta V}{2} \right) = T_1 V_1 + T_2 V_2 \tag{2.21}$$

And equation 2.20 is arranged by

$$T_4 + T_5 \frac{-\Delta v}{2} dt = T_4 V_4 + T_5 V_5 \tag{2.22}$$

From equation 2.17 to equation 2.22, the re-formed reference vector in a main sector is represented by

$$T_s \left| V_{ref} + \frac{\Delta V}{2} \right| \begin{bmatrix} cos\alpha \\ sin\alpha \end{bmatrix} = T_1 \frac{\sqrt{3} V_{DC}}{2} \begin{bmatrix} 1 \\ 0 \end{bmatrix} + T_2 \frac{\sqrt{3} V_{DC}}{2} \begin{bmatrix} 0 \\ 1 \end{bmatrix} \tag{2.23}$$

And the restraint reference vector in a diagonal sector is represented by

$$T_s \left| -\frac{\Delta V}{2} \right| \begin{bmatrix} cos\alpha \\ sin\alpha \end{bmatrix} = T_1 \frac{\sqrt{3} V_{DC}}{2} \begin{bmatrix} 1 \\ 0 \end{bmatrix} + T_2 \frac{\sqrt{3} V_{DC}}{2} \begin{bmatrix} 0 \\ 1 \end{bmatrix} \tag{2.24}$$

Six switching times can be solved by equation 2.23 and equation 2.24 and given by the followings;

$$\begin{aligned}
T_1 &= \frac{T_s}{V_{DC}} \left[\frac{\sqrt{3} V_{DC}}{2} \frac{1}{sin\alpha + cos\alpha} + |V_{ref}| \right] cos\alpha \\
T_2 &= \frac{T_s}{V_{DC}} \left[\frac{\sqrt{3} V_{DC}}{2} \frac{1}{sin\alpha + cos\alpha} + |V_{ref}| \right] sin\alpha \\
T_0 + T_7 &= T_s - T_1 - T_2 \\
T_4 &= \frac{T_s}{V_{DC}} \left[\frac{\sqrt{3} V_{DC}}{2} \frac{1}{sin\alpha + cos\alpha} + |V_{ref}| \right] cos\alpha \\
T_5 &= \frac{T_s}{V_{DC}} \left[\frac{\sqrt{3} V_{DC}}{2} \frac{1}{sin\alpha + cos\alpha} + |V_{ref}| \right] sin\alpha \\
T_0 + T_7 &= T_s - T_4 - T_5
\end{aligned} \tag{2.25}$$

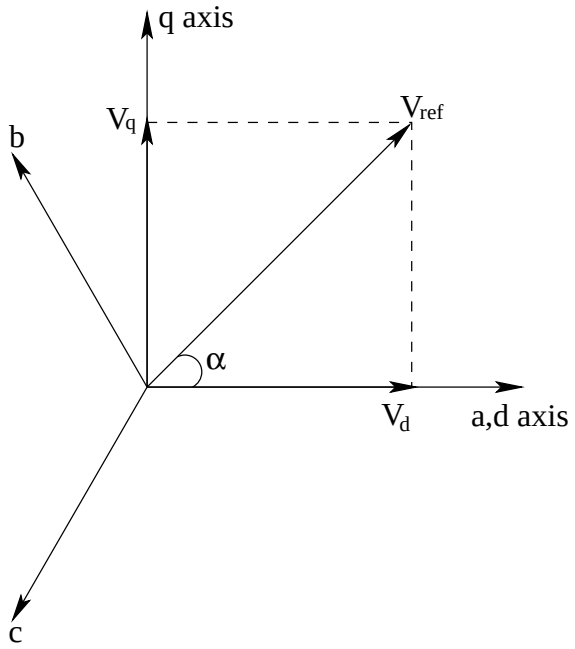

Figure 2.7: Voltage Space Vector and its Components in (d,q)

2.4 Steps of Design for SVM Generation

To implement the space vector modulation, the voltage equations in the abc reference frame can be transformed into the stationary dq reference frame [75] as shown in Figure 2.7.

From Figure 2.7, the relation between these two reference frames is as below

$$f_{dq0} = K_s f_{abc} \tag{2.26}$$

Where

$$K_s = \frac{2}{3}\begin{bmatrix} 1 & -1/2 & -1/2 \\ 0 & \sqrt{3}/2 & -\sqrt{3}/2 \\ 1/2 & 1/2 & 1/2 \end{bmatrix}$$

$f_{dq0} = [f_d, f_q, f_0]^T$

$f_{abc} = [f_a, f_b, f_c]^T$

and f denotes either a voltage or a current variable.

As described in Figure 2.7, this transformation is equivalent to an orthogonal projection of $[a, b, c]^t$ onto the two-dimensional perpendicular to the vector $[1, 1, 1]^t$ (the equivalent $d - q$ plane) in a three-dimensional coordinate system. As a result, six non-zero vectors and two zero vectors are possible. Six non-zero vectors (V_1 - V_6) shape the axis

of a hexagonal as shown in Figure 2.4 and feed electric power to the load. The angle between any adjacent two non-zero vectors is 60 degrees. Meanwhile, two zero vectors (V_0 and V_7) are at the origin and apply zero voltage to the load. The eight vectors are called the basic space vectors and are denoted by V_0, V_1, V_2, V_3, V_4, V_5, V_6 and V_7. The same transformation can be applied to the desired output voltage to get the desired reference voltage vector V_{ref} in the $d-q$ plane.

The objective of space vector modulation technique is to approximate the reference voltage vector V_{ref} using the eight switching patterns.

The space vector modulation can be implemented by the following steps:

Step 1. Determine V_d, V_q, V_{ref} and angle (α).

Step 2. Determine time duration T_1, T_2, T_0.

Step 3. Determine the switching time of each MOSFET (S_1 to S_6).

2.4.1 Determination V_d, V_q, V_{ref} and angle (α)

From Figure 2.7, the V_d, V_q, V_{ref} and angle (α) can be determine as follows:

$$\begin{aligned}
V_d &= V_{an} - V_{bn} \cdot cos60 - V_{cn} \cdot cos60 \\
&= V_{an} - \frac{1}{2}V_{bn} - \frac{1}{2}V_{cn} \\
V_q &= 0 + V_{bn} \cdot cos30 - V_{cn} \cdot cos30 \\
&= \frac{\sqrt{3}}{2}V_{bn} - \frac{\sqrt{3}}{2}V_{cn} \\
\begin{bmatrix} V_d \\ V_q \end{bmatrix} &= \frac{2}{3}\begin{bmatrix} 1 & -\frac{1}{2} & -\frac{1}{2} \\ 0 & \frac{\sqrt{3}}{2} & -\frac{\sqrt{3}}{2} \end{bmatrix}\begin{bmatrix} V_{an} \\ V_{bn} \\ V_{cn} \end{bmatrix} \\
|V_{ref}| &= \sqrt{V_d^2 + V_q^2} \\
\alpha &= tan^{-1}\left(\frac{V_d}{V_q}\right) = \omega t = 2\pi f t,
\end{aligned} \tag{2.27}$$

Where

f = Fundamental frequency

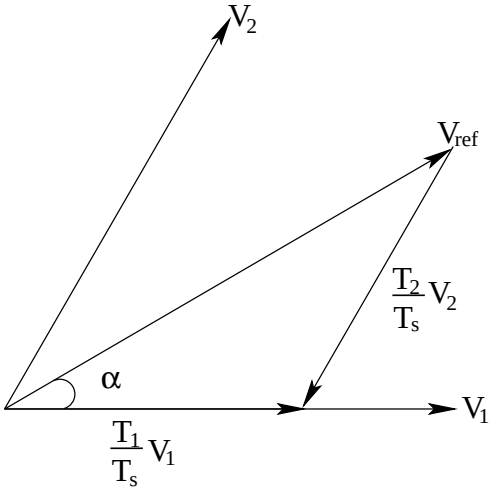

Figure 2.8: Reference Vector as a Combination of Adjacent Vectors at Sector I

2.4.2 Determination time duration T_1, T_2, T_0

From Figure 2.8, the switching time duration can be calculated as follows:

- Switching time duration at sector I

$$\begin{aligned} \int_0^{T_s} V_{ref}dt &= \int_0^{T_1} V_1 dt + \int_{T_1}^{T_1+T_2} V_2 dt + \int_{T_1+T_2}^{T_s} V_0 dt \\ T_s \cdot V_{ref} &= (T_1 \cdot V_1 + T_2 \cdot V_2) \\ T_s \cdot |V_{ref} \cdot \begin{bmatrix} cos(\alpha) \\ sin(\alpha) \end{bmatrix} &= T_1 \cdot \frac{2}{3} \cdot V_{DC} \cdot \begin{bmatrix} 1 \\ 0 \end{bmatrix} + T_2 \cdot \frac{2}{3} \cdot V_{DC} \begin{bmatrix} cos(\pi/3) \\ sin(\pi/3) \end{bmatrix} \end{aligned} \tag{2.28}$$

Where

$0 \leq \alpha \leq 60^o$

$$\begin{aligned} T_1 &= T_s \cdot a \cdot \frac{sin(\pi/3 - \alpha)}{sin(\pi/3)} \\ T_2 &= T_s \cdot a \cdot \frac{sin(\alpha)}{sin(\pi/3)} \\ T_0 &= T_s - (T_1 + T_2) \end{aligned} \tag{2.29}$$

Where

$$\begin{aligned} T_s &= \frac{1}{f_s} \\ a &= \frac{|V_{ref}|}{\frac{2}{3}V_{DC}} \end{aligned}$$

- Switching time duration at any sector

$$\begin{aligned} T_1 &= \frac{\sqrt{3}\cdot T_s\cdot|V_{ref}|}{V_{DC}}\left(sin\left(\frac{\pi}{3}-\alpha+\frac{n-1}{3}\pi\right)\right) \\ &= \frac{\sqrt{3}\cdot T_s\cdot|V_{ref}|}{V_{DC}}\left(sin\frac{n}{3}\pi-\alpha\right) \\ &= \frac{\sqrt{3}\cdot T_s\cdot|V_{ref}|}{V_{DC}}\left(sin\frac{n}{3}\pi cos\alpha-cos\frac{n}{3}\pi sin\alpha\right) \\ T_2 &= \frac{\sqrt{3}\cdot T_s\cdot|V_{ref}|}{V_{DC}}\left(sin\left(\alpha-\frac{n-1}{3}\pi\right)\right) \\ &= \frac{\sqrt{3}\cdot T_s\cdot|V_{ref}|}{V_{DC}}\left(-cos\alpha\cdot sin\frac{n-1}{3}\pi+sin\alpha\cdot cos30\frac{n-1}{3}\pi\right) \\ T_0 &= T_s-T_1-T_2 \end{aligned} \tag{2.30}$$

Where
n = 1 through 6 (that is, Sector I to VI)
$(n-1)\frac{\pi}{3}\leq\alpha\leq\frac{n\pi}{3}$

2.4.3 Determination of the switching time for MOSFET (S_1 to S_6)

Based on Figure 2.9, Figure 2.10 and Figure 2.11, the switching time at each sector has been summarized in Table 2.3 and it will be built in Simulink model to implement SVM.

2.5 Simulation Results

Simulation results were performed using simulink block as shown in Figure 2.12. The DC bus V_{DC} is equal to $325V$, is connected to the input of the inverter. For the linear operating range the V_{ref} must not exceeds the boundary of the hexagon. Therefore the maximum amplitude of the desired V_{ref} is calculated as

$$|V_{ref}|_{max} = \sqrt{\left(\frac{2}{3}V_{DC}\right)^2-\left(\frac{2}{6}V_{DC}\right)^2} \tag{2.31}$$

Sample circuit parameters are given in Table 2.4. Simulation space vector generator has been shown in Figure 2.12 Three phase PWM inverter output line to line voltage, output current, 3 phase to 2 phase dq transformation voltages and 3 phase to 2 phase dq transformation currents are shown in Figure 2.13, Figure 2.14, Figure 2.15, Figure

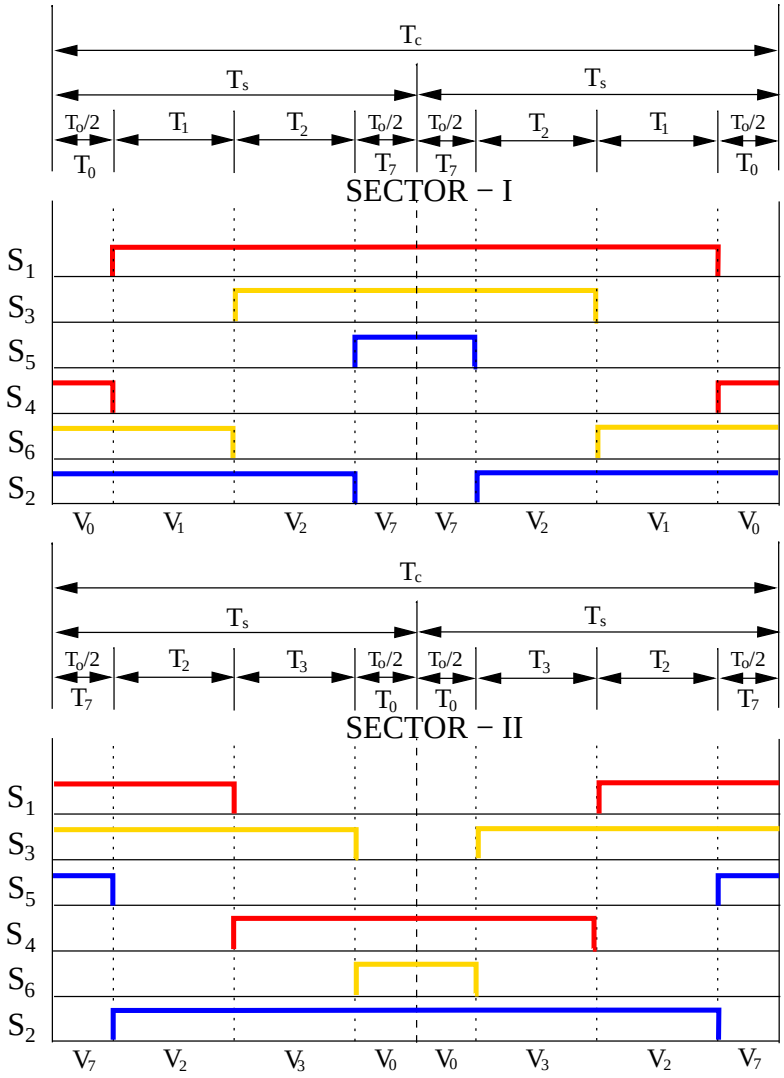

Figure 2.9: Optimal Switching Sequences for Sector I & II

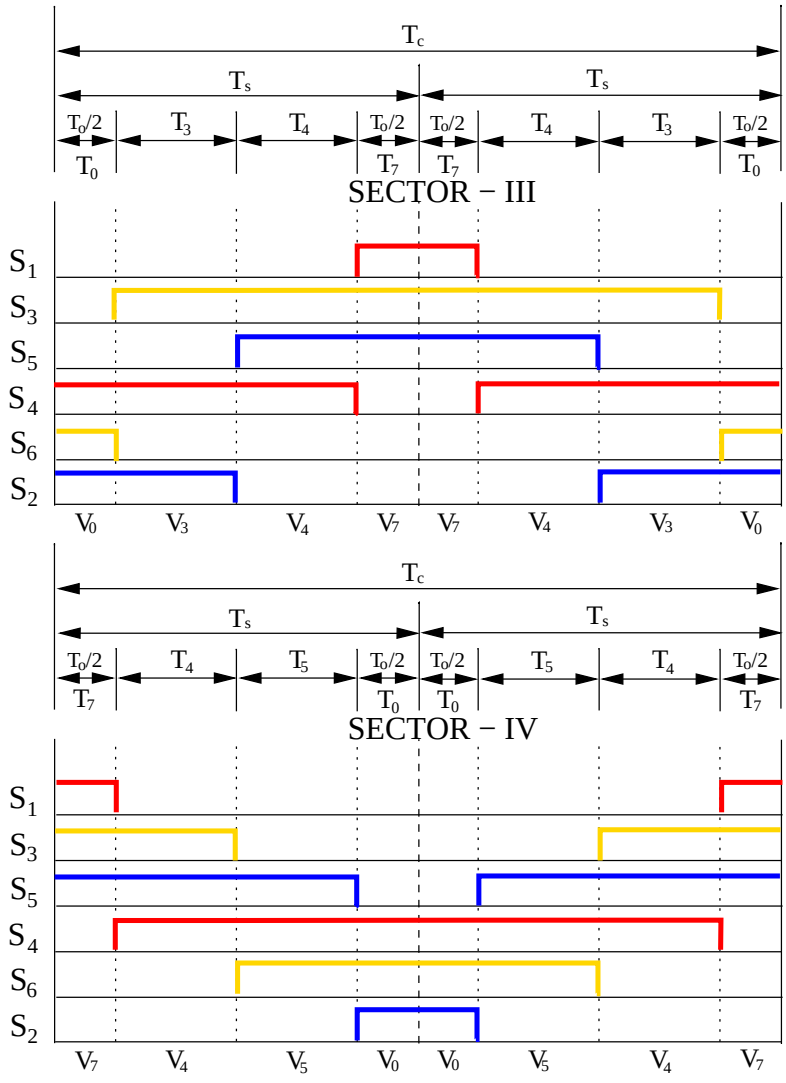

Figure 2.10: Optimal Switching Sequences for Sector III & IV

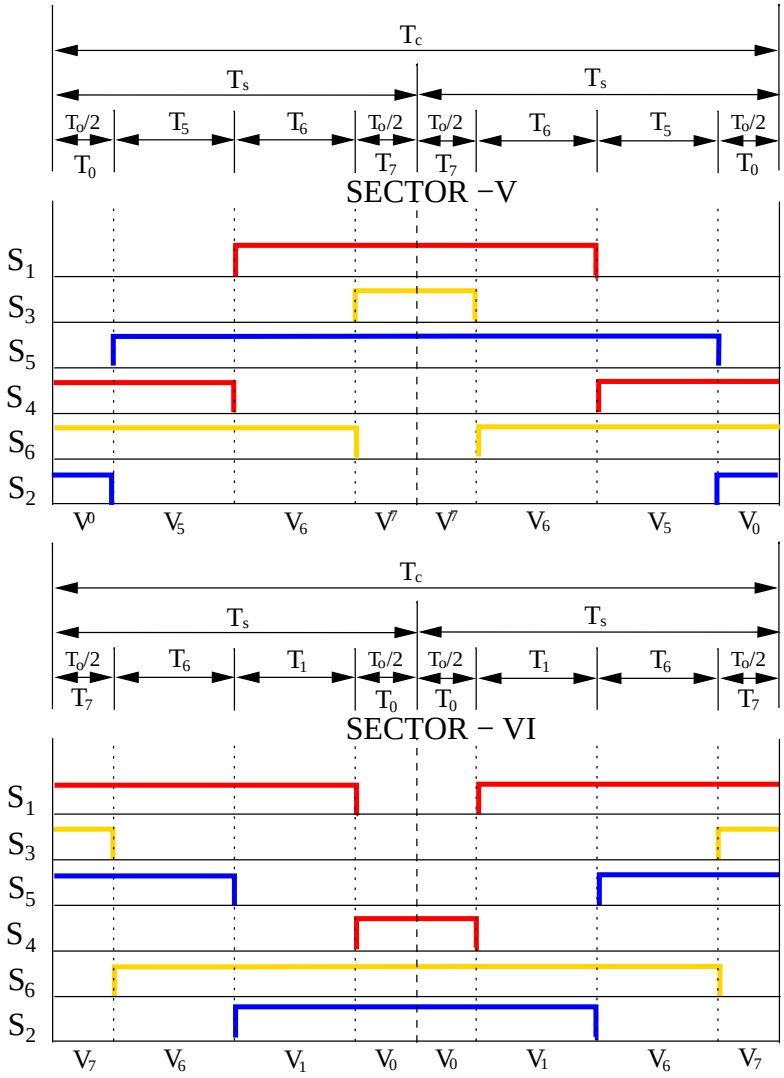

Figure 2.11: Optimal Switching Sequences for Sector V & VI

Table 2.3: Switching Time Calculation at Each Sector

Sector	Upper Switches (S_1, S_3, S_5)	Lower Switches (S_4, S_6, S_2)
1	$S_1 = T_1 + T_2 + T_7$ $S_3 = T_2 + T_7$ $S_5 = T_7$	$S_4 = T_0$ $S_6 = T_1 + T_0$ $S_2 = T_1 + T_2 + T_0$
2	$S_1 = T_2 + T_7$ $S_3 = T_2 + T_3 + T_7$ $S_5 = T_7$	$S_4 = T_3 + T_0$ $S_6 = T_0$ $S_2 = T_2 + T_3 + T_0$
3	$S_1 = T_7$ $S_3 = T_3 + T_4 + T_7$ $S_5 = T_4 + T_7$	$S_4 = T_3 + T_4 + T_0$ $S_6 = T_0$ $S_2 = T_3 + T_0$
4	$S_1 = T_7$ $S_3 = T_4 + T_7$ $S_5 = T_4 + T_5 + T_7$	$S_4 = T_4 + T_5 + T_0$ $S_6 = T_5 + T_0$ $S_2 = T_0$
5	$S_1 = T_6 + T_7$ $S_3 = T_7$ $S_5 = T_5 + T_6 + T_7$	$S_4 = T_5 + T_0$ $S_6 = T_5 + T_6 + T_0$ $S_2 = T_0$
6	$S_1 = T_1 + T_6 + T_7$ $S_3 = T_7$ $S_5 = T_6 + T_7$	$S_4 = T_0$ $S_6 = T_1 + T_6 + T_0$ $S_2 = T_1 + T_0$
	$T_7 = T_o/2$	$T_0 = T_o/2$

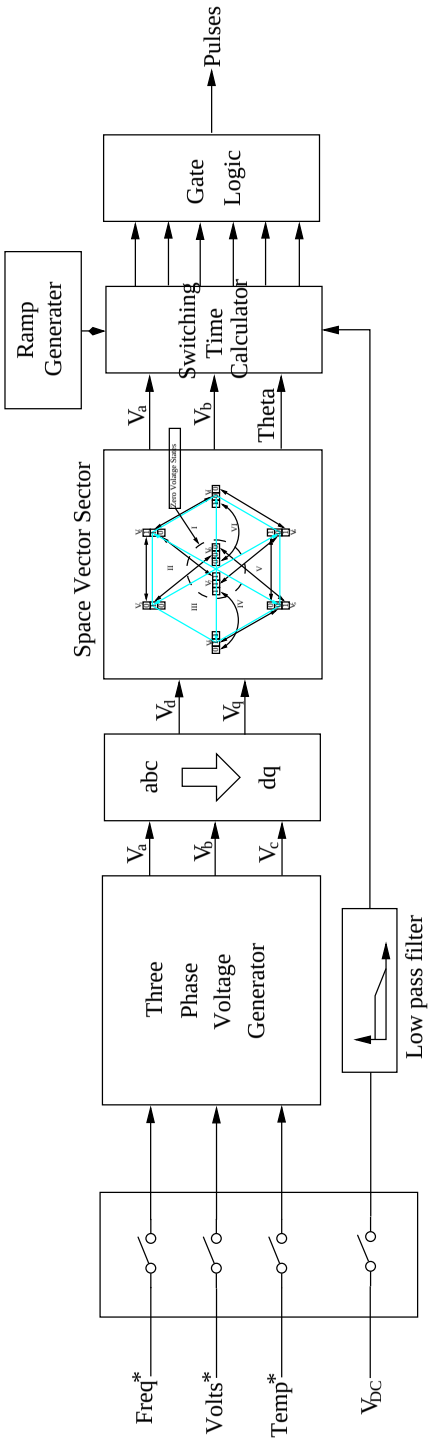

Figure 2.12: SVM Generator

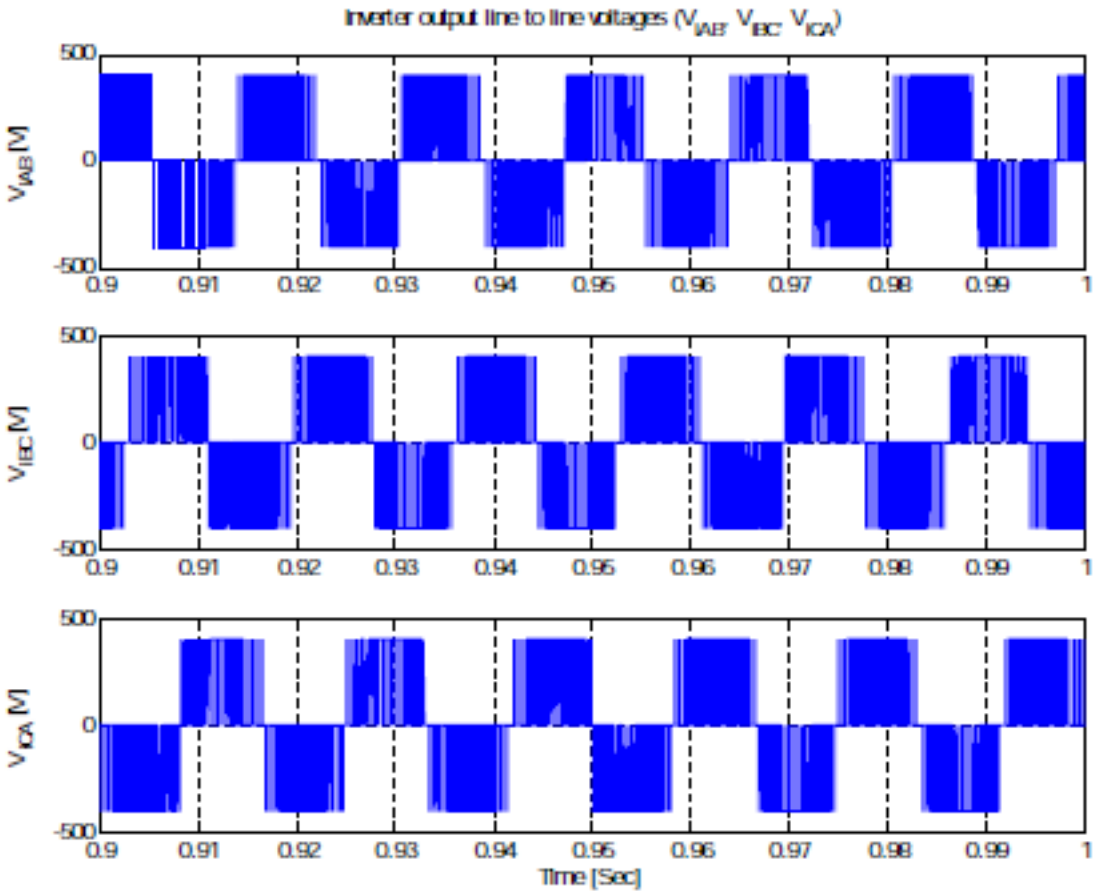

Figure 2.13: Simulation of Inverter Output Line to Line Voltages ($V_{lAB}, V_{lBC}, V_{lCA}$)

2.16 respectively. Simulation summaries and results are given in Table 2.5, Table 2.6 respectively.

A spectral analysis of all waveforms is performed and all harmonics are presented in Table 2.7. These results show that acceptable performances can be obtained at all testing frequencies since the total harmonic distortion (THD) did never reach 10%. At high switching frequency the PWM converter generate a voltage having amplitude close to the desired value.

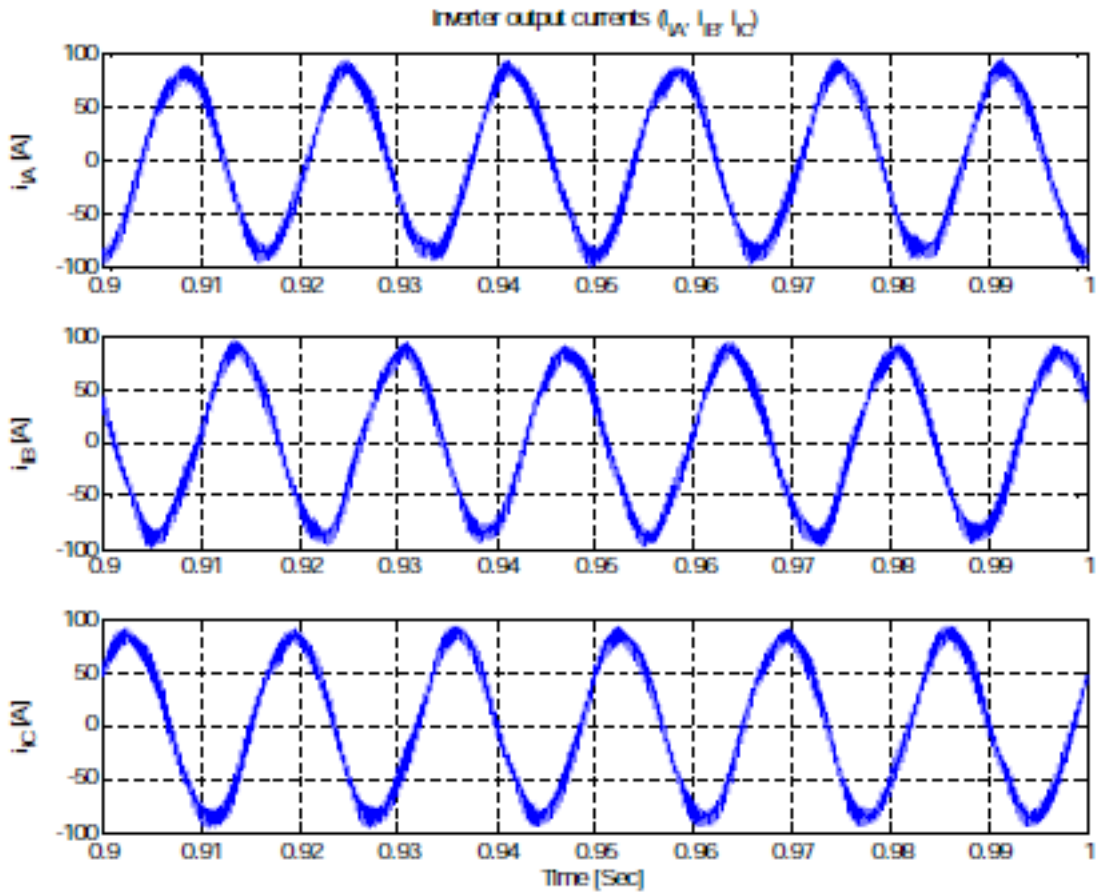

Figure 2.14: Simulation Results of Inverter Output Currents (i_{iA}, i_{iB}, i_{iC})

Table 2.4: Circuit Parameters

Parameter	Value
Utility	220V/50Hz
V_{DC}	325 volt
L_m	69.31mH
f_{sw}	2Khz

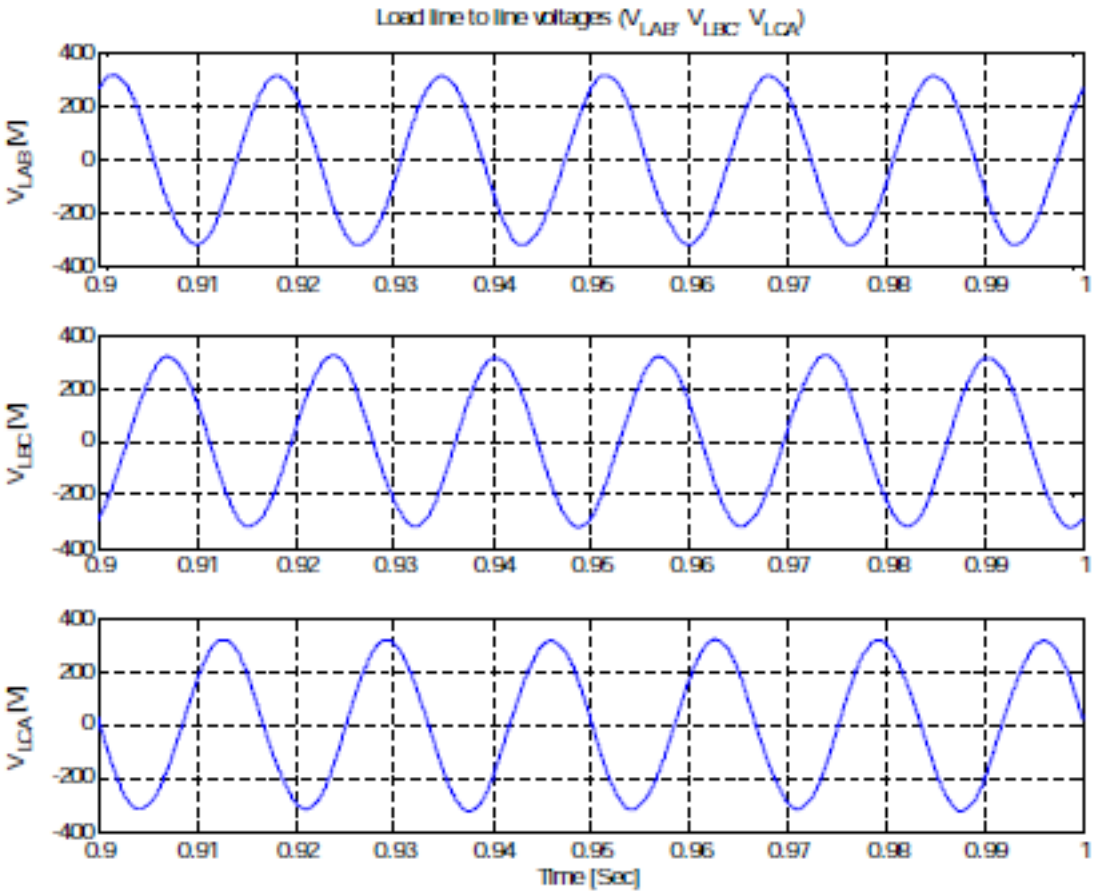

Figure 2.15: Simulation Results of Load Line to Line Voltages ($V_{LAB}, V_{LBC}, V_{LCA}$)

Table 2.5: Simulation Results

Switching Freq. in Hz	Set Temp. in ^0C	Final Temp. in ^0C	V_{ab} in Volt	Frequency in Hz	Load current in Amp.
200	1200	1167	139.21	41.01	9.036
2000	1200	1170	153.49	41.74	6.107
20000	1200	1168	151.33	41.74	5.186
200000	1200	1190	175.95	41.74	4.765

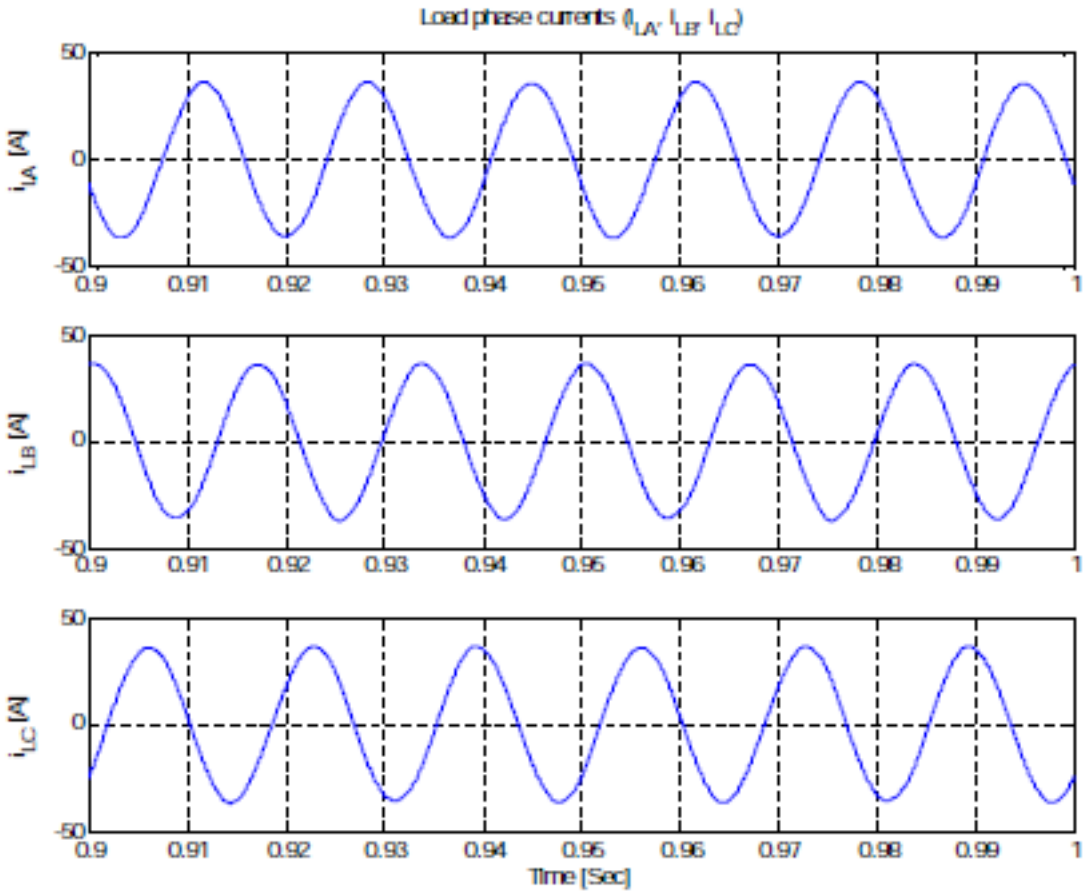

Figure 2.16: Simulation Results of Load Phase Currents (i_{LA}, i_{LB}, i_{LC})

Table 2.6: Simulation Summaries

Set Temp. in ^0C	Final Temp. in ^0C	V_{ab} in Volt	Frequency in Hz
150	145.8	15.20	16.42
530	499	67.22	18.44
1300	1275	165.84	45.21
1500	1484	191.75	52.17
1200	1170	153.49	41.74

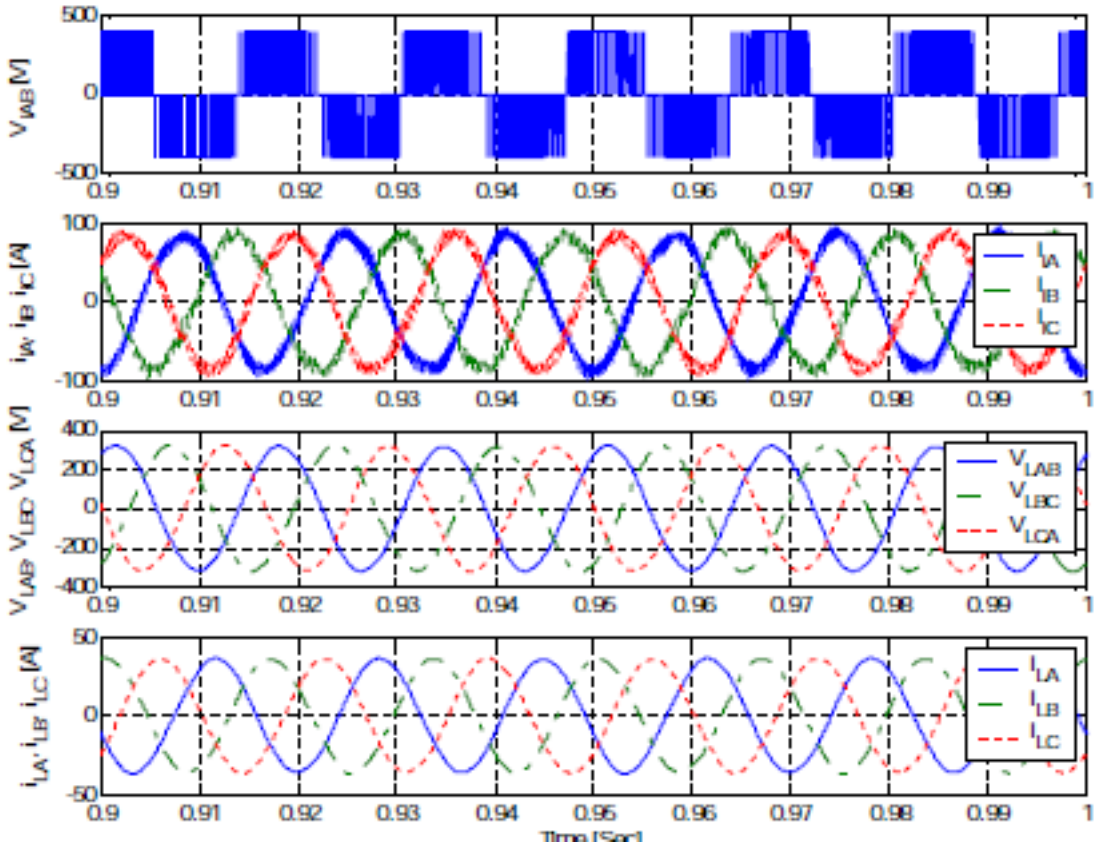

Figure 2.17: Simulation Waveforms. (a) Inverter Output Line to Line Voltage (V_{lAB}) (b) Inverter Output Current (i_{iA}) (c) Load Line to Line Voltage (V_{LAB}) (d) Load Phase Current (i_{LA})

Table 2.7: Spectral Analysis

h	Harmonic for different Switching frequencies			
	1 kHz	3 kHz	5 kHz	10 kHz
0	-4.58	-4.58	-4.16	-4.16
1	81.22	80.83	73.33	73.24
2	3.22	2.99	2.64	2.60
3	4.70	4.53	4.06	4.03
4	0.42	0.20	0.11	0.06
5	4.45	5.04	4.80	4.94
6	1.98	1.79	1.58	1.55
7	1.03	1.07	0.99	1.00

Table 2.8: Switching Vectors Part I

Sector	Switching Vector						Voltage	Time	Consecutive Time	Sample Time
	S_q	S_2	S_3	S_4	S_5	S_6				
SECTOR I	0	0	0	1	1	1	V_0	$\frac{T_0}{2}$	T_{C11}	T_{S-I}
	1	0	0	0	1	1	V_1	T_1		
	1	1	0	0	0	1	V_2	T_2		
	1	1	1	0	0	0	V_7	$\frac{T_0}{2}$		
	1	1	1	0	0	0	V_7	$\frac{T_0}{2}$	T_{C12}	
	1	1	0	0	0	1	V_2	T_2		
	1	0	0	0	1	1	V_1	T_1		
	0	0	0	1	1	1	V_0	$\frac{T_0}{2}$		
SECTOR II	1	1	1	0	0	0	V_7	$\frac{T_0}{2}$	T_{C21}	T_{S-II}
	1	1	0	0	0	1	V_2	T_2		
	0	1	0	1	0	1	V_3	T_3		
	0	0	0	1	1	1	V_0	$\frac{T_0}{2}$		
	0	0	0	1	1	1	V_0	$\frac{T_0}{2}$	T_{C22}	
	0	1	0	1	0	1	V_3	T_3		
	1	1	0	0	1	1	V_2	T_2		
	1	1	1	0	0	0	V_7	$\frac{T_0}{2}$		
SECTOR III	0	0	0	1	1	1	V_0	$\frac{T_0}{2}$	T_{C31}	T_{S-III}
	0	1	0	1	0	1	V_3	T_3		
	0	1	1	1	0	0	V_4	T_4		
	1	1	1	0	0	0	V_7	$\frac{T_0}{2}$		
	1	1	1	0	0	0	V_7	$\frac{T_0}{2}$	T_{C32}	
	0	1	1	1	0	0	V_4	T_4		
	0	1	0	1	0	1	V_3	T_3		
	0	0	0	1	1	1	V_0	$\frac{T_0}{2}$		

Table 2.9: Switching Vectors Part II

Sector	Switching Vector						Voltage	Time	Consecutive Time	Sample Time
	S_q	S_2	S_3	S_4	S_5	S_6				
SECTOR IV	1	1	1	0	0	0	V_7	$\frac{T_0}{2}$	T_{C41}	T_{S-IV}
	0	1	1	1	0	0	V_4	T_4		
	0	0	1	1	1	0	V_5	T_5		
	0	0	0	1	1	1	V_0	$\frac{T_0}{2}$		
	0	0	0	1	1	1	V_0	$\frac{T_0}{2}$	T_{C42}	
	0	0	1	1	1	0	V_5	T_5		
	0	1	1	1	0	0	V_4	T_4		
	1	1	1	0	0	0	V_7	$\frac{T_0}{2}$		
SECTOR V	0	0	0	1	1	1	V_0	$\frac{T_0}{2}$	T_{C51}	T_{S-V}
	0	0	1	1	1	0	V_5	T_5		
	1	0	1	0	1	0	V_6	T_6		
	1	1	1	0	0	0	V_7	$\frac{T_0}{2}$		
	1	1	1	0	0	0	V_7	$\frac{T_0}{2}$	T_{C52}	
	1	0	1	0	1	0	V_6	T_6		
	0	0	1	1	1	0	V_5	T_5		
	0	0	0	1	1	1	V_0	$\frac{T_0}{2}$		
SECTOR VI	1	1	1	0	0	0	V_7	$\frac{T_0}{2}$	T_{C61}	T_{S-VI}
	1	0	1	0	1	0	V_6	T_6		
	1	0	0	0	1	1	V_1	T_1		
	0	0	0	1	1	1	V_0	$\frac{T_0}{2}$		
	0	0	0	1	1	1	V_0	$\frac{T_0}{2}$	T_{C62}	
	1	0	0	0	1	1	V_1	T_1		
	1	0	1	0	1	0	V_6	T_6		
	1	1	1	0	0	0	V_7	$\frac{T_0}{2}$		

2.6 Conclusions

The main finding of this chapter reveals following:

1. Space vector modulation requires only a reference space vector to generate three phase sine waves.
2. The amplitude and frequency of load voltage can be varied by controlling the reference space vector.
3. This algorithm is flexible and suitable for advanced vector control.
4. The strategy of the switching minimizes the distortion of load current as well as loss due to optimum number of commutations in the inverter.
5. The effectiveness of the SVM to reduced the switching power losses is proved.
6. SVM is one of the best solutions to achieve good voltage transfer and reduce harmonic distortion in the output of three phase inverter for IDH.
7. It also provides excellent output performance optimized efficiency and high reliability compared to similar three phase inverter with conventional pulse width modulations.

Chapter 3

CONFIGURATION PROPOSALS FOR AN OPTIMAL ELECTROMAGNETIC COUPLING IN IDH SYSTEM

3.1 Introduction

Induction Dielectric Heating (IDH) is a mature technique for heating conducting materials (CM) and non-conducting materials (NCM). To reduce process cycle time with repeated quality, a suitable electromagnetic coupling that in turns generates intense heat throughput at very high rates, at well-defined locations and without considering magnetic permeability has been enabled.

When it comes to induction heating, one must keep in mind that ferromagnetic materials loose their magnetic properties above Curie temperature [4], [11], [70], thus good electric conductor condition exist as to be taken into account for a proper work-piece candidate in a IDH system, whereas low conducting materials will require high frequency for the excitation coil in order to get the above advantages. Other way to overcome the poor electromagnetic coupling in low conductive work-pieces is by way of assembling a high melting temperature condition [86], which is due to its high conductivity which heats indirectly the low conductive insert so as to avoid high frequency supportive equipment thus lowering the capital costs.

Despite IDH is a well-established heating method; the fit a favourable IDH scheme realized on empirical rules, relating size, frequency and the skin depth of the work-piece.

In this chapter the mathematical model for steady state IDH process has been developed and its numerical solution using Matlab and finite element method (FEM) has been obtained. It has been devoted to develop analytic parameters, which are intended to be taken as guidance to set optimal IDH configurations for putting together inductor and work-piece to achieve the highest electromagnetic coupling. It should match optimal conditions that are already known for induction heating practitioners [106], [110]. The simplest and existing geometrical coordinates have been used in massive induction heating systems. Which are the cylindrical and the spherical coordinates.

IDH system can be represented as a three phase high frequency electrical transformer, the more intense heat the influence on the idle coil impedance when the secondary loop is assembled, the greater the occurrence of eddy current on CM and displacement current (rate of change of voltage with respect to time) on NCM. Thus, a proposed reflection coefficient and transmission coefficient has been developed, which is the common factor that precedes both secondary resistance and secondary inductance as appearing in the effective impedance formula for an ideal electrical transformer. The larger reflection coefficient, the better is the electromagnetic coupling of the work-piece. To undertake the task, a dimensionless treatment of simplified governing differential equation of the process has been derived. The above approach has been presented for cylindrical systems [28], [106] and spherical systems, by considering boundary values: either a longitudinal or a transverse magnetic flux. In this chapter same treatment also will be given to cylindrical and spherical work-pieces, namely steel and lemon being excited by a travelling wave.

3.2 Impedance Parameters for an IDH System

A lumped parameter model has been represented in a mathematical model of a physical system where field variables have been simplified. The mathematical analysis of an electrical circuit is much simpler than solving the electromagnetic equations for the actual IDH physical system. Thus impedances, as lumped parameters, are electrical equivalent to those electromagnetic fields distributed in an existing inductor or an element of a circuit. Thereby, magnetic strength and current density distributions for a given IDH configuration, the basic impedance parameters such as resistances and inductances have been

stemmed from and then treated in such a way that a reflection coefficient and transmission coefficient has been obtained as a result.

The properties of an electromagnetic wave (direction of propagation, velocity of propagation, wavelength, frequency, attenuation, phase, intrinsic, skin depth etc.) can be determined by examining the solutions to the wave equations that define the electric and magnetic fields of the wave.

The mathematical model has been developed for two cases as follows:

1. Conducting material (CM)

2. Non-conducting material (NCM)

To obtain the mathematical model, Maxwell's equation and Ohm's law have been used. Displacement current is neglected for CM and eddy current is neglected for NCM. Maxwell's equations provide the following system:

$$\nabla X H = \text{curl} H = J + \frac{\partial D}{\partial t} \tag{3.1}$$

$$\nabla . B = \text{div} B = 0 \tag{3.2}$$

$$\nabla X E = \text{curl} E = -\frac{\partial B}{\partial t} \tag{3.3}$$

$$\nabla . D = \text{div} D = \sigma \tag{3.4}$$

$$\upsilon B = H \tag{3.5}$$

Where

E = Electric field intensity in V/m
H = Magnetic field intensity in A/m
B = Magnetic inductance (flux density) in Wb/m^2
D = Electric displacement field in C/m^2
J = Current density in A/m^2
υ = Magnetic reactivity
σ = Electrical conductivity in $S.m^{-1}$
μ = Magnetic permeability in H/m

With other co-relationship

$$D = \varepsilon E \text{ ,For non-conducting material (Dielectric)} \tag{3.6}$$

$$B = \mu H \text{ ,Magnetic inductance} \tag{3.7}$$

$$J = \sigma E \text{ ,For conducting material (Metal)} \tag{3.8}$$

valid in the whole space. From Ohm's law,

$$J = J_d + J_e + J_D \tag{3.9}$$

Where
J_d = Driving current
J_e = Eddy current
J_D = Displacement current inside the materials

$$J = 0 \text{ in the space outside the materials.} \tag{3.10}$$

This work overlooks the function of the accumulative charges, that is $\sigma = 0$. According to the relationship between D, J, E, B and D,

$$\nabla X H = J + \frac{\partial D}{\partial t} = \sigma E + \frac{\partial}{\partial t}(\varepsilon E) \tag{3.11}$$

The corresponding vector from

$$\nabla X H = (\sigma + j\varepsilon\omega)E \tag{3.12}$$

$$\nabla X E = -j\omega\mu H \tag{3.13}$$

$$\nabla . E = 0 \tag{3.14}$$

$$\nabla . H = 0 \tag{3.15}$$

$$\nabla X \nabla E = \nabla(\nabla . E) - \nabla^2 E$$

Substituting values from equation 3.13 and equation 3.14

$$-\nabla^2 E = -j\omega\mu(\nabla X H) \tag{3.16}$$

By substituting equation 3.12, results as

$$\nabla^2 E = j\omega\mu(\sigma + j\omega\varepsilon)E \tag{3.17}$$

$$\nabla^2 E = \gamma^2 E \tag{3.18}$$

Where

$\gamma^2 = j\omega\mu(\sigma + j\omega\varepsilon)$

γ (gamma) is called propagation constant in m^{-1} and has real and imaginary parts,

$$\gamma = \alpha + j\beta \tag{3.19}$$

Where
α = Attenuation constant in neper/m (Np/m)
β = Phase constant in (rad/m)

The attenuation constant defines the rate at which the fields of the wave is attenuated as the wave propagates. An electromagnetic wave propagates in an ideal (lossless) media without attenuation (α= 0). The phase constant defines the rate at which the phase changes as the wave propagates.

Taking only the x-component of E, variation with respect to z,

$$\frac{\partial^2 E_x}{\partial t^2} = -\mu_0 \varepsilon_0 \omega_2 E_x$$

$$\frac{\partial^2 E_x}{\partial t^2} + \mu_0 \varepsilon_0 \omega_2 \bar{E}_x = 0 \tag{3.20}$$

It is a second order differential equation having complete solution

$$E_x = E_{x0} e^{j\omega t} e^{\pm \gamma z} \tag{3.21}$$

$$E_x = E_{x0} e^{-\alpha z} e^{j(\omega t - \beta z)} \tag{3.22}$$

Where

$-\gamma x = -\alpha x - j\beta x$

The factor $e^{-\alpha z}$ shows the attenuation of wave. The phase constant β for a lossy dielectric is different from phase constant of a perfect dielectric of same dielectrics constant and permeability, β increases with conductivity. Hence wave length corresponding to given frequency becomes smaller and velocity of propagation is less.

The propagation constant can be obtained from equation 3.2

$$\gamma^2 = j\omega\mu(\sigma + j\omega\varepsilon)$$

$$\gamma = j\omega\sqrt{\mu\varepsilon}\sqrt{1 - j(\frac{\sigma}{\omega\varepsilon})} \tag{3.23}$$

γ can be separated into α and β such that

$$\gamma^2 = (\alpha + j\beta)^2 = j\omega\mu(\sigma + j\omega\varepsilon) \tag{3.24}$$

$$\alpha^2 - \beta^2 = -\omega^2\mu\varepsilon \tag{3.25}$$

$$2\alpha\beta = \omega\mu\varepsilon \tag{3.26}$$

From equation 3.25 and equation 3.26, separate α and β

$$\alpha = \omega\sqrt{\frac{\mu\varepsilon}{2}\left([\sqrt{1+(\frac{\sigma}{\omega\varepsilon})^2}-1]\right)} \tag{3.27}$$

$$\beta = \omega\sqrt{\frac{\mu\varepsilon}{2}\left([\sqrt{1+(\frac{\sigma}{\omega\varepsilon})^2}+1]\right)} \tag{3.28}$$

Considering only E_x component to E varying w.r.t z

$$\begin{aligned}\nabla XE &= \frac{\partial E_x}{\partial z}1_y \\ &= 1_y\frac{\partial}{\partial z}E_{x0}e^{-\gamma z} \\ &= -1_y\gamma E_{x0}e^{-\gamma z}\end{aligned}$$

Substituting equation 3.13

$$-j\omega\mu H = -1_y\gamma E_{x0}e^{-\gamma z}$$

H has H_y component corresponding to E_x

$$H_y = \frac{\gamma}{j\omega\mu}E_x \tag{3.29}$$

So the intrinsic impedance

$$\eta = \frac{E_x}{H_y} = \frac{j\omega\mu}{\gamma} \tag{3.30}$$

Substituting γ from equation 3.23

$$\eta = \sqrt{\frac{\mu}{\varepsilon(1+j\frac{\sigma}{j\omega\varepsilon})}} = \sqrt{\frac{j\omega\mu}{\sigma+j\omega\varepsilon}} \tag{3.31}$$

η is a complex quantity

$$\eta = \eta_m\angle\theta_\eta \tag{3.32}$$

With

$$E_x = E_{x0}e^{-\alpha z}e^{j(\omega t-\beta z)} \tag{3.33}$$

$$= E_{x0}e^{-\alpha z}(cos(\omega t-\beta z)+jsin(\omega t-\beta z)) \tag{3.34}$$

The magnetic field intensity becomes

$$\begin{aligned} H_y &= \frac{E_{x0}}{\eta} e^{-\alpha z} e^{j(\omega t - \beta z)} \\ &= \frac{E_{x0}}{\eta} e^{-\alpha z} (cos(\omega t - \beta z) + jsin(\omega t - \beta z)) \\ &= \frac{E_{x0}}{\eta_m} e^{-\alpha z} (cos(\omega t - \beta z - \theta_\eta) + jsin(\omega t - \beta z - \theta_\eta)) \end{aligned} \tag{3.35}$$

The electric and magnetic fields is no longer in time phase.

The factor $e^{-\alpha z}$ causes an exponential decrease in amplitude with increasing values of z; η is a complex quantity in the first quadrant, so the electric field leads the magnetic field in time phase.

Since P is given by the cross product of E and H, the direction of power flow at any point is normal to both the E and H vectors. This certainly agrees with our experience with the uniform plane wave, for propagation in the $+z$ direction was associated with an E_x and H_y component,

$$E_x a_x X H_y a_y = P_z a_z \tag{3.36}$$

Thus,

$$\begin{aligned} P_z &= E_x H_y \\ &= \frac{E_{x0}^2}{\eta_m} e^{-2\alpha z} (cos(\omega t - \beta z) + jsin(\omega t - \beta z)) \\ &(cos(\omega t - \beta z - \theta_\eta) + jsin(\omega t - \beta z - \theta_\eta)) \\ &= \frac{1}{2} \frac{E_{x0}^2}{\eta_m} e^{-2\alpha z} [cos(2\omega t - 2\beta z - 2\theta_\eta) + cos\theta_\eta] \end{aligned} \tag{3.37}$$

From equation 3.37, it can be seen that the power density has only a second harmonic component and a DC component. Since the first term has zero average value over an integral number of periods, the time average value of the Poynting vector

$$P_{z,av} = \frac{1}{2} \frac{E_{x0}^2}{\eta_m} e^{-2\alpha z} [cos(2\omega t - 2\beta z - 2\theta_\eta) + cos\theta_\eta] \tag{3.38}$$

Note that the power density attenuates as $e^{-2\alpha z}$, where as E_x and H_y fall off as $e^{-\alpha z}$

The dividing line between two classes is not sharp and some media has considered as conducting material (conductors) in one part of high frequency range, but as non-conducting material (dielectric) (with loss) in another part of the range.

In the Maxwell's equation $\nabla X H = \sigma E + j\omega\varepsilon E$, the ratio $\frac{\sigma}{\omega\varepsilon}$ is therefore just the ratio of conduction current density to displacement current density in the medium. Conducting material has $\frac{\sigma}{\omega\varepsilon} >> 1$ over entire high frequency range. Non-conducting material has $\frac{\sigma}{\omega\varepsilon} << 1$ under the high frequency range.

The term $\frac{\sigma}{\omega\varepsilon}$ is referred to as the loss tangent (similar to loss tangent in case of a capacitor) or dissipation factor. In practice, following observations are true:

1. For good conductors σ and ω are nearly independent of frequency.
2. For most dielectrics σ and ω are functions of frequency, but the ratio $\frac{\sigma}{\omega\varepsilon}$ is often constant over the frequency range of interest.

Based on the value of $\frac{\sigma}{\omega\varepsilon}$, it can be approximate the relations for attenuation constant, phase constant and intrinsic impedance for CM and NCM.

3.3 Conducting Material

For the development of mathematical model for conducting material following assumptions have been made,

1. All CM are cylindrical, magnetic and have no net electric charge.
2. The system is rotationally symmetric about the z-axis i.e. θ for conducting material e.g. steel.
3. The rate of change of output voltage with respect to time is neglected for conducting material (CM).
4. The distribution of electrical current and travelling magnetic flux in the coil is uniform.
5. The self inductance effect in the coil is taken into account.
6. The current has a steady state quality and as a result, the electromagnetic field quantities are harmonically oscillating functions with a fixed single frequency.

3.3.1 Wave propagation in conducting material (CM)

For conducting material $\sigma >> \omega\varepsilon$

$$\frac{\sigma}{\omega\varepsilon} >> 1 \tag{3.39}$$

The propagation constant γ can be written as

$$\begin{aligned}
\gamma^2 &= j\omega\mu(\sigma + j\omega\varepsilon) \\
&= j\omega\mu\sigma\left(1 + j\frac{\omega\varepsilon}{\sigma}\right) \\
&\approx j\omega\mu\sigma \\
\gamma &= \sqrt{j\omega\mu\sigma} \qquad (3.40) \\
&= \sqrt{\omega\mu\sigma}\angle 45^0 \\
&= \sqrt{\omega\mu\sigma}(cos45 + jsin45) \\
&= \sqrt{\frac{\omega\mu\sigma}{2}} + j\sqrt{\frac{\omega\mu\sigma}{2}} \\
&= (1+j)\sqrt{\frac{\omega\mu\sigma}{2}} \qquad (3.41)
\end{aligned}$$

$$\text{So } \alpha = \beta = \sqrt{\frac{\omega\mu\sigma}{2}} = \sqrt{\pi f\mu\sigma} \tag{3.42}$$

The velocity of propagation

$$\nu = \frac{\omega}{\beta} = \sqrt{\frac{2\omega}{\mu\sigma}} \tag{3.43}$$

The intrinsic impedance of the CM

$$\eta = \sqrt{\frac{j\omega\mu}{\sigma + j\omega\varepsilon}} = \sqrt{\frac{j\omega\mu}{\sigma}} = \sqrt{\frac{\omega\mu}{\sigma}}\angle 45^0 \tag{3.44}$$

In a conductor, α and β are large. The wave attenuates greatly as it progresses and phase shift per unit length is also large. The velocity of the wave is small. The intrinsic impedance is small and has a reactive component with impedance angle of 45^0.

3.3.2 Mathematical model for CM (Steel)

Let (a_r, a_θ, a_z) be the natural tangent system associated with cylindrical coordinate, (r, θ, z) such that the O_z-axis is the symmetry axis of the induction dielectric heating

(IDH). The current density is supposed to be in the form $J = J(r,z)e^{j\omega t}a_\theta$, where ω is the angular frequency of the current and t is the time. It is also assumed that the components of the fields H, E, B in the system (a_r, a_θ, a_z) depend only on r, z and t (not on θ). Equation 3.1 yields then that $H(r,z)$ is of the from

$$H(r,z) = (H_r(r,z)a_r + H_z(r,z)a_z)e^{j\omega t} \tag{3.45}$$

Let A be a magnetic vector potential, i.e., a magnetic field satisfying

$$B = \nabla X A \tag{3.46}$$

A is divergence free (coulomb gauge). Using equation 3.5, equation 3.45 and equation 3.46, it can be shown that A may be expressed in terms of a continuous scalar potential ψ depending only on r and z:

$$A = e^{j\omega t}\psi(r,z)a_\theta \tag{3.47}$$

Using the notation $B(r,z) = (B_r(r,z)a_r + B_z(r,z)a_z)e^{j\omega t}$, from equation 3.46

$$\begin{aligned} B_r &= -\frac{\partial \psi}{\partial z} \\ B_z &= \frac{1}{r}\frac{\partial r\psi}{\partial r} \end{aligned} \tag{3.48}$$

From equation 3.3

$$\nabla X E + j\omega B = 0 \tag{3.49}$$

and using equation 3.46

$$\nabla X (E + j\omega A) = 0 \tag{3.50}$$

Include the self inductance effect in the induction coil as eddy current represented by $J_e = \sigma E$ as per equation 3.8. The displacement current is neglected for conducting material, then

$$\begin{aligned} J &= J_d + J_e = J_d + \sigma_{co}E \text{ , Driving and eddy current in the coil} \\ &= J_e = \sigma_w E \text{ , Eddy current in the work-piece} \end{aligned} \tag{3.51}$$

Where

σ_{co} = The electrical conductivity of the coil

σ_w = The electrical conductivity of the work-piece

Setting $J_d = J_0 cos\omega t$ as the driving current in the coil, to find a solution of the from

$$\nabla X((\frac{J_e}{\sigma_{co}} + j\omega\psi)a_\theta) = 0 \text{ ,For coil}$$
$$\nabla X((\frac{J_e}{\sigma_w} + j\omega\psi)a_\theta) = 0 \text{ ,For work-piece} \tag{3.52}$$

It follows that for coil $(\frac{J_e}{\sigma_{co}}r + j\omega\psi r)$ and for work-piece $(\frac{J_e}{\sigma_w}r + j\omega\psi r)$ are a constant in each connected components of a conductor and shows that this constant is equal to $v_k/2\pi$.

$$J = \sigma_{co}(-j\omega\psi + \frac{v_k}{2\pi r}) \text{ ,Coil}$$
$$J = \sigma_w(-j\omega\psi + \frac{v_k}{2\pi r}) \text{ ,Work-piece} \tag{3.53}$$

Where

v_k = Total voltage imposed in the conductor

Using equation 3.1, equation 3.5, equation 3.48 and equation 3.53, to get inside the conducting materials (coils and work-pieces) the equation

$$-\left(\frac{\partial}{\partial r}\left(\frac{\upsilon}{r}\frac{\partial r\psi}{\partial r}\right) + \frac{\partial}{\partial z}\left(\upsilon\frac{\partial\psi}{\partial z}\right)\right) + j\sigma_{co}\omega\psi = \sigma_{co}\frac{v_k}{2\pi r} \text{ ,Coil}$$
$$-\left(\frac{\partial}{\partial r}\left(\frac{\upsilon}{r}\frac{\partial r\psi}{\partial r}\right) + \frac{\partial}{\partial z}\left(\upsilon\frac{\partial\psi}{\partial z}\right)\right) + j\sigma_w\omega\psi = \sigma_w\frac{v_k}{2\pi r} \text{ ,Work-piece} \tag{3.54}$$

In a similar way the relation from equation 3.1, equation 3.5, equation 3.10 and equation 3.48 are combined together will provide the following equation in the space outside the conductors.

$$\left(\frac{\partial}{\partial r}\left(\frac{\upsilon}{r}\frac{\partial r\psi}{\partial r}\right) + \frac{\partial}{\partial z}\left(\upsilon\frac{\partial\psi}{\partial z}\right)\right) = 0 \tag{3.55}$$

Since there are no surface current, the following interface condition holds at the boundary of any conductor

$$\left[\frac{\upsilon}{r}\left(\frac{\partial(r\psi)}{\partial r}n_r + \frac{\partial(r\psi)}{\partial z}n_z\right)\right] = 0 \tag{3.56}$$

Where $[\psi]$ denotes the jump of a function ψ at the boundary of the conducting material and $n = n_r a_r + n_z a_z$ is the normal vector on the interface.

For electromagnetic computations, consider a circular in the (r, z)-plan, surrounding the induction dielectric heating system and big enough for the magnetic field to be weak at the boundaries of the outer surface.

The Bio-Savart hypothesis implies that the field B behave like $1/(r^3+z^3)$ far from the conductors. For big values of r, the behaviour of ψ can be considered to be similar to $1/r^2$. Therefore, on the boundaries of the outer surface which are parallel to the symmetry axis, so called Robin condition [[55] p.162].

$$\frac{\partial(r\psi)}{\partial r} + \psi = 0 \tag{3.57}$$

For those boundaries of the outer surface which are perpendicular to the symmetry axis, a Robin like condition is difficult to enforce. Instead, the condition

$$\frac{\partial(r\psi)}{\partial z} = 0 \tag{3.58}$$

Which stems from the assumptions that the radial component of the magnetic field is close to zero on these boundaries.

Finally, the natural symmetry condition along the revolution axis is

$$\psi = 0 \tag{3.59}$$

To sum up, the electromagnetic model to be solved consists of equation 3.53 and equation 3.54, together with the interface condition equation 3.55, the boundary conditions equation 3.58 and equation 3.57, as well as the symmetry condition equation 3.59.

In order to study the thermal effects of the electromagnetic phenomena, the above model will be coupled with the heat equation. Assume that the work-pieces do not interact thermally. These assumptions will allow solving the heat equation individually for each work-piece. The Joule effect power term is $\sigma^{-1}|J_m|^2$, where J_m is the mean current density, equal to $J/\sqrt{2}$ in our case. The value of J is directly obtained by equation 3.53. Therefore, the equation to be solved in order to get the temperature field in the work-piece is

$$\rho C_p \frac{\partial T}{\partial t} - (\lambda \nabla T) = \frac{\sigma_w}{2} \left| \left(-j\omega\psi + \frac{v_k}{2\pi r} \right) \right|^2 \tag{3.60}$$

Equation 3.60 is completed by the following radiation condition on the boundary of the work-piece, which is justified if the work-piece is convex and there is a large difference in temperature between the work-piece and the surrounding space:

$$\lambda \frac{\partial T}{\partial n} + \kappa(T^4 - T_{amb}^2) = 0 \tag{3.61}$$

Where

κ = The product of the Stefan Boltzmann constant by the material emissivity coefficient

$\partial T/\partial n$ = The normal derivative of T on the boundary of the work-piece

T_{amb} = The ambient temperature

One can also consider an empirical conversion law, replacing equation 3.61 by the condition

$$\lambda\frac{\partial T}{\partial n} + \kappa(T^4 - T_{amb}^4) + \zeta(T - T_{amb}) = 0 \tag{3.62}$$

Where

ζ = Proportionality coefficient

The complete model consists in coupling the electromagnetic problem equation 3.53-equation 3.59 with the thermal problem equation 3.60, equation 3.61, or equation 3.62, where T depends only on the spatial coordinates r, z and on the time t.

This model includes two kinds of nonlinearities: the first due to the heat source term in the heat equation 3.57 and the second due to the dependence of physical properties of the conducting materials on the temperature and possibly on the magnetic field.

3.4 Non-Conducting Material

For the development of mathematical model for non-conducting material following assumptions have been made,

1. All NCM are isotropic, non-magnetic and have no net electric charge.
2. The system is rotationally symmetric about the z-axis i.e. ϕ for non-conducting material e.g. lemon.
3. The eddy current is neglected for non-conducting material (NCM).
4. The distribution of potential in the coil is uniform.
5. The self capacitance effect in the coil is taken into account.
6. The voltage has a steady state quality and as a result, the electromagnetic field quantities are harmonically oscillating functions with a fixed single frequency.

3.4.1 Wave propagation in non-conducting material (NCM)

For non-conducting material

$$\sigma << \omega\varepsilon \text{ or}$$
$$\frac{\sigma}{\omega\varepsilon} << 1$$

It can be written as

$$\sqrt{1+\frac{\sigma^2}{\omega^2\varepsilon^2}} \approx \left(1+\frac{\sigma^2}{2\omega^2\varepsilon^2}\right) \tag{3.63}$$

by using binomial theorem

$$(1+x)^n = 1 + nx + \frac{n(n-1)}{2!}x^2 + \frac{n(n-1)(n-2)}{3!}x^3 + ... \tag{3.64}$$

Equation 3.27 and equation 3.28 then becomes

$$\begin{aligned}\alpha &= \omega\sqrt{\frac{\mu\varepsilon}{2}\left(\sqrt{1+\left(\frac{\sigma}{\omega\varepsilon}\right)^2}-1\right)} \\ &\approx \omega\sqrt{\frac{\mu\varepsilon}{2}\left(1+\frac{\sigma^2}{2\omega^2\varepsilon^2}-1\right)} \\ &= \frac{\sigma}{2}\sqrt{\frac{\mu}{\varepsilon}}\end{aligned} \tag{3.65}$$

$$\begin{aligned}\beta &= \omega\sqrt{\frac{\mu\varepsilon}{2}\left(\sqrt{1+\left(\frac{\sigma}{\omega\varepsilon}\right)^2}+1\right)} \\ &\approx \omega\sqrt{\frac{\mu\varepsilon}{2}\left(1+\frac{\sigma^2}{2\omega^2\varepsilon^2}+1\right)} \\ &= \omega\sqrt{\mu\varepsilon}\left(1+\frac{\sigma^2}{8\omega^2\varepsilon^2}\right)\end{aligned} \tag{3.66}$$

$\omega\sqrt{\mu\varepsilon} = (\frac{\omega}{\nu})$ is the phase shift for a non-conducting material.

$$\begin{aligned}\text{Velocity of wave } \nu &= \frac{\omega}{\beta} \\ &= \frac{1}{\sqrt{\mu\varepsilon\left(1+\frac{\sigma^2}{8\omega^2\varepsilon^2}\right)}} \\ &\approx \frac{1}{\sqrt{\mu\varepsilon}}\left(1-\frac{\sigma^2}{8\omega^2\varepsilon^2}\right)\end{aligned} \tag{3.67}$$

$\frac{1}{\sqrt{\mu\varepsilon}}$ is the velocity of the wave in the NCM when the conductivity is zero i.e. in perfect dielectric. The effect of a small amount of loss is to reduce slightly the velocity of propagation of the wave.

$$\begin{aligned}\text{Intrinsic impedance } \eta &= \sqrt{\frac{j\omega\mu}{\sigma + j\omega\varepsilon}} \\ &= \sqrt{\frac{\mu}{\varepsilon}\left(\frac{1}{1+\frac{\sigma}{j\omega\varepsilon}}\right)} \\ &\approx \sqrt{\frac{\mu}{\varepsilon}}\left(1 + j\frac{\sigma}{2\omega\varepsilon}\right) \end{aligned} \tag{3.68}$$

$\sqrt{\frac{\mu}{\varepsilon}}$ is the intrinsic impedance of the NCM with $\sigma = 0$. The chief effect of loss is to add a small reactive component to the intrinsic impedance.

The above approximations may be made in the cases where $\frac{\sigma}{\omega\varepsilon} < 0.1$.

3.4.2 Mathematical model for NCM (Lemon)

Let (a_r, a_θ, a_ϕ) be the natural tangent system associated with spherical coordinate (r, θ, ϕ) such that the O_θ-axis is the symmetry axis of the induction dielectric heating (IDH). The current density is supposed to be in the form $J = J(r, \theta)e^{j\omega t}a_\phi$, where ω is the angular frequency of the current and t is the time. It is also assumed that the components of the fields H, E, B in the system (a_r, a_θ, a_ϕ) depend only on r, θ and t (not on ϕ). Equation 3.1 yields then that $H(r, \theta)$ is of the from

$$H(r, \theta) = (H_r(r, \theta)a_r + H_\theta(r, \theta)a_\theta)e^{j\omega t} \tag{3.69}$$

Let A be a magnetic vector potential, i.e., a magnetic field satisfying

$$B = \nabla X A \tag{3.70}$$

A is divergence free (coulomb gauge). Using equation 3.5, equation 3.69 and equation 3.70, it can be shown that A may be expressed in terms of a continuous scalar potential ψ depending only on r and θ:

$$A = e^{j\omega t}\psi(r, \theta)a_\phi \tag{3.71}$$

Using the notation $B(r,\theta) = (B_r(r,\theta)a_r + B_\theta(r,\theta)a_\theta)e^{j\omega t}$, from equation 3.70

$$B_r = \frac{1}{rsin\theta}\frac{\partial(\psi sin\theta)}{\partial\theta}$$
$$B_\theta = -\frac{1}{r}\frac{\partial r\psi}{\partial r} \tag{3.72}$$

From equation 3.3

$$\nabla X E + j\omega B = 0 \tag{3.73}$$

and using equation 3.46

$$\nabla X(E + j\omega A) = 0 \tag{3.74}$$

Include the self inductance effect in the induction coil as displacement current represented by $J_D = \partial D/\partial t = j\omega D = j\omega\varepsilon E$ as per equation 3.8. The eddy current is neglected for non-conducting material, then

$$J = J_d + J_D = J_d + j\omega\varepsilon_{co}E \text{ ,Driving and displacement current in the coil}$$
$$= J_D = j\omega\varepsilon_w E \text{ ,Displacement current in the work-piece} \tag{3.75}$$

Where

ε_{co} = The electrical permittivity of the coil

ε_w = The electrical permittivity of the work-piece

Setting $J_d = J_0 cos\omega t$ as the driving current in the coil, to find a solution of the form

$$\nabla X((\frac{J_D}{j\omega\varepsilon_{co}} + j\omega\psi)a_\phi) = 0 \text{ ,For coil}$$
$$\nabla X((\frac{J_D}{j\omega\varepsilon_w} + j\omega\psi)a_\phi) = 0 \text{ ,For work-piece} \tag{3.76}$$

It follow that for coil $(\frac{J_D}{j\omega\varepsilon_w}r + j\omega\psi r)$ and for work-piece $(\frac{J_D}{j\omega\varepsilon_w}r + j\omega\psi r)$ are a constant in each connected components of a lemon and shown that this constant is equal to $v_k/2\pi$.

$$J = j\omega\varepsilon_{co}(-j\omega\psi + \frac{v_k}{2\pi r}) \text{ ,Coil}$$
$$J = j\omega\varepsilon_w(-j\omega\psi + \frac{v_k}{2\pi r}) \text{ ,Work-piece} \tag{3.77}$$

Where

v_k = Total voltage imposed in the lemon (NCM)

Using equation 3.1, equation 3.5, equation 3.72 and equation 3.77, inside the non-conducting materials (coils and work-pieces) the equation

$$\begin{aligned} -\left(\frac{\partial}{\partial r}\left(\frac{\upsilon}{r^2 sin\theta}\frac{\partial r\psi sin\theta}{\partial r}\right)+\frac{\partial}{\partial\theta}\left(\frac{\upsilon}{r}\frac{\partial r\psi}{\partial\theta}\right)\right)-\omega^2\varepsilon_{co}\psi = j\omega\varepsilon_{co}\frac{v_k}{2\pi r} \text{ ,Coil} \\ -\left(\frac{\partial}{\partial r}\left(\frac{\upsilon}{r^2 sin\theta}\frac{\partial r\psi sin\theta}{\partial r}\right)+\frac{\partial}{\partial\theta}\left(\frac{\upsilon}{r}\frac{\partial r\psi}{\partial\theta}\right)\right)-\omega^2\varepsilon_{w}\psi = j\omega\varepsilon_{w}\frac{v_k}{2\pi r} \text{ ,Work-piece} \end{aligned} \tag{3.78}$$

In a similar way the relation from equation 3.1, equation 3.5, equation 3.10 and equation 3.72 are combined together will provide the following equation in the space outside the conductors.

$$\left(\frac{\partial}{\partial r}\left(\frac{\upsilon}{r^2 sin\theta}\frac{\partial(r\psi sin\theta)}{\partial r}\right)+\frac{\partial}{\partial\theta}\left(\frac{\upsilon}{r}\frac{\partial r\psi}{\partial\theta}\right)\right)=0 \tag{3.79}$$

Since there are no surface current, the following interface condition holds at the boundary of any non-conductor material

$$\left[\frac{\upsilon}{r}\left(\frac{1}{r sin\theta}\frac{\partial(r\psi sin\theta)}{\partial r}n_r+\frac{\partial(r\psi)}{\partial\theta}n_\theta\right)\right]=0 \tag{3.80}$$

Where $[\psi]$ denotes the jump of a function ψ at the boundary of the non-conducting material and $n = n_r a_r + n_\theta a_\theta$ is the normal vector on the interface.

For electromagnetic computations, consider a sphere in the (r,θ)-plan, surrounding the IDH system and big enough for the magnetic field to be weak at the boundaries of the outer surface.

The Bio-Savart hypothesis implies that the field B behave like $1/(r^3+\theta^3)$ far from the lemon. For big values of r, the behaviour of ψ can be considered to be similar to $1/r^2$. Therefore, on the boundaries of the outer surface which are parallel to the symmetry axis, so called Robin condition [[55] p.162].

$$\frac{\partial(r\psi sin\theta)}{\partial r}+\psi=0 \tag{3.81}$$

For those boundaries of the outer surface which are perpendicular to the symmetry axis, a Robin like condition is difficult to enforce. Instead, the condition

$$\frac{\partial(r\psi)}{\partial\theta}=0 \tag{3.82}$$

Which stems from the assumptions that the radial component of the magnetic field is close to zero on these boundaries.

Finally, the natural symmetry condition along the revolution axis is

$$\psi = 0 \tag{3.83}$$

To sum up, the electromagnetic model to be solved consists of equation 3.77 and equation 3.78, together with the interface condition equation 3.79, the boundary conditions equation 3.82 and equation 3.81, as well as the symmetry condition equation 3.83.

In order to study the thermal effects of the electromagnetic phenomena, the above model will be coupled with the heat equation. Assume that the work-pieces do not interact thermally. These assumptions will allow solving the heat equation individually for each work-piece. The Rubbing effect power term is $|J_m|^2/j\omega\varepsilon$, where J_m is the mean current density, equal to $J/\sqrt{2}$ in our case. The value of J is directly obtained by equation 3.77. Therefore, the equation to be solved in order to get the temperature field in the work-piece is

$$\rho C_p \frac{\partial T}{\partial t} - (\lambda \nabla T) = \frac{j\omega\varepsilon_w}{2} \left| \left(-j\omega\psi + \frac{v_k}{2\pi r} \right) \right|^2 \tag{3.84}$$

Equation 3.84 is completed by the following radiation condition on the boundary of the work-piece, which is justified if the work-piece is convex and there is a large difference in temperature between the work-piece and the surrounding space:

$$\lambda \frac{\partial T}{\partial n} + \kappa(T^4 - T_{amb}^2) = 0 \tag{3.85}$$

Where

κ	=	The product of the Stefan Boltzmann constant by the material emissivity coefficient
$\partial T/\partial n$	=	The normal derivative of T on the boundary of the work-piece
T_{amb}	=	The ambient temperature

One can also consider an empirical conversion law, replacing equation 3.85 by the condition

$$\lambda \frac{\partial T}{\partial n} + \kappa(T^4 - T_{amb}^4) + \zeta(T - T_{amb}) = 0 \tag{3.86}$$

Where

ζ	=	Proportionality coefficient

The complete model consists in coupling the electromagnetic problem equation 3.77-equation 3.83 with the thermal problem equation 3.84, equation 3.85 or equation 3.86, where T depends only on the spatial coordinates r, θ and on the time t.

This model includes two kinds of nonlinearities: the first due to the heat source term in the heat equation 3.81 and the second due to the dependence of physical properties of the non-conducting materials on the temperature and possibly on the magnetic field.

3.5 Depth of Penetration

Penetration Depth is a measure of how deep light or any electromagnetic radiation can penetrate into a material. A number of things can influence penetration depth, including properties of the material itself, the intensity and frequency of the radiation, and various environmental factors. It has been defined as the depth at which the intensity of the radiation inside the material falls to 1/e (about 37%) of its original value at (or more properly, just beneath) the surface.

When electromagnetic radiation is incident on the surface of a material, it may be (partly) reflected from that surface and there will be a field containing energy transmitted into the material. This electromagnetic field interacts with the atoms and electrons inside the material. Depending on the nature of the material, the electromagnetic field might travel very far into the material, or may die out very quickly. For a given material, penetration depth will generally be a function of wavelength. The depth of penetration, δ, is defined as the depth, which has been attenuated to $\frac{1}{e}$ or approximately 37% of the original value.

The amplitude of the wave decreases by a factor $e^{-\alpha x}$, where α is attenuation constant, it is apparent that a distance x which makes $\alpha x = 1$, the amplitude is only $\frac{1}{e}$ times its value at $x = 0$. This distance is equal to δ, the depth of penetration,

$\alpha x = 1$ or $\alpha\delta = 1$, $\delta = \frac{1}{\alpha}$

$$\delta = \frac{1}{\alpha} = \frac{1}{\omega\sqrt{\frac{\mu\varepsilon}{2}\left(\sqrt{1+\frac{\sigma^2}{\omega^2\varepsilon^2}}-1\right)}} \tag{3.87}$$

For a conducting material $\frac{\sigma}{\omega\varepsilon} >> 1$, so

$$\delta = \frac{1}{\alpha} = \sqrt{\frac{2}{\omega\mu\sigma}} = \sqrt{\frac{1}{\pi f\mu\sigma}} \tag{3.88}$$

3.6 Wave Reflection and Transmission

When wave propagating in a uniform medium encounters an interface with a different medium, a portion of the wave is reflected from the interface while the remainder of the wave is transmitted. The reflected and transmitted waves can be determined by enforcing the fundamental electromagnetic field boundary conditions at the media interface.

Given a z-directed, x-polarized uniform plane wave incident on a planar media interface located on the x-y plane, the phaser fields associated with the incident, reflected and transmitted fields may be written as:

Incident wave fields

$$E_x^i = E_{x0}e^{-\gamma z}$$
$$H_y^i = \frac{E_{x0}e^{-\gamma z}}{\eta_1} \tag{3.89}$$

Reflected wave fields

$$E_x^r = \Gamma E_{x0}e^{-\gamma z}$$
$$H_y^r = \Gamma\frac{E_{x0}e^{-\gamma z}}{\eta_1} \tag{3.90}$$

Transmitted wave fields

$$E_x^t = \Upsilon E_{x0}e^{-\gamma z}$$
$$H_y^t = \Upsilon\frac{E_{x0}e^{-\gamma z}}{\eta_2} \tag{3.91}$$

Where

Γ = Reflection coefficient
Υ = Transmission coefficient
η_1 = Reflected intrinsic impedance
η_2 = Transmission intrinsic impedance

Enforcement of the boundary conditions (continuous tangential electric field and continuous tangential magnetic field) yields

$E_x^i + E_x^r + E_x^t$ at $z = 0 \rightarrow 1 + \Gamma = \Upsilon$

$H_x^i + H_x^r + H_x^t$ at $z = 0 \rightarrow \frac{1-\Gamma}{\eta_1} = \frac{\Upsilon}{\eta_2}$

Solving these two equations for the reflection and transmission coefficients gives

Reflection coefficients $\Gamma = \frac{\eta_2-\eta_1}{\eta_2+\eta_1}$

Transmission coefficient $\Upsilon = \frac{2\eta_2}{\eta_2+\eta_1}$

The different condition of intrinsic impedance has been represented as per material characteristics shown in Table 3.1.

Table 3.1: Effects of Intrinsic Impedance

Case	Intrinsic impedance	Reflection Coefficient	Transmission Coefficient	Remark
I	$\eta_1 = \eta_2$	$\Gamma = 0$	$\Upsilon = 1$	Total transmission, No reflection
II	$\eta_1 = 0$	$\Gamma = 1$	$\Upsilon = 2$	Total reflection without inversion of E
III	$\eta_2 = 0$	$\Gamma = -1$	$\Upsilon = 0$	Total reflection with inversion of E
IV	$\eta_2 > \eta_1$	$0 < \Gamma < 1$	$1 < \Upsilon < 2$	
V	$\eta_2 > \eta_1$	$0 < \Gamma < 1$	$0 < \Upsilon < 1$	

Table 3.2: Characteristics of Materials

Sr. No.	Types of Material	Conductivity σ s/m	Permittivity ε F/m	Permeability μ H/m
1	Water	$2X10^{-4}$	80	0.999991
2	Aluminum	$3.54X10^{7}$	1	1.000021
3	Copper	$5.80X10^{7}$	1	0.999991
4	Stainless steel	10^{6}	1	1
5	Lemon / Orange	4	80	1
6	Tomatoes	2.5	80	1

3.7 Operating Parameters

Values of electrical conductivity, permittivity and permeability employed for calculation are presented in Table 3.2 and operating parameters are listed in Table 3.3. The system under consideration includes a right cylindrical conductor for steel and sphere for lemon load in the direction of O_z and O_θ respectively, which are surrounded by a multi turn cylindrical induction coil.

Therefore, it is realistic to assume that the coil is always at room temperature. Assume a total voltage of the coil is $V_{coil} = 200V$ with a frequency of 10 Hz to 1000 K Hz. The driving current density in the IDH coil is calculated by $J_0 = \sigma_{co} V_{coil}/(2\pi R_{co} N)$,

Where
V_{coil} = Total voltage of the coil
R_{co} = The mean value of the coil radius
N = The number of coil turns

For the magnetic permeability (μ), assume that it is everywhere the constant value of free space $\mu = \mu_r \mu_0 \simeq \mu_0$ (i.e. $\mu_r \simeq 1$).

Table 3.3: Operating Parameters

Sr. No.	Description (Units in mm)	Symbol	Value For steel	Value For lemon
1	Work-piece radius	r_w	55	35
2	Work-piece height	h_w	40	-
3	Coil inner radius	r_{co}	85	85
4	Coil width	L_{co}	20	20
5	Coil wall thickness	l_{co}	5	5
6	Height of coil turns	h_{co}	40	40
7	Distance between coil turn	d_{co}	2.5	2.5

Where

μ_r = The relative magnetic permeability

The quantity $\delta_w = (2/\mu_w\sigma_w\omega)^{1/2}$ has the dimension of length and is called the skin depth (or penetration depth). It is a measure of the field penetration depth into the materials. In our calculation the corresponding skin depth of the steel and lemon work-pieces are $\delta_w = 2.5mm$ and $\delta_w = 1.5mm$ respectively.

It should be mentioned here that since IDH is a very complicated process, one can not expect accurate simulation of the whole chain of coupled phenomena - electromagnetic, thermal, mechanical, hydrodynamic and metallurgical - during a heating process. The most important and controllable process is electromagnetic which is analyzed here.

3.8 Numerical Solution

The standard finite element method has been adopted for the discrimination of equation 3.53, equation 3.54, equation 3.77 and equation 3.78. Finite differences in time and standard finite elements in space have been used to solve the heat equation. The mesh used for the thermal problem is same as the part of the mesh used for the electromagnetic problem inside the materials. It is worth noticing that the skin effect requires a particularly refined mesh close to the boundary of the materials. On the other hand, coarse mesh size would result an inaccurate solution of heat equation. Therefore, a reasonable compromise has to be found.

The electromagnetic problem is solve by stationary time, while the heat equation gives

rise to an evaluative problem. Due to the different time scale of the two phenomena, it is assume that the solution of the electromagnetic problem is valid on a time interval and the physical properties of the work-pieces do not change much, due to the increases in temperature resulting from the Joule / Rubbing effect. Then these results are used to compute the source term to be plugged into the heat equation. The evaluative heat equations have been solved using finite difference on the same time interval. The new values of the temperature field thus obtained have been used to update the values of the physical coefficient of the work-pieces. This will allow us to proceed to another computation of magnetic potential, followed by the computations of the temperature field and so on.

A numerical simulation code has been developed based on the above model. It can be dealt with any IDH system having an axis symmetric geometry. Only sinusoidal voltage is allowed, but the restriction on the shape of the voltage does not have a big effect from the energetic point of view. The possibility of having several electric current generators, characterized by different frequency, voltage amplitudes and possibly different phases, has been taken into account.

3.9 Simulation Results

Attenuation constant, phase constant and propagation constant for conducting material (stainless steel) simulation results are shown in Figure 3.1, Figure 3.2 and Figure 3.3, respectively. Figure 3.4 shows skin depth for conducting material. Velocity of propagation and intrinsic impedance for stainless steel are shown in Figure 3.5 and Figure 3.6, respectively. The velocity of propagation and intrinsic impedance for conducting material is small and a reactive component with impedance angle of 45^0 determined from equation 3.44 and simulation shown in Figure 3.7. Figure 3.8, Figure 3.9, Figure 3.10 and Figure 3.11 show simulation of loss tangent, electric field intensity, magnetic field intensity and power density for conducting material, respectively.

Attenuation constant, phase constant and propagation constant for non-conducting material (lemon/orange) simulation results are shown in Figure 3.12, Figure 3.13 and Figure 3.14, respectively. Figure 3.15 shows skin depth for non-conducting material. Velocity of propagation and intrinsic impedance for lemon/orange are shown in Figure 3.16

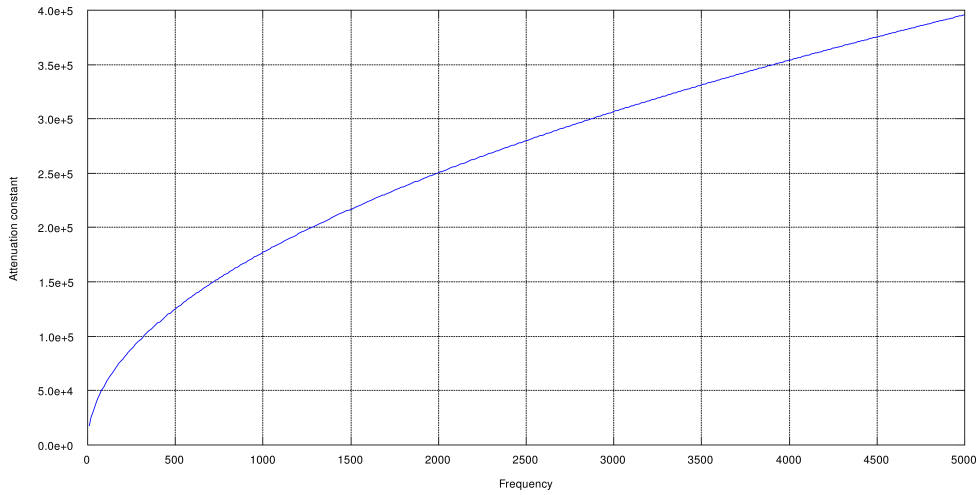

Figure 3.1: Attenuation Constant for Stainless Steel

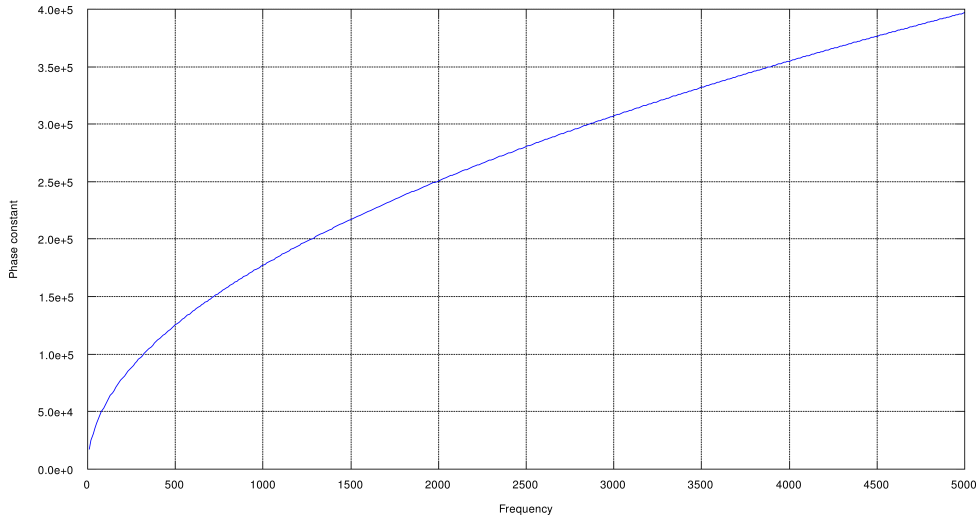

Figure 3.2: Phase Constant for Stainless Steel

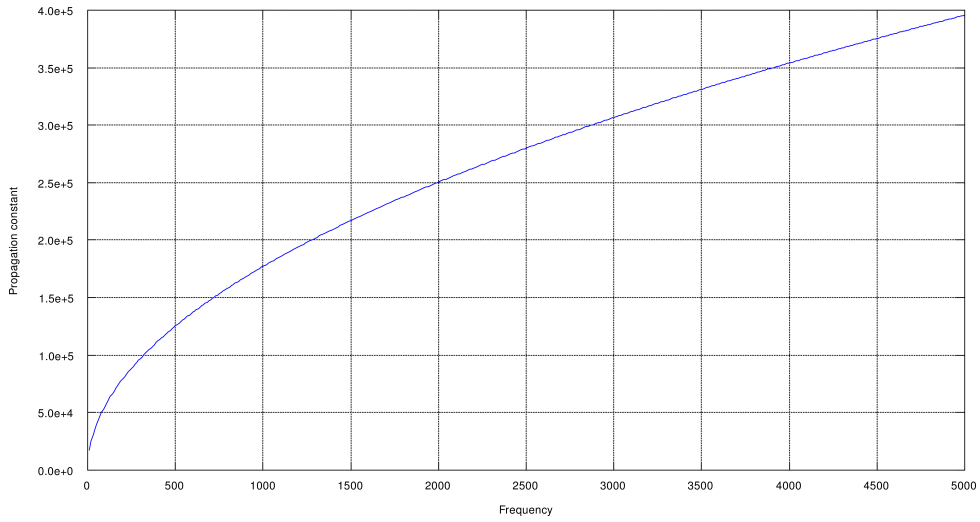

Figure 3.3: Propagation Constant for Stainless Steel

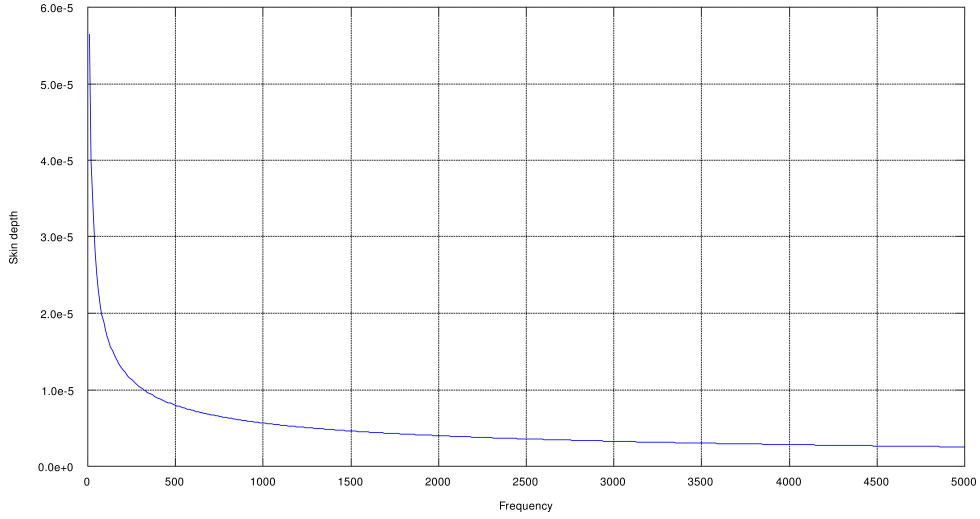

Figure 3.4: Skin Depth for Stainless Steel

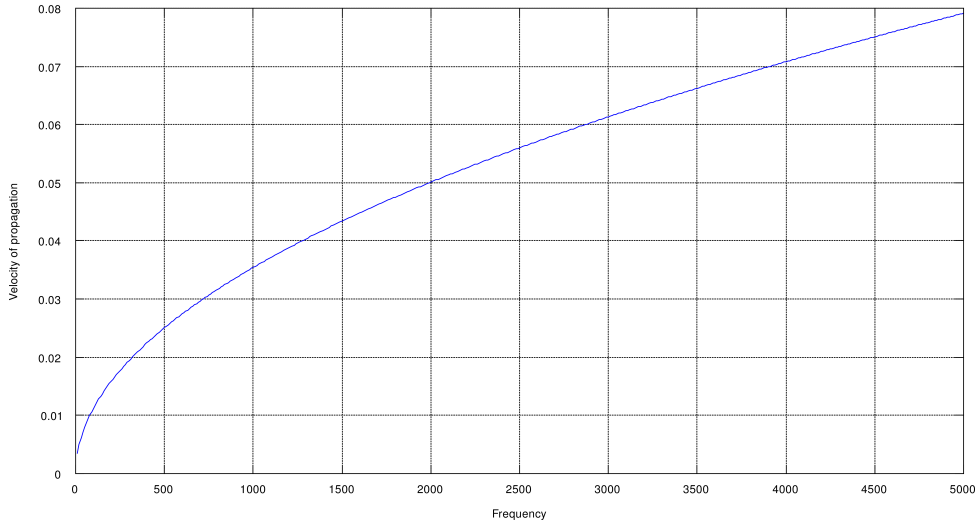

Figure 3.5: Velocity of Propagation for Stainless Steel

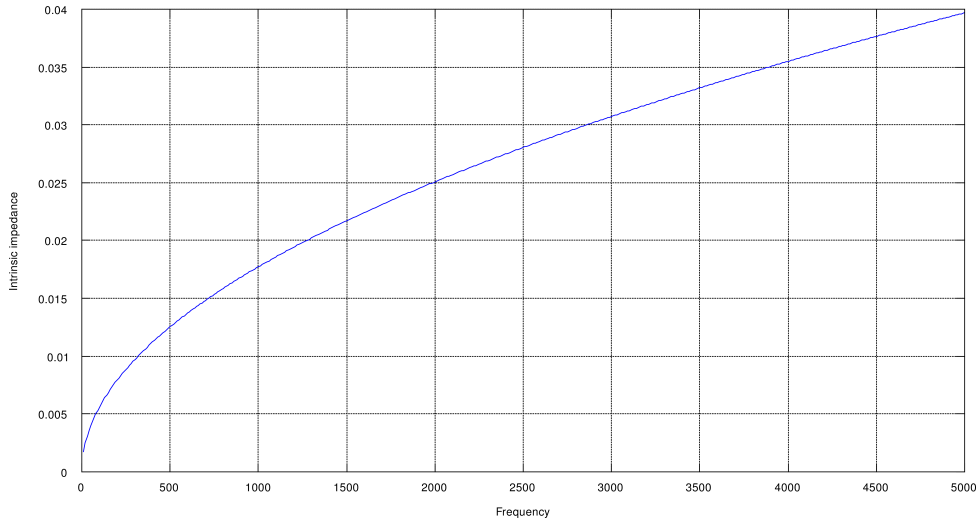

Figure 3.6: Intrinsic Impedance for Stainless Steel

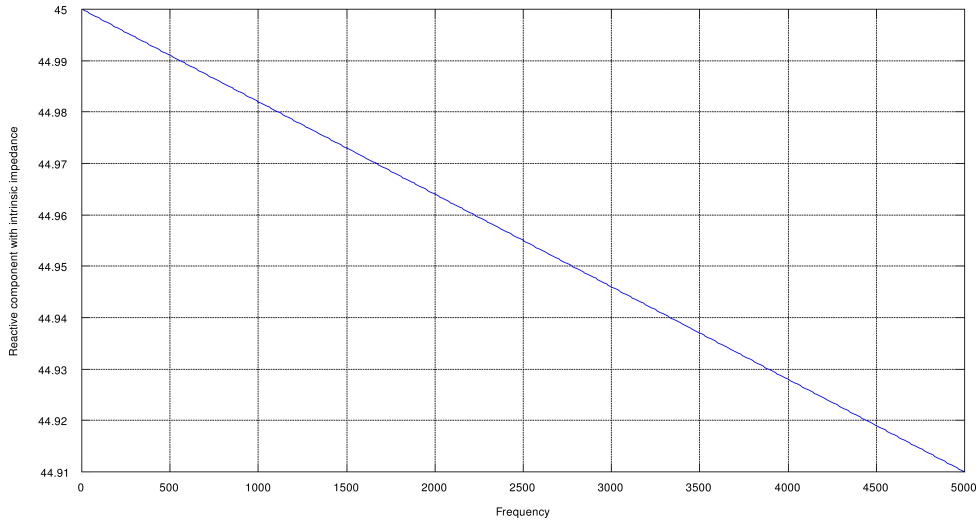

Figure 3.7: Reactive Component With Intrinsic Impedance for Stainless Steel

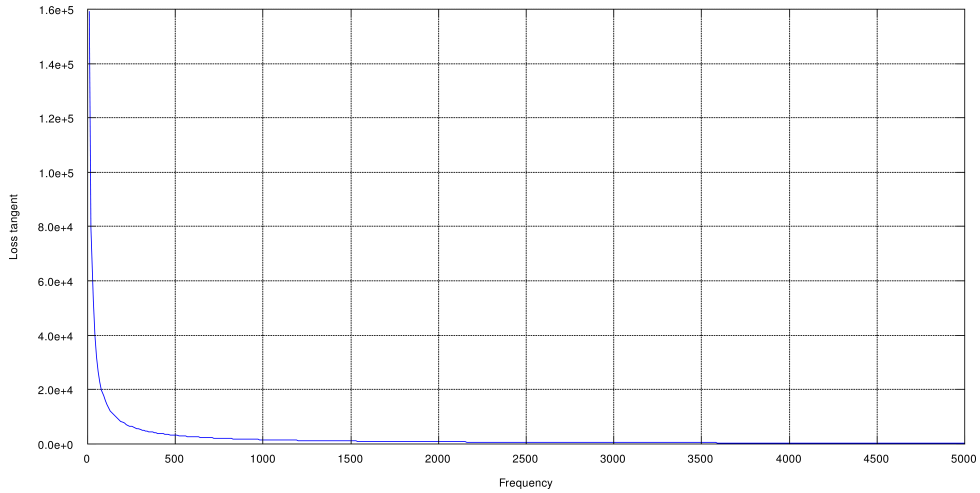

Figure 3.8: Loss Tangent for Stainless Steel

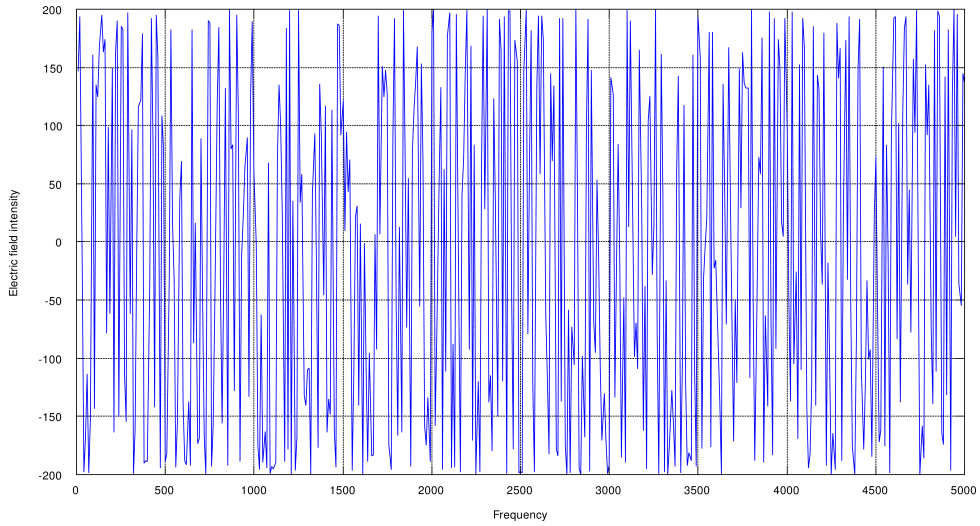

Figure 3.9: Electric Field Intensity for Stainless Steel

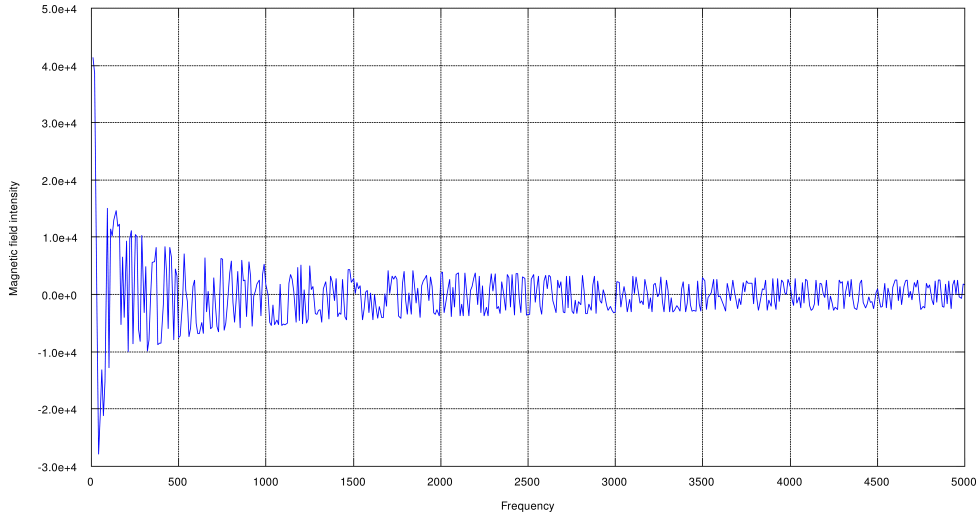

Figure 3.10: Magnetic Field Intensity for Stainless Steel

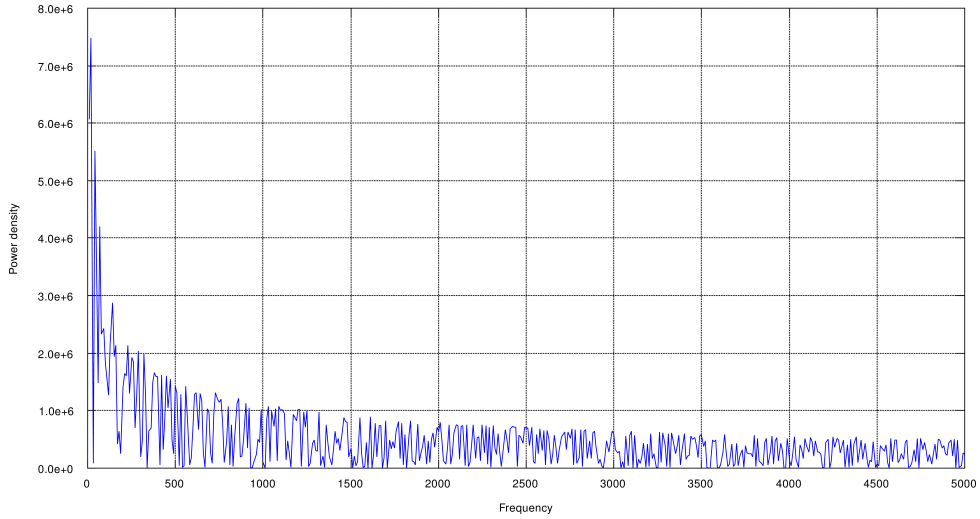

Figure 3.11: Power Density for Stainless Steel

and Figure 3.17, respectively. The velocity of propagation and intrinsic impedance for non-conducting material is remaining constant and a small reactive component with intrinsic impedance determined from equation 3.68 and simulation shown in Figure 3.18. Figure 3.19, Figure 3.20, Figure 3.21 and Figure 3.22 show simulation of loss tangent, electric field intensity, magnetic field intensity and power density for non-conducting material, respectively.

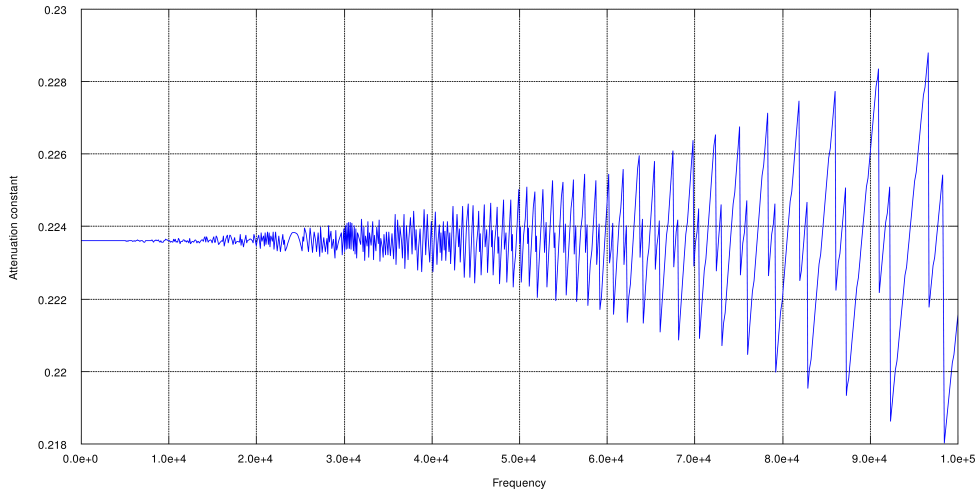

Figure 3.12: Attenuation Constant for Lemon / Orange

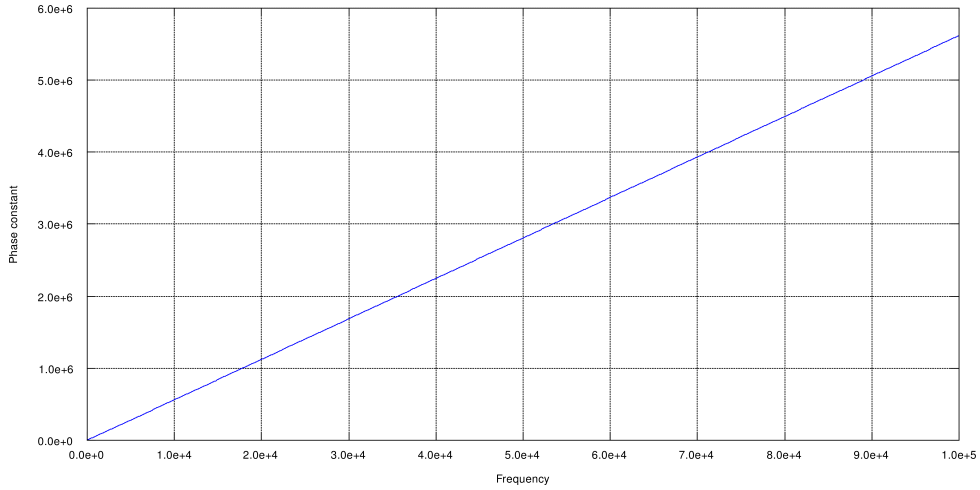

Figure 3.13: Phase Constant for Lemon / Orange

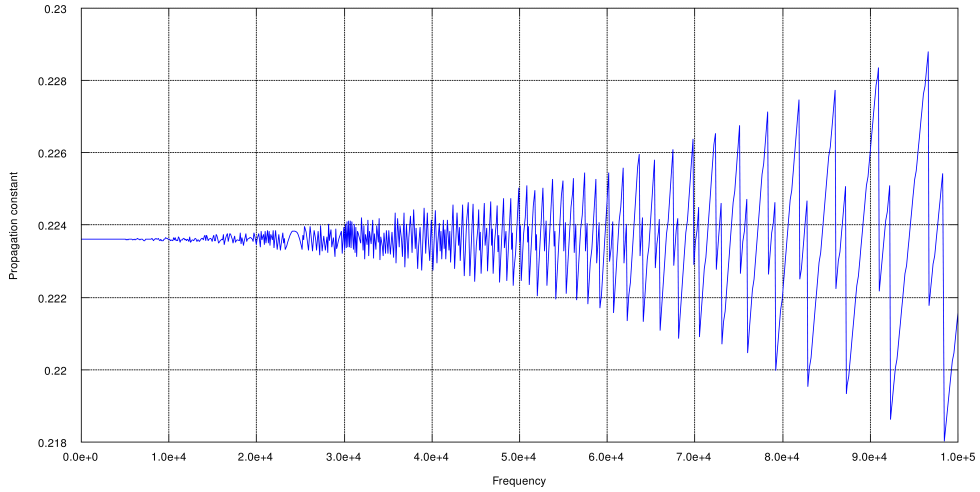

Figure 3.14: Propagation Constant for Lemon / Orange

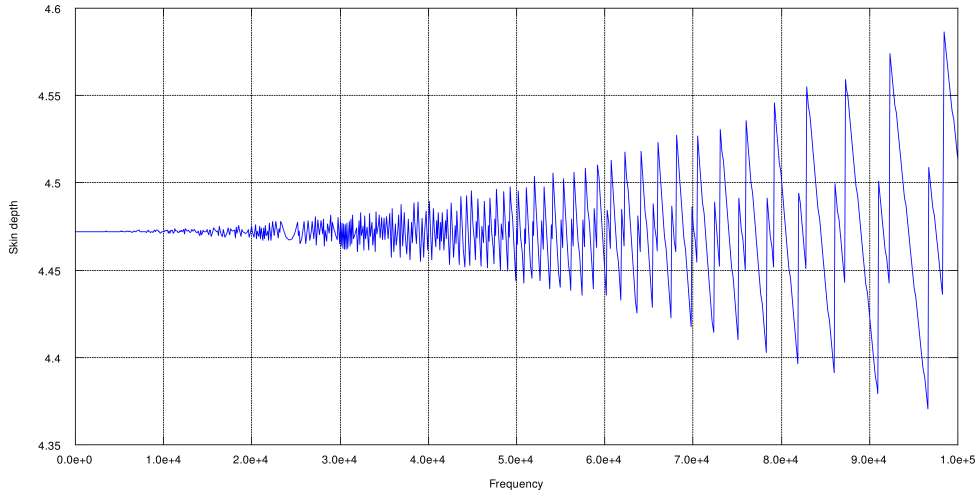

Figure 3.15: Skin Depth for Lemon / Orange

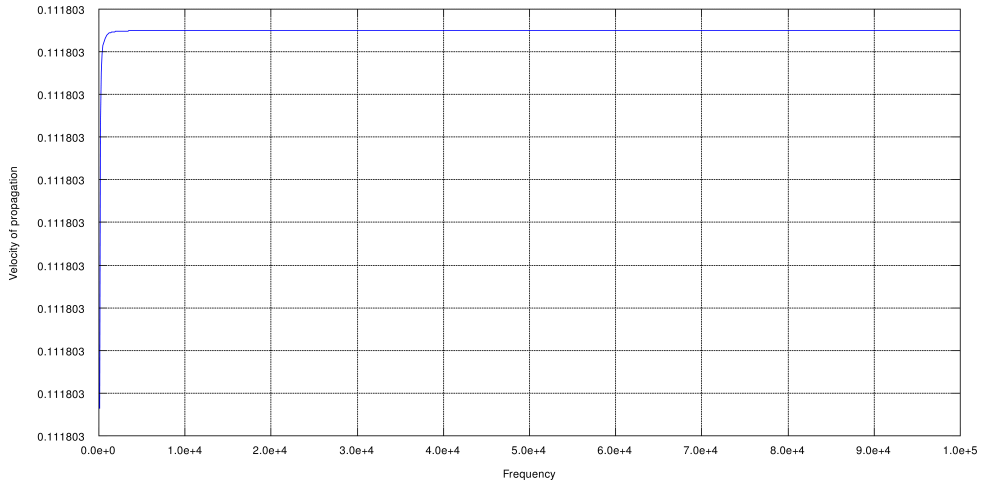

Figure 3.16: Velocity of Propagation for Lemon / Orange

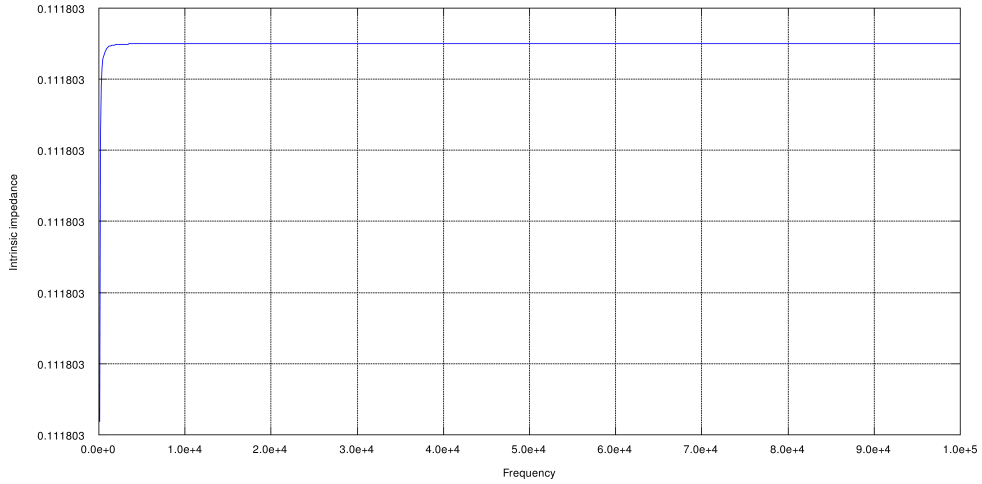

Figure 3.17: Intrinsic Impedance for Lemon / Orange

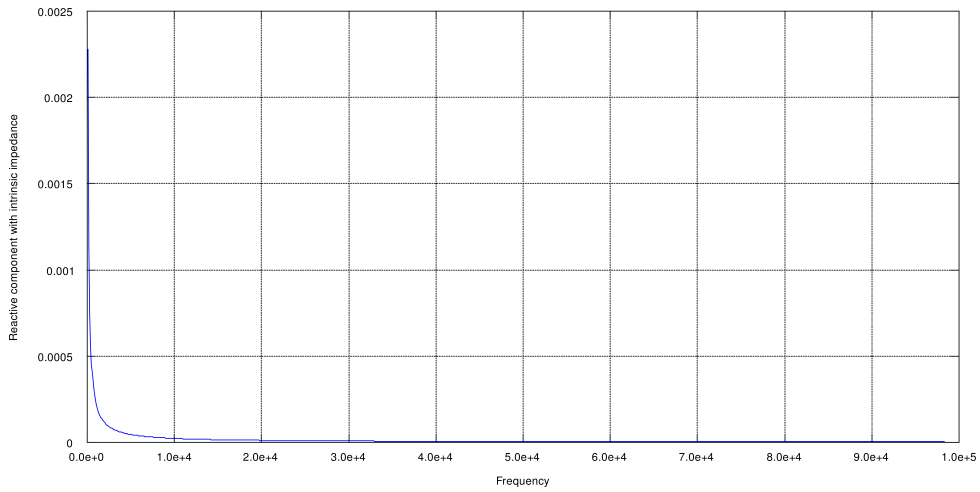

Figure 3.18: Reactive Component With Intrinsic Impedance for Lemon / Orange

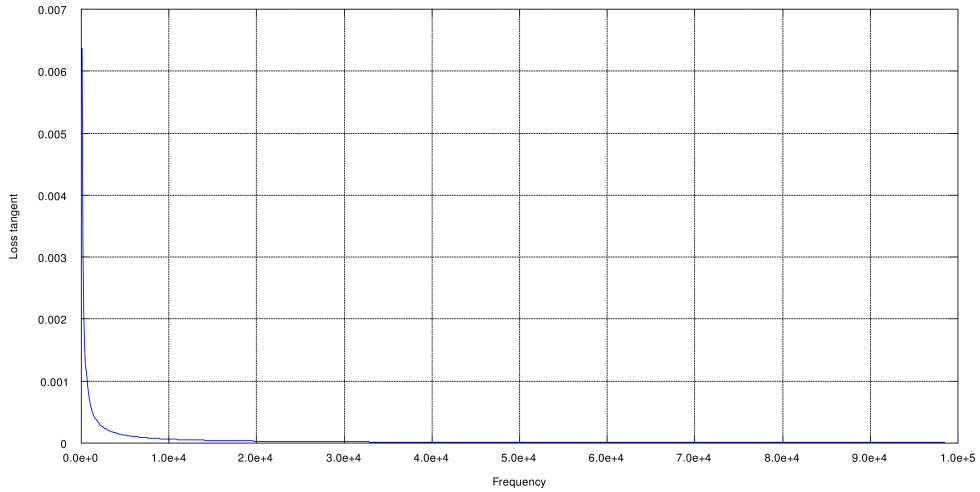

Figure 3.19: Loss Tangent for Lemon / Orange

The finite element mesh analysis is shown in Figure 3.23 for non-conducting material (lemon). Figure 3.24, Figure 3.25, and Figure 3.26 show different temperature analysis, Skin depth analysis using finite element method (FEM), respectively. The displacement current are shown in Figure 3.27 and Figure 3.28 for non-conducting material at different frequency using FEM. Figure 3.29, Figure 3.30, Figure 3.31, and Figure 3.32 show magnetic field density and magnetic field intensity for lemon at different frequency using FEM, respectively.

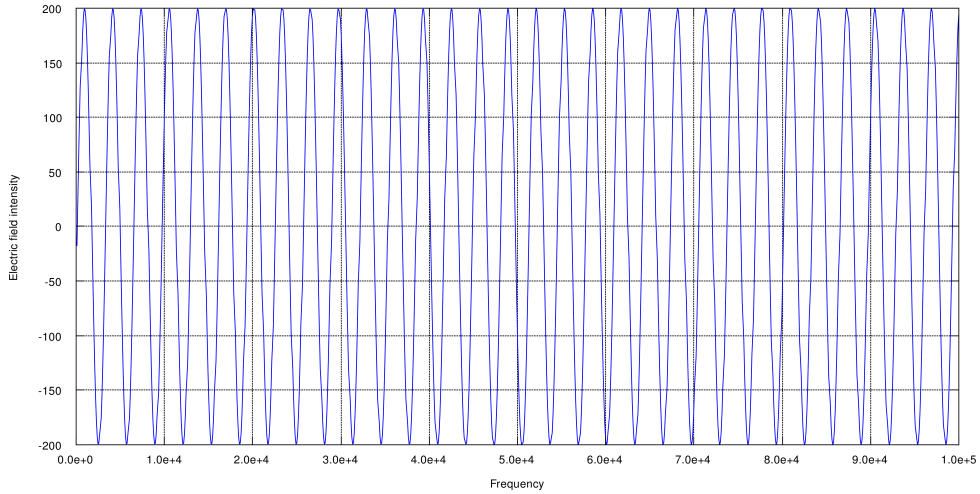

Figure 3.20: Electric Field Intensity for Lemon / Orange

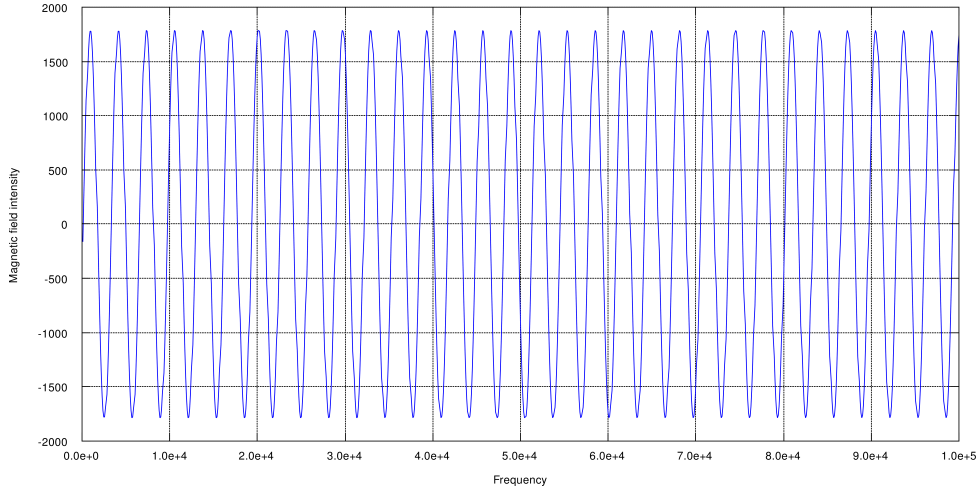

Figure 3.21: Magnetic Field Intensity for Lemon / Orange

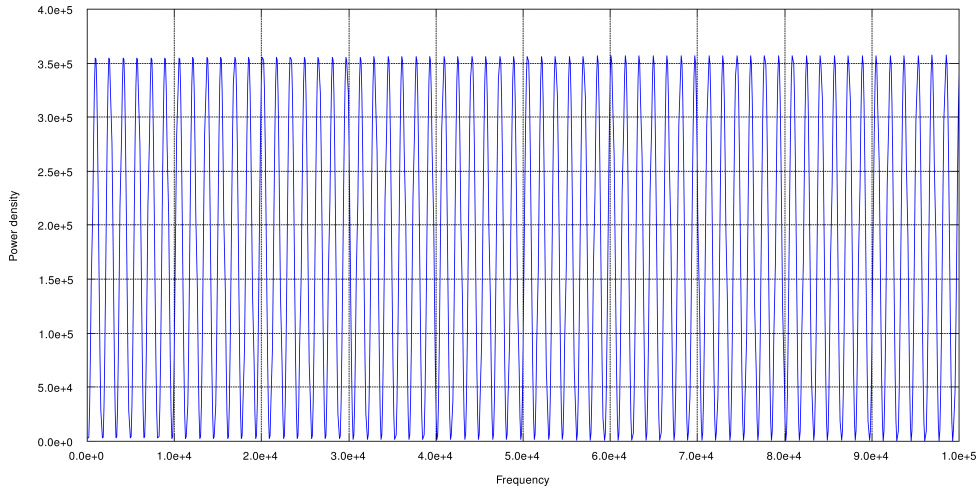

Figure 3.22: Power Density for Lemon / Orange

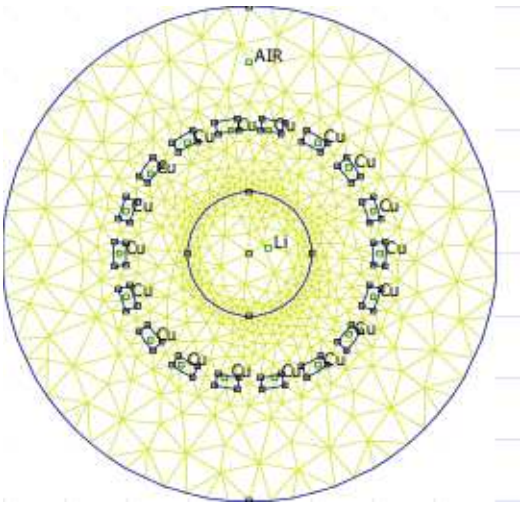

Figure 3.23: Mesh Analysis for Lemon

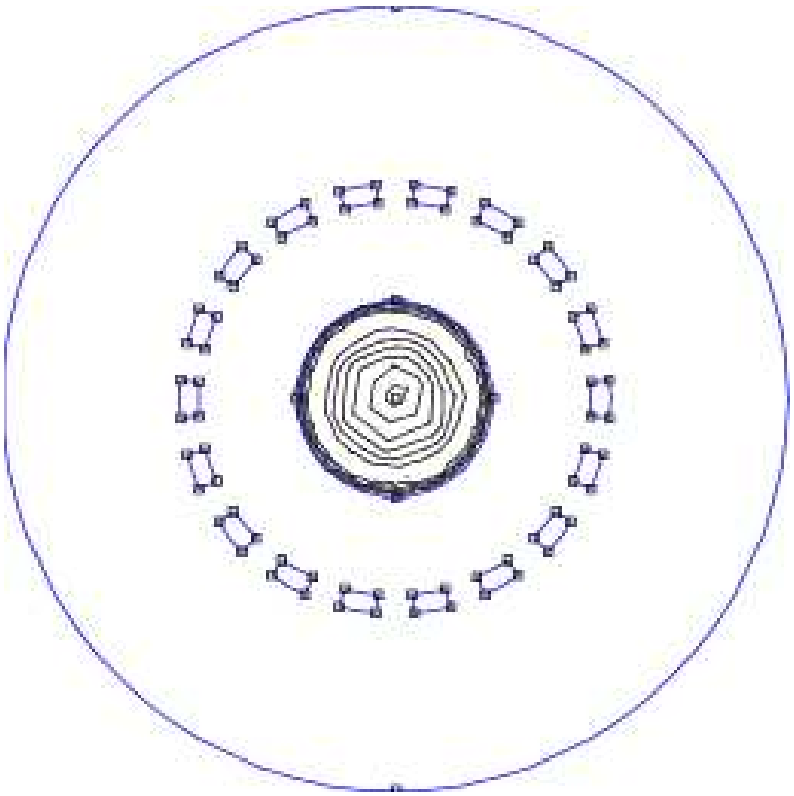

Figure 3.24: Temperature Analysis Using FEM

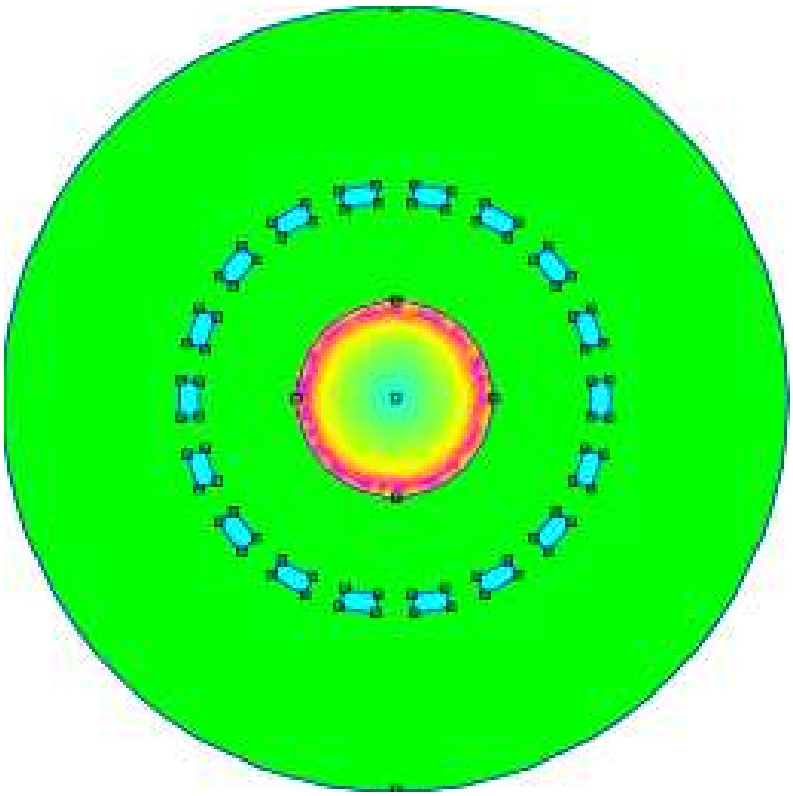

Figure 3.25: Skin Depth Analysis Using FEM

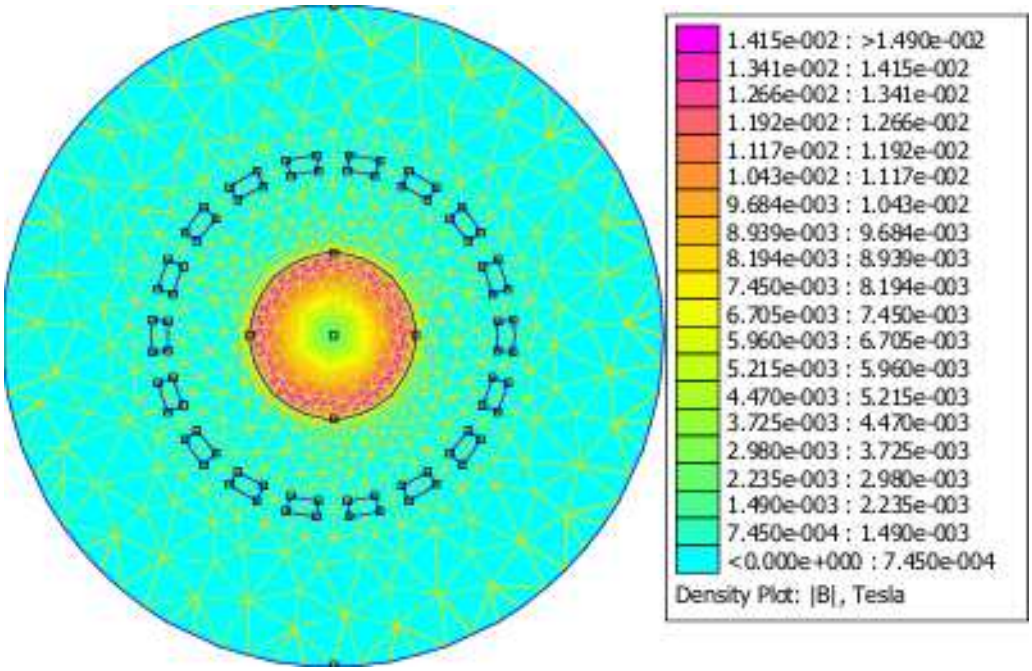

Figure 3.26: Temperature and Skin Depth Analysis With Density Using FEM for Lemon

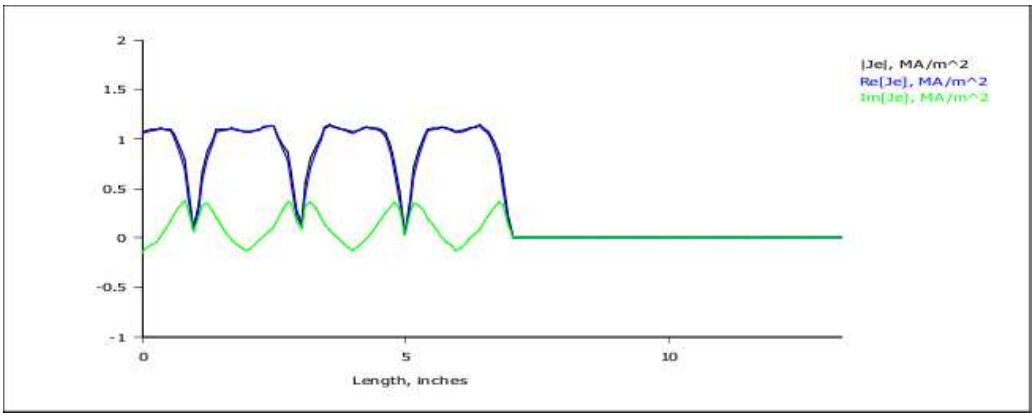

Figure 3.27: Displacement Current for Lemon Using FEM at 10 MHz

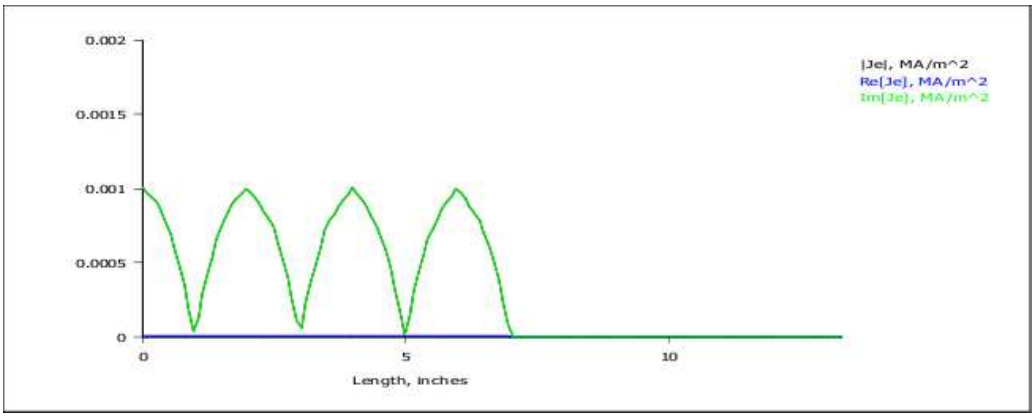

Figure 3.28: Displacement Current for Lemon Using FEM at 1KHz

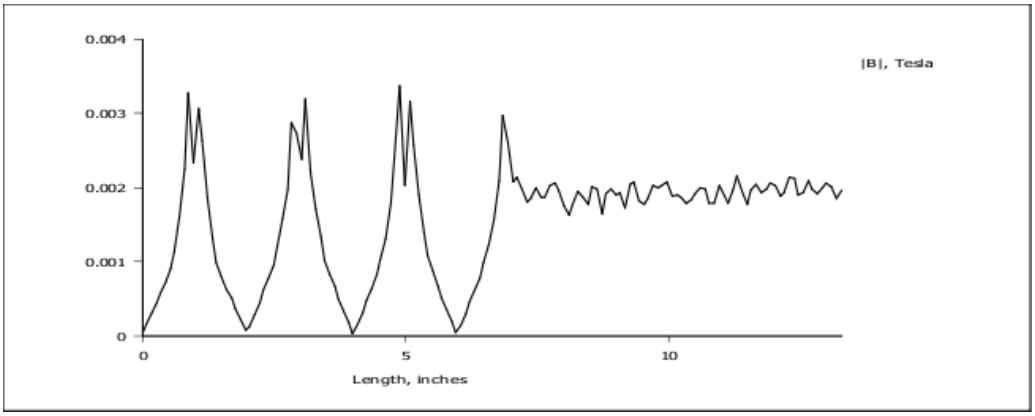

Figure 3.29: Magnetic Field Density for Lemon Using FEM at 10MHZ

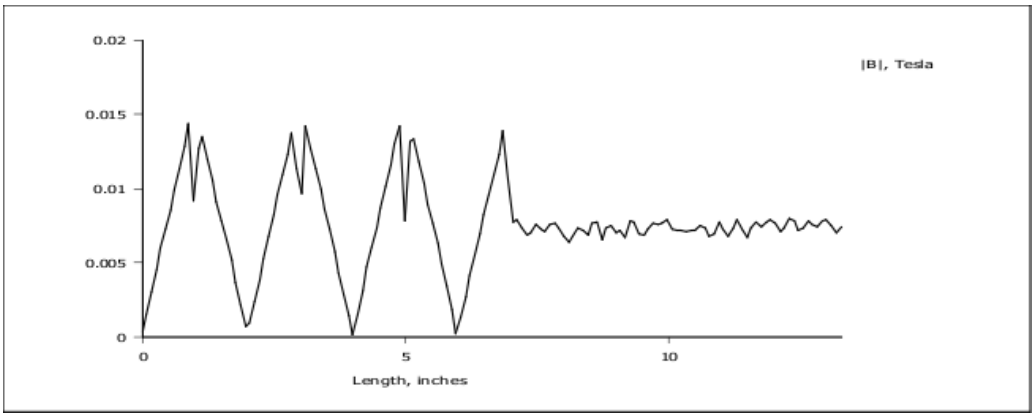

Figure 3.30: Magnetic Field Density for Lemon Using FEM at 1KHz

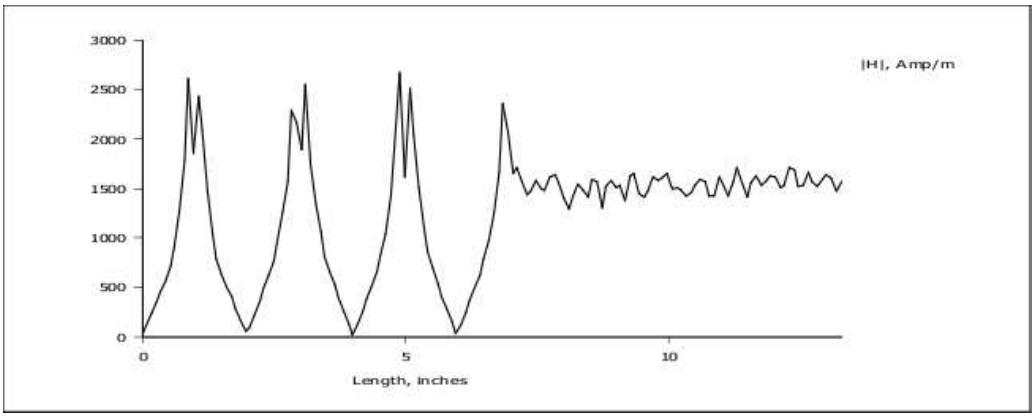

Figure 3.31: Magnetic Field Intensity for Lemon Using FEM at 10MHz

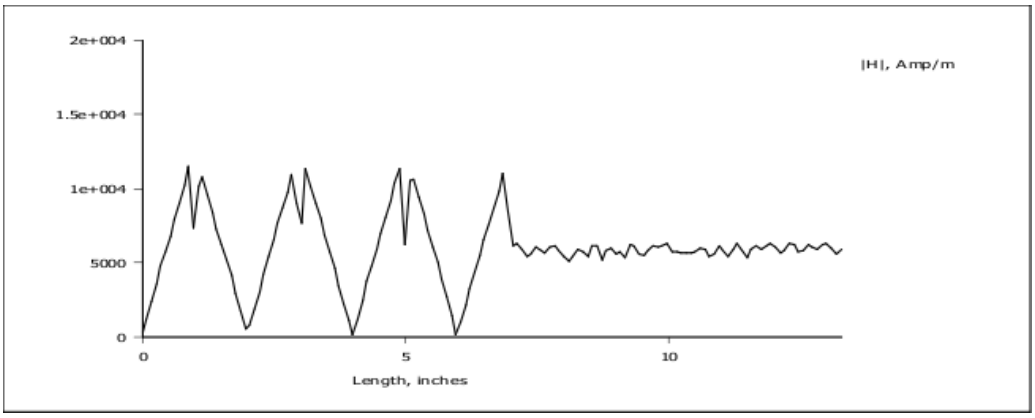

Figure 3.32: Magnetic Field Intensity for Lemon Using FEM at 1KHz

3.10 Conclusions

A mathematical model for obtaining a reflection coefficient, transmission coefficient and electromagnetic wave properties for the work-piece contribution to the impedance of a given IDH system has been derived. This is intended to asses how work-piece is linked to the excitation loop, thus in order to find out conditions where the eddy current or displacement current occurrence is enhanced. Empirical rules already known by IDH practitioners have been proved and the finding can be extrapolated to design new possibilities. The proposed approach has been validated using MATLAB and FEM software.

The main finding of this chapter reveals following:

1. As frequency increases, the current becomes concentrated along the outer surface of the object.

2. The electromagnetic shield may be necessary to prevent waves from radiating out of the shielded volume or to prevent waves from penetrating into the shielded volume.

3. Attenuation constant, phase constant and propagation constant increases with increase in frequency in conducting material and non-conducting material.

4. Intrinsic impedance increases with increase in frequency in conducting material and is remaining constant with increase in frequency for non-conducting material.

5. Velocity of propagation and intrinsic impedance of conducting material exponentially increases with increase in frequency and reactive component of conducting material remains constant at 45^0.

6. Velocity of propagation and intrinsic impedance of non-conducting material remains constant with increase in frequency and reactive component of non-conducting material is small.

Chapter 4

SIMULATION RESULTS FOR THE IDH

4.1 Introduction

The principle of induction dielectric heating (IDH) has been used in various applications such as brazing, surface hardening, forging, annealing, melting, drying and dehydration for food etc. Each application has different appropriate frequency required. In food application frequency depends on work-pieces geometry and skin depth requirement [13], [60]. A large number of topologies have been developed. Among them, current-fed and voltage-fed inverters are most commonly used [37]. The advantages of current fed inverter are short-circuiting protection capability and superior no-load performance because of its current-limiting DC link characteristic. Voltage-fed or Current-fed inverter for IDH applications have employed many switches such as Thyristors, GTO's, Bipolar power transistor, IGBT's, MCT's, MOSFET's, SIT. Also in recent year, MOSFET are used in induction heating system, which has the advantage of low conduction loss, high speed switching time and very little gate drive power.

When a work-piece is inserted into an induction coil, variation of induction heating load parameters can affect resonant frequency, resulting in reduction of load power. Therefore, it is necessary to track operating frequency in order to obtain high power factor.

This chapter describes the three phase MOSFET based inverter for dehydration of food (lemon) application. The operating frequency has been adjusted by the micro controller to maintain constant leading phase angle when parameters of IDH load are varied. The

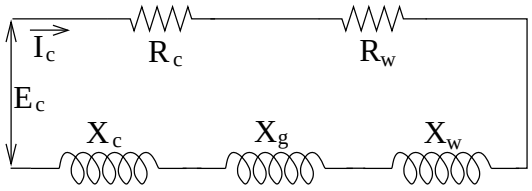

Figure 4.1: The Equivalent Circuit of Induction Coil and Work-piece

output power can be controlled by input setting. The load voltage is controlled to protect the MOSFETs.

4.2 Principle of Induction Dielectric Heating

The IDH method is one of most suitable methods for such heating due to the non-contact between the induction coil and the work-pieces. It is heated by being placed inside the magnetic field, induced in the coil when energized, causes eddy currents in the work-pieces and increases the heating effect. An equivalent circuit of the induction coil and work-piece is shown in Figure 4.1.

$$\text{Work resistance, } R_w = K(\mu_r p A_w) \text{ ohms} \tag{4.1}$$

$$\text{Coil resistance, } R_c = K\left(\frac{k_r \pi d_c \delta_c}{2}\right) \text{ ohms} \tag{4.2}$$

$$\text{Gap reactance, } X_g = K(A_g) \text{ ohms} \tag{4.3}$$

$$\text{Work reactance, } X_w = K(A_r q A_w) \text{ ohms} \tag{4.4}$$

$$\text{Coil reactance, } X_c = K\left(\frac{k_r \pi d_c \delta_c}{2}\right) \text{ ohms} \tag{4.5}$$

$$K = 2\pi f \mu_0 [\frac{N_c^2}{l_c}] \text{ Ohms per square meter} \tag{4.6}$$

Where

μ_r	=	The relative magnetic permeability
A_w	=	The cross section are of work-piece
A_g	=	The area of gap
k_r	=	The coil correction factor that ranging from 1-1.5
N_c	=	The number of turns of induction coil
l_c	=	The length of gap
δ_c	=	The resistivity of copper
d_c	=	The diameters of induction coil
		(p and q are function for a solid cylinder)

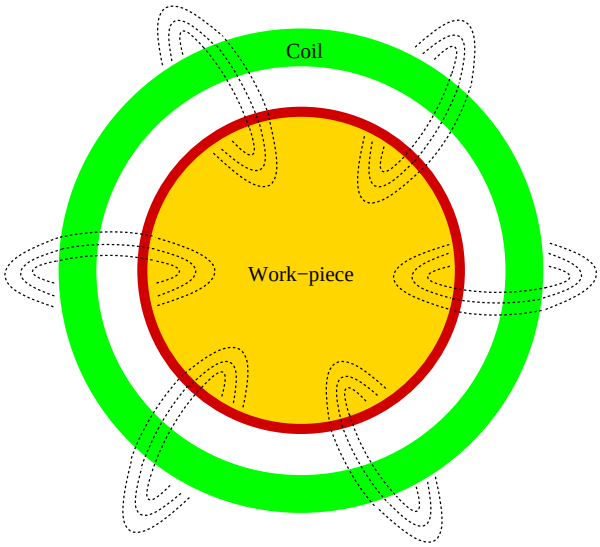

Figure 4.2: Practical Representations of IDH Coil

As shown in Figure 4.1 and from above equations, it can be seen that the parameters of induction heating load (induction coil and work-piece) depend on several variables including the shape of the heating coil, the space between the work-piece and coil, their electrical conductivities and magnetic permeability and the frequency [13], [60].

4.3 System Considerations

This section describes the load impedance characterization of an induction dielectric heating. This impedance model is needed for suitable power supply design. Finally the basic operating limitations of a load, three phase inverter are briefly reviewed [47], [58], [75], [79], [85], [89], [96], [107], [111], [113].

4.3.1 Considerations of coil design

A block diagram of an IDH coil and equivalent circuit modelled are shown in Figure 4.2 and Figure 4.3, respectively. The heating coil is modelled as a transformer with a single turn secondary winding. The equivalent model can be represented in a simplified form by an equivalent induction and resistance. The circuit represented in Figure 4.3 can also be characterized by a dimensionless parameter called the quality factor 'Q' of the coil.

The core rating is generated based on data about the frequency, resistivity, magnetic

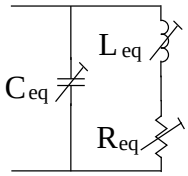

Figure 4.3: Equivalent Electric Circuit Model of IDH Coil

permeability, coil dimensions, coil resistivity and an acceptable lower and upper bound on the number of volts per turn. On the other hand power rating is governed by the heating rate requirement and any additional primary coil losses. The choice for operating frequency is based upon the form in which the solid material enters the pot, the electromagnetic properties of the material and the conducting or non-conducing material. These aforementioned items taken together are often used to identify skin depth of the material. This term corresponds to an effective distance from the surface where induced currents will flow.

Heat will be generated in work-piece and will be partially conducted away to the surrounding medium. The generated and conducted heat can either be used to surface heat the material. The effective parameters for the equivalent resistance and inductance will vary throughout the heating cycle. This comes about as a result of the changes in impedance in the material and also changes in the amount of coil flux coupling the material. The change can also be expressed as a variation in the Q of the coil. Electromagnetic type materials exhibit an increase in Q over the duration of the heating cycle. On the other hand non-magnetic metals exhibit small variations in Q over the duration of the heating cycle. The power supply designers' main objective therefore is to determine the maximum range over which the Q of the coil will vary. The maximum Q at the rated coil voltage is then established as the baseline value for purposes of designing the power supply. Secondly, these base values are then used to specify a transformer turns ratio. The purpose of the transformer is to match as closely as possible the coil voltage to the power supply voltage. Maximum power transfer can be achieved if the reactive component of the load is compensated. This can be done using different circuit topologies incorporating capacitors. Capacitors value can be chosen to compensate for the reactive power assuming a fixed value for the reactive component of the load. Under these conditions the transformer can be matched to the power supply. However exact matching is not the case in practice.

This comes about as a result of a change in the equivalent inductance during a heating cycle. The problem is particularly acute for ferrous metals. Initial coupling between the coil and load is good. However the coupling decreases over a period of time as successive layers of the heated material exceed the Curie point. This gradual process corresponds to a slow decrease in the inductance of the load i.e., (order of minutes). Consequently the power transfer will decrease.

4.3.2 Coil specification

The foregoing discussions can conveniently be summarized in the form of the following coil specifications

1. Coil voltage
2. Power rating
3. Operating frequency
4. Range of Q
5. Range of L_{eq}.

The above design data can in many cases be obtained using simple design rules [60] however, for special cases (for example, partially conducting refractoriness, or coils whose length to width ratio is small) it will be necessary to characterize coil impedance, as a function of frequency, using a finite element software package.

Nevertheless, whichever approach is taken, the requirements are subsequently used for purposes of designing the matching transformer and the power supply.

4.3.3 Power supply requirements

AC to DC rectifier topology (1 or 3 phase) and inverter topology commonly used in IDH is shown in Figure 4.4. It is referred to as either a voltage driven power supply or a current driven power supply. This chapter concerns itself primarily with power supplies that operate on the principle of three phase inverter. The load (comprised of an inductance, capacitances and resistance) should at all times be presenting itself as a leading power factor to the source. Hence the capacitor voltage should lag the driving current source

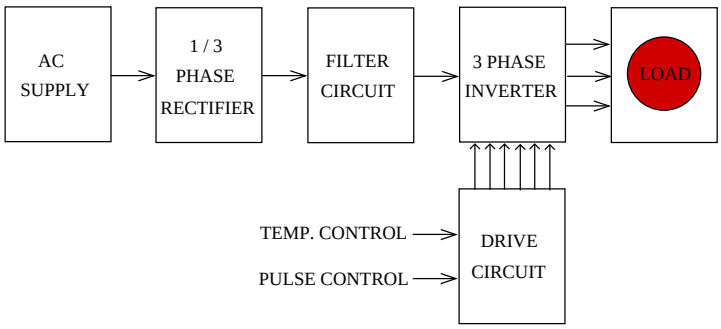

Figure 4.4: Structure of The IDH

inverter. Alternatively the operating frequency should always reside above the resonant frequency of the tuned circuit. Similarly the total current (i_o) for the voltage source driven circuit lead the applied voltage. This is the case if the applied frequency is less than the resonant frequency.

Converters use semiconductor switches such as MOSFET's and IGBT's. The proper operating of the switches requires that a reverse voltage be maintained across the switch, for a minimum interval of time subsequent to the current extinction. This interval is referred to as the turn off time for the device; it is another way of stating a leading power factor load. The power supply control circuit should also guarantee that current and capacitor voltages be maintained within safe operating levels. Finally, the power supply should be able to control and maintain the power applied to the load subject to safe operating conditions. Taken together these operating modes can be summarized as follows.

1. Constant output power operation
2. Capacitor voltage limited operation
3. Load current limited operation
4. Turn off time limited operation
5. Fault operation

4.4 Operation of Proposed Inverter

Figure 4.5 illustrates the power circuit of proposed IDH that employs six switches at primary side of isolating transformer to establish some part of three phase utility voltages on the primary winding. Being the converter supplied by voltage source, the input phases should never be short circuited and owing to presence of inductive loads, the load currents should not be interrupted. With these constrains in 1 phase to 3 phase converter, there are 8 permitted switching combinations, which are shown in Table 4.1

For each combination, the input and output line voltages can be expressed in term of space vectors as

$$v_i = \frac{2}{3}\left(v_{ab} + v_{bc}e^{j2\pi/3} + v_{ca}e^{j4\pi/3}\right) = V_i e^{j\alpha_i} \tag{4.7}$$

$$v_o = \frac{2}{3}\left(v_{AB} + v_{BC}e^{j2\pi/3} + v_{CA}e^{j4\pi/3}\right) = V_o e^{j\alpha_o} \tag{4.8}$$

In the same way, the input and output line currents can be expressed as given below.

$$i_i = \frac{2}{3}\left(i_a + i_b e^{j2\pi/3} + i_c e^{j4\pi/3}\right) = I_i e^{j\beta_i} \tag{4.9}$$

$$i_o = \frac{2}{3}\left(i_A + i_B e^{j2\pi/3} + i_C e^{j4\pi/3}\right) = I_o e^{j\beta_o} \tag{4.10}$$

It may be noted from above equations that the resulting output voltage has been expressed as a function of the input voltages and the resulting input current of primary side has been represented as function of the output currents of secondary side.

As shown in Table 4.1, for the 6 combinations of group I, each output phase is connected to a different input phase. In the 2 combinations of group II, all the output phase is short-circuited.

Each combination of group I determines an output voltage vector having a phase angle α_0 which is dependent on the phase angle α_i of the corresponding input voltage vector. In the same way, the input current vector has phase angle β_i which is related to the phase angle β_0 of the output vector. Hence, in order to apply the SVM technique, these combinations cannot be usefully employed.

Finally, the 2 configurations of group II determine zero output voltage and zero input current vectors.

Duration of non zero intervals, T_{ON}, are given by equation 4.11:

$$t_{ON} = D(kT_s)\frac{T_s}{2} \tag{4.11}$$

Table 4.1: Switching Vectors, Phase Voltages and Output Line to Line Voltage

Voltage Vectors	Switching Vector			Line to Neutral Voltage			Line to line voltage		
	a	b	c	V_{ab}	V_{bc}	V_{ca}	V_{ab}	V_{bc}	V_{ca}
Group I									
V_1	1	0	0	2/3	-1/3	-1/3	1	0	-1
V_2	1	1	0	1/3	1/3	-2/3	0	1	-1
V_3	0	1	0	-1/3	2/3	-1/3	-1	1	0
V_4	0	1	1	-2/3	1/3	1/3	-1	0	1
V_5	0	0	1	-1/3	-1/3	2/3	0	-1	1
V_6	1	0	1	1/3	-2/3	1/3	1	-1	0
Group II									
V_0	0	0	0	0	0	0	0	0	0
V_7	1	1	1	0	0	0	0	0	0

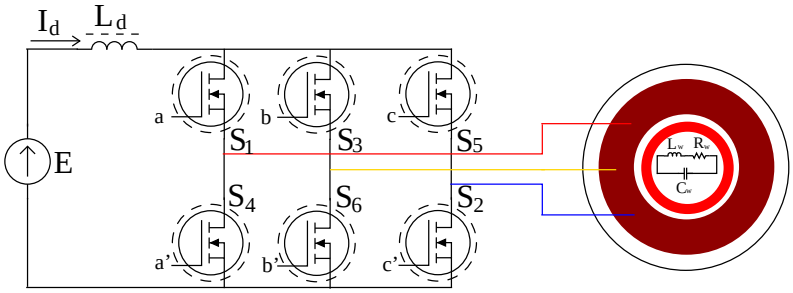

Figure 4.5: Three Phase Inverter for IDH

$$D(kT_s) = \frac{V_{ref}}{v_{\max}(kT_s)} \tag{4.12}$$

Where

T_s = Switching period

D = Duty cycle

V_{ref} = Reference adjusting voltage

Secondary side of isolation transformer is coupled to parallel resonance tank circuit through matching (or filter) coil L_C.

4.5 Analysis of Three Phase Inverter

The three phase inverter is shown in Figure 4.5. Its analysis is based on the following assumptions:

1. The quality factor of three phase inverter load $Q = \omega L_w/R_w$ is larger than 2.5 (high Q load).

2. The inverter circuit inductance ratio factor $(L_d/L_w) > 10$.

3. The three phase inverter switches are ideal.

4. The internal resistance of the three phase inverter DC source is negligible.

The transient behaviour of the IDH circuit represented by the following Laplace transformer equations:

$$\begin{aligned} sL_dI_d(s) + (-1)^{n-1}U_c(s) &= \frac{E}{s} + L_di(0) \\ -U_c(s) + (R_w + sL_w)I(s) &= Li(0) \\ -(-1)^{n-1}I_d(s) + C_wsU_c(s) + I(s) &= C_wu_c(0) \end{aligned} \tag{4.13}$$

Where

$I_d(s)$ = The Laplace transforms of the three phase inverter input current $i_d(t)$
$I(s)$ = Load current $i(t)$
$U_c(s)$ = Voltage $u_c(t)$

With their initial values $i_d(0)$, $i(0)$, $u_c(0)$ and $(-1)^{n-1}$ is a sign changing factor, reflecting to the three phase inverter switching, where n is a number of half periods counting from inverter starting instant $(n_{st} = 1)$

The solution of the IDH system equation 4.13 is

$$I_d(s) = \frac{1}{sL_dL_wC_wM(s)}[(C_wL_ws^2 + C_wR_ws + 1)E + A_{I_d}] \tag{4.14}$$

$$U_c(s) = \frac{(-1)^{n-1}(R_w + L_ws)}{sL_dL_wC_wM(s)}(E - A_{u_c}) \tag{4.15}$$

$$I(s) = \frac{(-1)^{n-1}}{sL_dL_wC_wM(s)}(E + A_I) \tag{4.16}$$

Where

$$M(s) = s^3 + \frac{R_w}{L_w}s^2 + \frac{L_d + L_w}{L_dL_wC_w}s + \frac{R_w}{L_dL_wC_w} \tag{4.17}$$

and A_{I_d}, A_I and A_{u_c} are the corresponding initial condition polynomials:

$$\begin{aligned} A_{I_d} &= (L_d L_w C_w s^3 + L_d R_w C_w s^2 + L_d s) i_d(0) \\ &\quad - (-1)^{n-1}(L_w C_w s^2 + R_w C_w s) u_c(0) + (-1)^{n-1} s L_w i(0) \end{aligned} \tag{4.18}$$

$$A_I = L_d s i_d(0) + (-1)^{n-1} L_d C_w s^2 u_c(0) + (-1)^{n-1}(L_d L_w C_w s^3 + L_w s) i(0) \tag{4.19}$$

$$A_{U_c} = -L_d s i_d(0) - (-1)^{n-1} L_d C_w s^2 u_c(0) + (-1)^{n-1} \frac{L_d L_w s^2}{L_w s + R_w} i(0) \tag{4.20}$$

For the first half period

$$A_{I_d} = A_I = A_{U_c} = 0$$

To obtain the values of $I_d(s)$, $U_c(s)$ and $I(s)$ it is essential ton obtain the roots of equation 4.17. It is preferable to normalize parameters.

The inductance ration factor is defined as:

$$K = \frac{L_d}{L_w} \tag{4.21}$$

a load quality factor and a resonant frequency

$$Q = \frac{\omega_0 L_w}{R_w} \tag{4.22}$$

$$\tag{4.23}$$

Where

$$\omega_0 = \frac{1}{\sqrt{L_w C_w}} \tag{4.24}$$

and a normalized frequency

$$\eta_f = \frac{\omega}{\omega_n} \tag{4.25}$$

Where

ω_n = The natural angular frequency

Power consumption of $10 - 1000kW$ with frequency range of 0.5 to $10MHz$ the range of Q, K and η_f has been provided by equation 4.26.

$$\begin{aligned} 2.5 < Q < 20 \\ 10 < K < 200 \\ 1.01 < \eta_f < 1.1 \end{aligned} \tag{4.26}$$

Therefore, the approximate analytical expressions for three phase inverter currents and voltage $i_d(t)$, $i(t)$ and $u_c(t)$ are obtained for these ranges of parameters.

The characteristic equation as described in equation 4.17 having order more than two needs iterative method is non-linear algebraic equation. According to this method, the third-order equation of the form

$$s^3 + k_1 s^2 + k_2 s + k_3 = 0 \tag{4.27}$$

after separating the real root $s_1 = -a$ may be written as

$$(s + a)[s^2 + (k_1 - a)s + (k_2 - b)] = 0 \tag{4.28}$$

Performing all the operations in equation 4.28 and comparing the coefficients of equal powers of s in equation 4.27 and equation 4.28,

$$b = (k_1 - a)a \tag{4.29}$$

$$a = \frac{k_3}{k_2 - b} \tag{4.30}$$

Thus, from equation 4.29 and equation 4.30 unknowns are a and b. To find them, the iteration method is used. Start with a zero iteration value: $a_0 = 0$, which gives in accordance with equation 4.29 $b_0 = 0$ and then, in accordance with equation 4.30, the first iteration value of a is $a_1 = k_3/k_2$. The next iteration value of b, i.e., b_1 is substituting value into equation 4.29. Hence, the following recurrent formula for the real root a_{j+1} can be employed:

$$a_{j+1} = \frac{k_3}{k_2 - b_3} \tag{4.31}$$

Where

$$b_j = (k_1 - a_j)a_j \tag{4.32}$$

and $j = 0, 1, 2, ...$ is the number of iterations. This iteration process is repeated up to the required accuracy.

Substituting, equation 4.21, equation 4.22 into equation 4.17 yields

$$M(s) = s^3 + \frac{\omega_0}{Q}s^2 + \frac{\omega_0^2(K+1)}{K}s + \frac{\omega_0^3}{KQ} = 0 \tag{4.33}$$

Thus, the coefficients of equation 4.27 area

$$k_1 = \frac{\omega_0}{Q} \tag{4.34}$$

$$k_2 = \frac{\omega_0^2(K+1)}{K} \tag{4.35}$$

$$k_3 = \frac{\omega_0^3}{KQ} \tag{4.36}$$

Starting with $a_0 = 0$ and $b_0 = 0$, in accordance with equation 4.31

$$a_1 = \frac{k_3}{k_2} = \frac{\omega_0}{Q(K+1)} \tag{4.37}$$

and with equation 4.32

$$b_1 = (k_1 - a_1)a_1 = \frac{\omega_0^2 K}{Q^2(K+1)^2} \tag{4.38}$$

The accuracy of root iteration may be estimated by applying a conversion rate factor $d_i = a_j/a_{j+1}$. At the first iteration:

$$d_1 = \frac{a_1}{a_2} = 1 - \frac{b_1}{k_2} = 1 - \frac{K^2}{Q^2(K+1)^3} \tag{4.39}$$

The limit accuracy is $d_\infty = 1$, which means that the root value was calculated exactly. As can be seen from equation 4.39 d_1 approaches one as Q and K become larger. Substituting into equation 4.39 the lowest values of Q and K equation 4.26.

$$d_1 \simeq 1 - \frac{1}{Q^2 K} = 1 - 0.61 * 10^{-1} = 0.984$$

Thus, even under adverse conditions, i.e., by using the lowest Q and K, the accuracy of the first iteration is sufficient. Therefore

$$s_1 = -a_1 \simeq -\frac{\omega_0}{Q(K+1)} \tag{4.40}$$

Substituting now equation 4.37 and equation 4.38 into the second factor of equation 4.28 yields the following quadrant equation:

$$s^2 + \frac{\omega_0 K}{Q(K+1)}s + \frac{\omega_0^2(K+1)}{K} = 0 \tag{4.41}$$

Which gives the next two roots:

$$s_{2,3} = \gamma \pm j\omega_n = \frac{\omega_0 K}{2Q(K+1)} \pm j\omega_0\sqrt{\frac{K+1}{K}} \tag{4.42}$$

Where

$\omega_n = \omega_0\sqrt{\frac{K+1}{K}}$ = The natural angular frequency

With roots equation 4.41, equation 4.42 the solution of equation 4.14, equation 4.15 and equation 4.16 is

$$\begin{aligned} i_d(t) &= \frac{E}{R}[1 + A_1 e^{-\frac{\omega_0 t}{Q(K+1)}} + A_2 e^{-\frac{\omega_0 K t}{2Q(K+1)}} cos(\omega_n t + \alpha_1)] \\ u_c(t) &= E[1 + B_1 e^{-\frac{\omega_0 t}{Q(K+1)}} + B_2 e^{-\frac{\omega_0 K t}{2Q(K+1)}} cos(\omega_n t + \alpha_2)] \\ i(t) &= \frac{E}{R}[1 + C_1 e^{-\frac{\omega_0 t}{Q(K+1)}} + C_2 e^{-\frac{\omega_0 K t}{2Q(K+1)}} cos(\omega_n t + \alpha_3)] \end{aligned} \tag{4.43}$$

Where $A_1, A_2, \alpha_1, B_1, B_2, \alpha_2, ...$ are constants of integration or residues, which are dependent on the initial conditions and may be found with the partial-fraction expression techniques. In the first half period the initial conditions equation 4.18, equation 4.19 and equation 4.20 are zero. Taking the residues of the both the real and complex poles and after simplifying due to the conditions imposed by equation 4.21 to equation 4.26, we obtain the values of the first half period:

$$i_d(T/2) = \frac{E}{R}\left(1 - e^{-\frac{\pi}{(K+1)Q\eta_f}}\right) \tag{4.44}$$

$$u_c(T/2) = E\left(1 - \frac{K}{K+1}e^{-\frac{\pi}{(K+1)Q\eta_f}} + \frac{\sqrt{\frac{Q^2}{Q^2+1}}}{K} e^{-\frac{\pi K\sqrt{\frac{K}{K+1}}}{2Q(K+1)\eta_f}} cos(\frac{\pi}{\eta_f} + \phi_1 + \phi_2)\right) \tag{4.45}$$

$$i(T/2) = \frac{E}{R}\left(1 - e^{-\frac{\pi}{(K+1)Q\eta_f}} + \frac{1}{K\sqrt{3.06+Q^2}} e^{-\frac{\pi K\sqrt{\frac{K}{K+1}}}{2Q(K+1)\eta_f}} cos(\frac{\pi}{\eta_f} + \phi_2)\right) \tag{4.46}$$

Where

ϕ_1 = $arctan(2Q)$

ϕ_2 = $arctan(2Q/3.5)$

η_f = ω/ω_n

It is the normalized frequency or operating frequency factor and ω is the inverter operating angular frequency.

According to equation 4.45 the first commutation reverse voltage may be estimated. Expressions equation 4.44, equation 4.45 and equation 4.46 allow us to calculate the initial conditions for the second half period of the three phase inverter start up.

To check the accuracy of the above approximate formulas computer aided simulation of the transient behaviour of the inverter in its starting process was performed. The differential equation 4.13 has been solved by the Runge Kutta method and the results

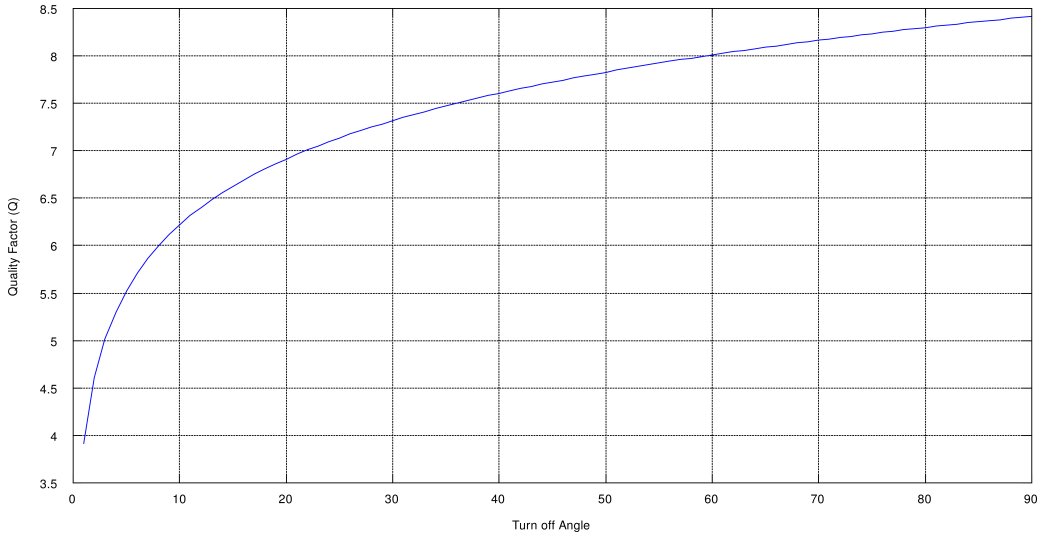

Figure 4.6: The Region of the Three Phase Inverter Parameters Q and β_s Determine the Starting Process

obtained by this computation were compared with the results obtained by approximate formulas equation 4.44, equation 4.45 and equation 4.46. The difference in the results at the end of the first half period is less than 5%. When $Q = 10$, $K = 100$, error is less than 1%. It is evident that this accuracy is high enough for the practical inverter analysis.

The turn off (dead time) angle β_d is of most importance for the reliable start-up process. This angle represents the time ($t_{off} = \beta_d/\omega$) that is available for the reliable switching of the inverter MOSFET's.

The computer-aided turn-off angle β_d shows that its varying may be monotonous or oscillating, depending on the circuit parameters and operating frequency factor. By the monotonous change the turn-off angle β_{dmin} takes place at the second commutation cycle. However, by the oscillating change it takes place at the following half-periods. Figure 4.6 shows two regions of the inverter parameters, i.e., Q and steady state turn off angle β_s which determine the kind of angle β_d changing. The steady state turn off angle β_s is related to the factor η_f [16] as

$$tan\beta_s = \left(\eta_f - \frac{1}{\eta_f}\right) Q \tag{4.47}$$

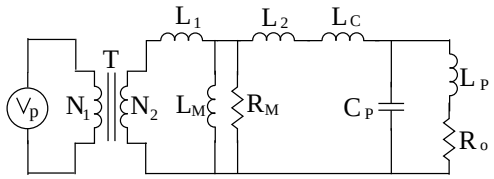

Figure 4.7: Circuit of Proposed IDH Equivalent

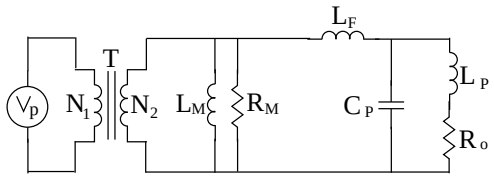

Figure 4.8: Simplified Circuit

Thus, for the known β_s, the frequency factor η_f may be determined with equation 4.22 and taking into account that $\eta_f = \omega/\omega_n$ and $\omega_n = \omega_0\sqrt{(K+1)/K}$, as

$$\eta_f = \left(1 - \frac{\sqrt{\frac{K+1}{k}}Rtan\beta_s}{2\pi f L_w}\right)^{-\frac{1}{2}} \tag{4.48}$$

When η_f changes from 1.01 to 1.1 [see (equation 4.26)], β_s changes from 5^o to 75^o in equation 4.47.

4.6 Calculation of Switching Frequency

Circuit of proposed 3 phase IDH equivalent to switching transformer (ST) is shown in Figure 4.7. R_M indicates core losses. L_M, L_{l1} and L_{l2} are mutual and leakage inductances of isolation transformer. Figure 4.8 shows the simplified circuit where L_F is obtained as follows:

$$L_F = L_C + L_{l1} + L_{l2} \tag{4.49}$$

Secondary side of isolation transformer provides a rectangular voltage V_S. An LC circuit feeds an inductive load with typical power factor less than 0.1 [94]. Parallel resonance

tank equivalent impedance matching coil is given by

$$Z_T(j\omega) = j\omega L_F + \frac{1}{j\omega C_P + \frac{1}{j\omega L_P + R_o}} \tag{4.50}$$

To obtain proper switching angular frequency, ω_0, imaginary part of equation 4.50 should be taken equal to zero. Due to low power factor of the induction coil, it is possible to assume $R_0^2 << (\omega_0 L_P)^2$, therefore equation 4.50 can be simplified as equation 4.51:

$$Z_T(j\omega) \approx j\omega L_F + \frac{\frac{R_O}{\omega_0^2 L_P^2} - j\omega_0 \left[C_P - \frac{1}{\omega_0^2 L_P}\right]}{\omega_0^2 \left[C_P - \frac{1}{\omega_0^2 L_P}\right]^2} \tag{4.51}$$

Imaginary part of equation 4.51, taken equal with zero, is solved to obtain f_0 by the following equation:

$$\omega_0 = \sqrt{\frac{L_P + L_F}{C_P L_P L_F}}; \omega_0 = 2\pi f_0 \tag{4.52}$$

Equation 4.52 shows the proper switching frequency, f_0, to transfer maximum power to the load. The value of impedance Z_T at frequency f_0 is obtained as equation 4.53:

$$Z_T(j\omega) \approx R_O \left(\frac{L_F}{L_P}\right)^2 \tag{4.53}$$

Maximum transferred power to R_0 at switching frequency f_0, is achieved by equation 4.51. V_{S1} and N_2/N_1 are effective main components of secondary voltage and winding ratio of transformer, respectively.

$$\begin{aligned} P_O &= \frac{V_S^2}{Z_T(j\omega_0)} \approx \frac{V_{S,1}^2}{R_O \left(\frac{L_F}{L_P}\right)^2} \\ P_O &\approx \left(\frac{2\sqrt{2}}{\pi} . \frac{N_2}{N_1} . \frac{L_P}{L_F}\right)^2 . \frac{V_{ref}^2}{R_O} \end{aligned} \tag{4.54}$$

It is clear from equation 4.54 that output can also be determined by winding ratio of high frequency transformer. Also the type of isolation transformer must be selected according to operation frequency.

4.7 Calculation of Matching Coil Value

There are several methods to determine matching coil value. To obtain a good filtering performance of output stage and almost sinusoidal waveform on the induction coil,

Table 4.2: Circuit Parameters

Parameter	**Value**	**Parameter**	**Value**
Utility	380V/50H$_Z$	N$_1$/N$_2$	1
V$_{ref}$	300V	L$_F$	200μH
L$_P$	10μH	C$_P$	26.96μF
R$_o$	50mΩ	L$_M$	20mH

following relationship may be assumed.

$$L_F >> L_P \tag{4.55}$$

Also, start-up current must be limited by L_F. The maximum possible start-up primary current variation, neglecting transformer inrush current, can be approximated by equation 4.56:

$$\max\triangle I_{primary_{startup}} \approx \frac{1}{L_F}\left(\frac{N_2}{N_1}\right)^2 \frac{T_s}{2}\sqrt{2}V_m \tag{4.56}$$

V_m is the peak voltage of the utility. Maximum allowable switching devices current found from the specifications supplied by manufacturer must be greater than maximum primary start-up current. Thus L_F can be determined by considering equation 4.55 and equation 4.56.

4.8 Simulation Results

Sample circuit parameters are given by Table 4.2. The switching frequency calculated from equation 4.52 is $9931.80H_Z$. Consequently, from equation 4.50 we have $Z_T(j\omega_o) = 1.969\angle -10°$, which gives a power factor close to 1 (0.9999) as shown in Figure 4.9. Figure 4.10, Figure 4.11, Figure 4.12 and Figure 4.13, Figure 4.14, Figure 4.15 show waveforms of supply voltage and primary side output voltage, respectively. Secondary side of isolation transformer, load voltage and induction coil current are shown in Figure 4.16, Figure 4.17, Figure 4.18 and Figure 4.19, Figure 4.20, Figure 4.21 respectively. Simulation summaries are given in Table 4.3. Figure 4.22, Figure 4.23, Figure 4.24 show FFT of output voltages.

Table 4.3: Simulation Summaries

Parameter	**Value**	**Parameter**	**Value**
V_{ab}	84.874V	I1	92.275A
V_{bc}	84.882V	I2	92.274A
V_{ca}	84.883V	I3	92.265A
PF	0.9999	THD(V_O)	0.7%
F_s	9956H_Z	Pout	7831.61W

Table 4.4: Simulation Results

Frequency in H_z	**Output Voltage in volt**
0.5k	732.00
1.0k	416.24
1.5k	324.20
2.0k	159.41
5.0k	90.50
10.0k	84.874

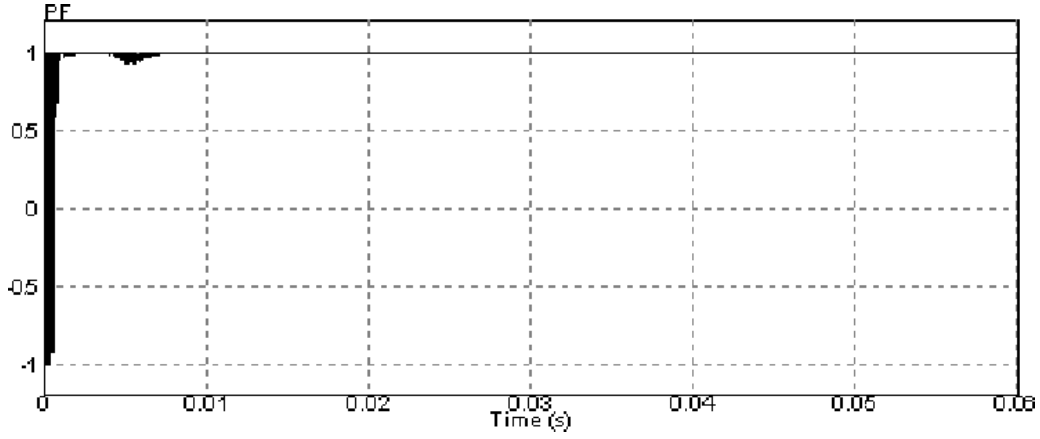

Figure 4.9: Power Factor

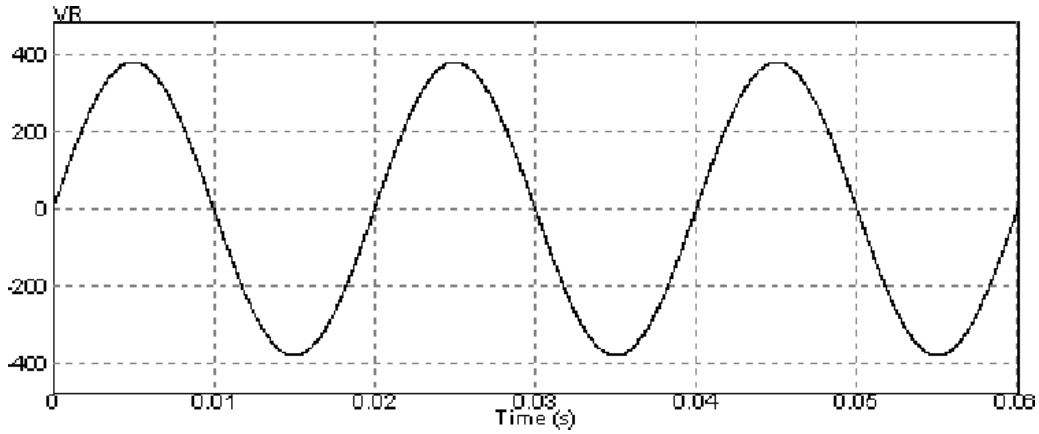

Figure 4.10: R Phase Supply Voltage Waveform

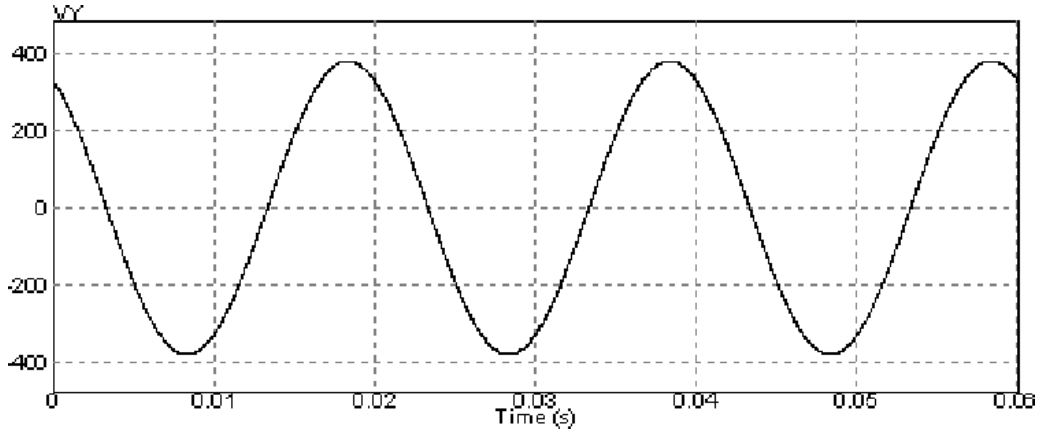

Figure 4.11: Y Phase Supply Voltage Waveform

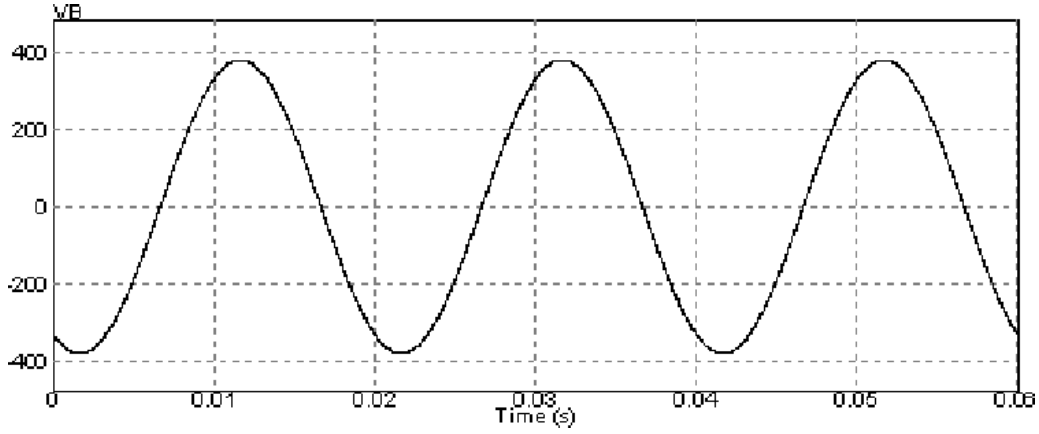

Figure 4.12: B Phase Supply Voltage Waveform

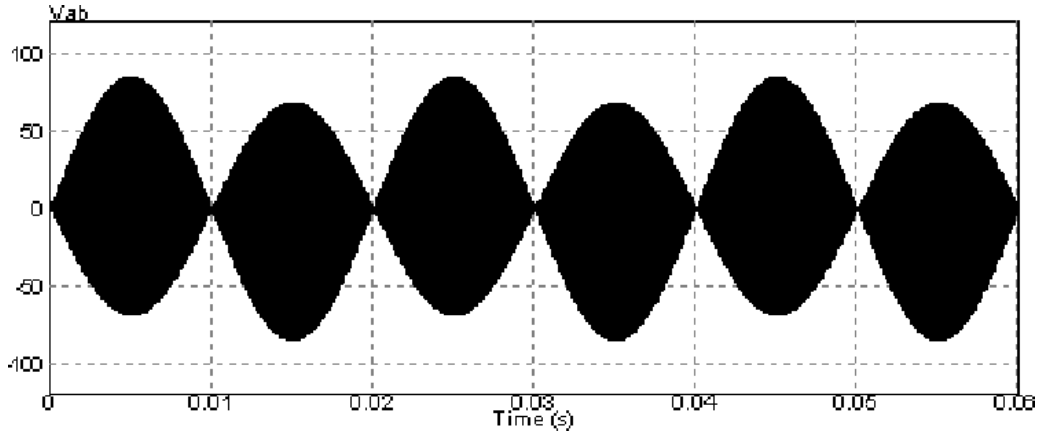

Figure 4.13: Waveform of Primary Output Voltage for V_{ab}

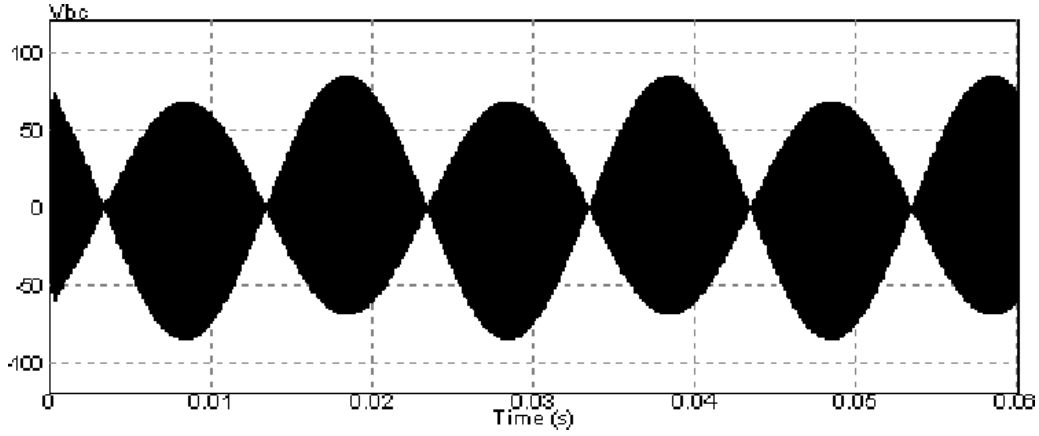

Figure 4.14: Waveform of Primary Output Voltage for V_{bc}

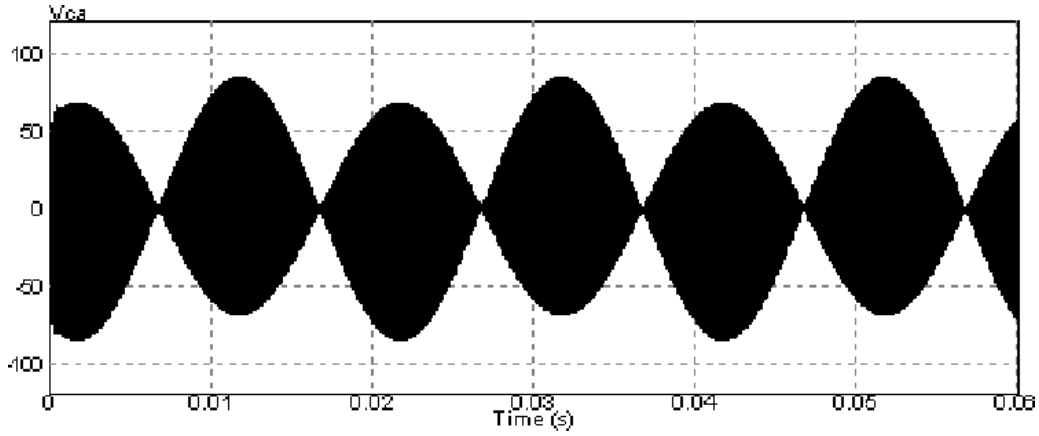

Figure 4.15: Waveform of Primary Output Voltage for V_{ca}

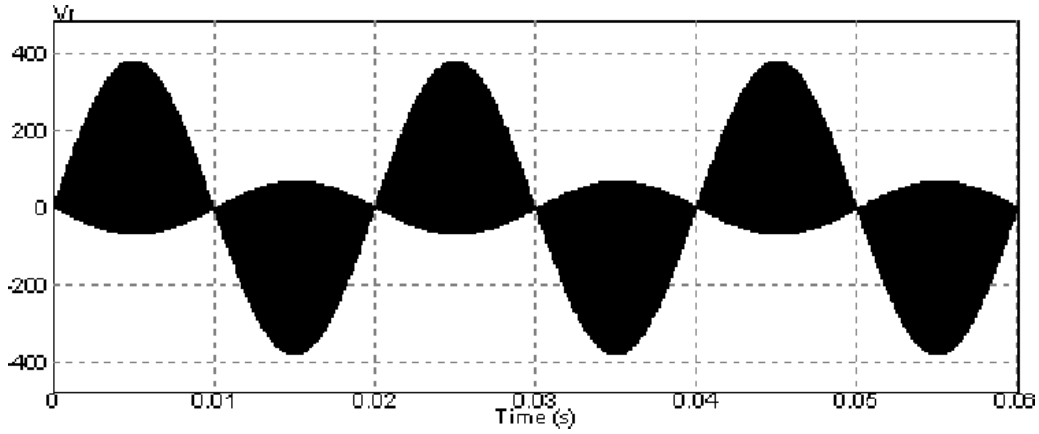

Figure 4.16: Secondary Side Output Voltage V_r

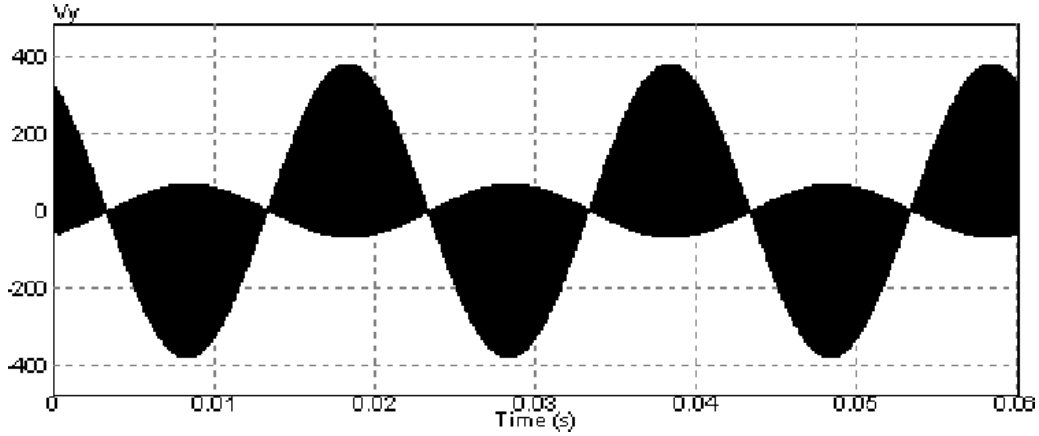

Figure 4.17: Secondary Side Output Voltage V_y

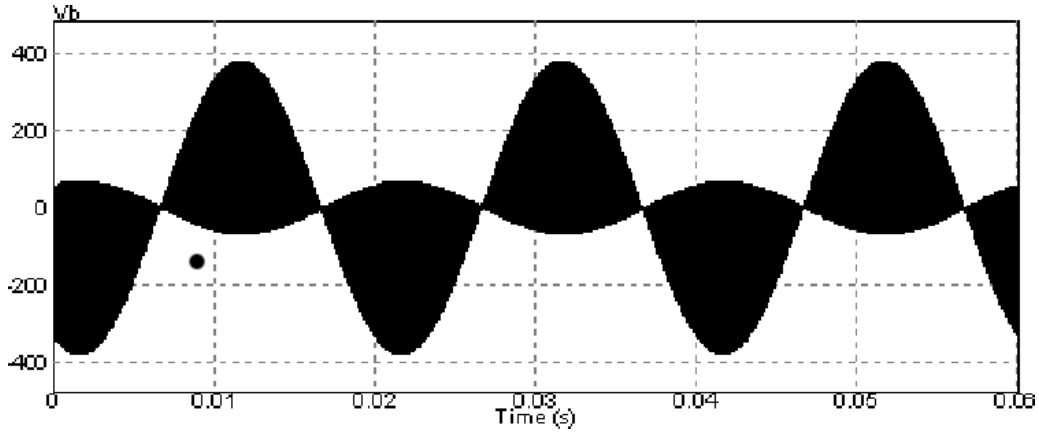

Figure 4.18: Secondary Side Output Voltage V_b

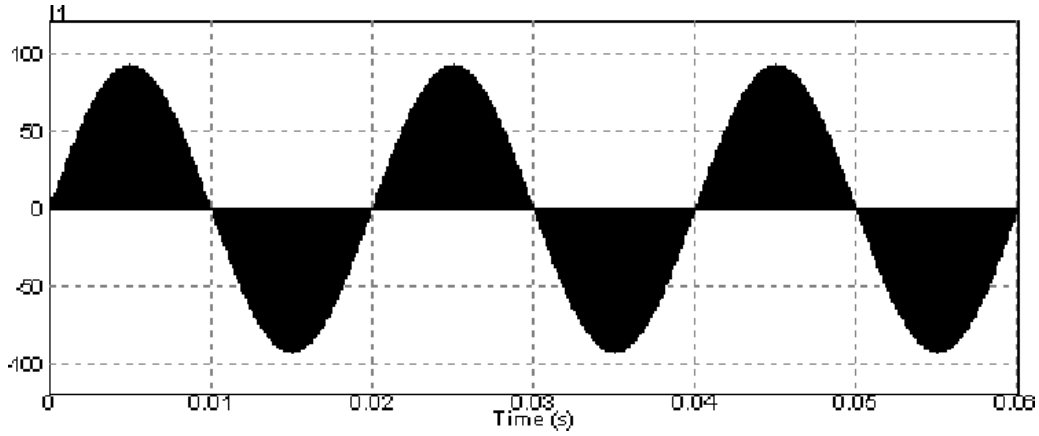

Figure 4.19: Induction Coil Current I_1

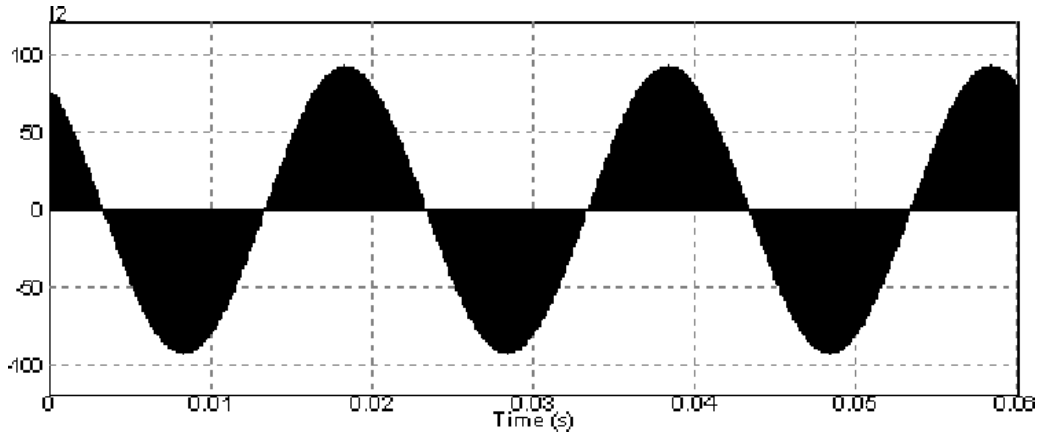

Figure 4.20: Induction Coil Current I_2

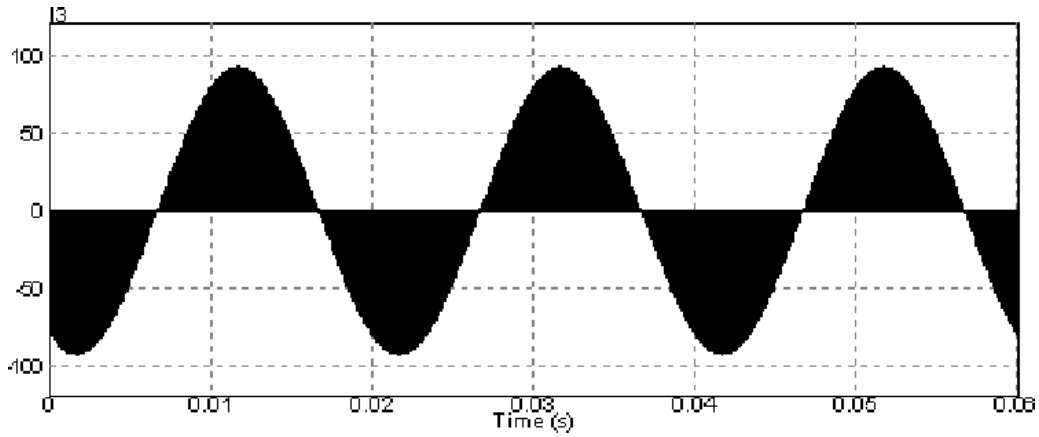

Figure 4.21: Induction Coil Current I_3

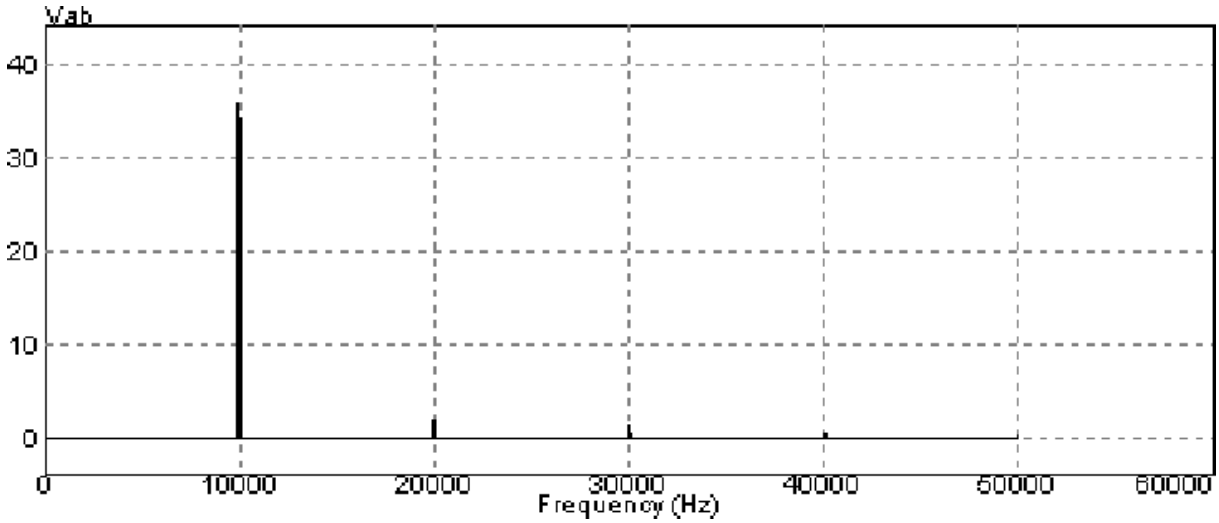

Figure 4.22: FFT of Output Voltage for V_{ab}

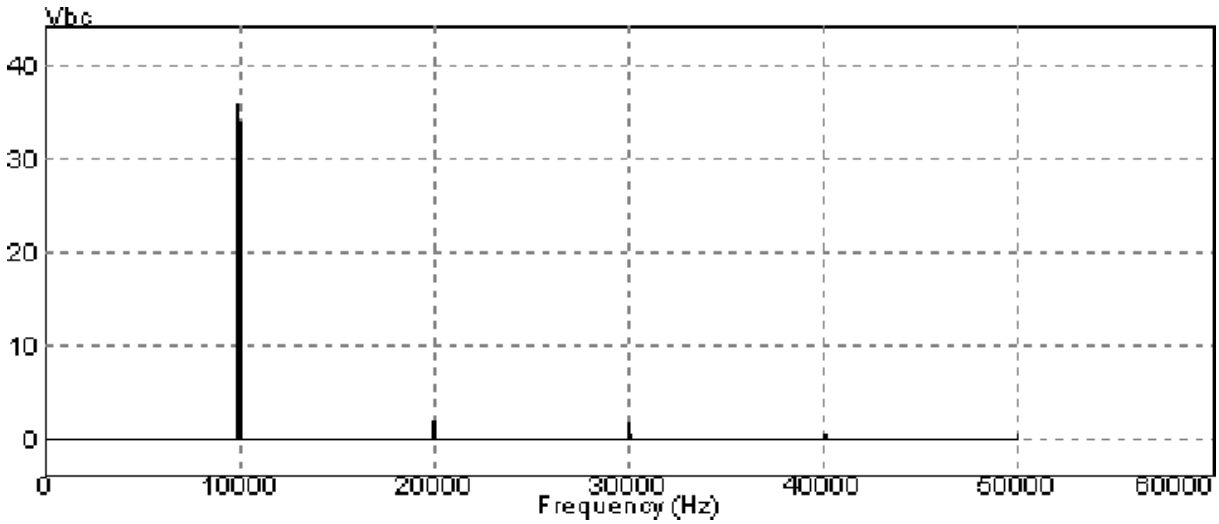

Figure 4.23: FFT of Output Voltage for V_{bc}

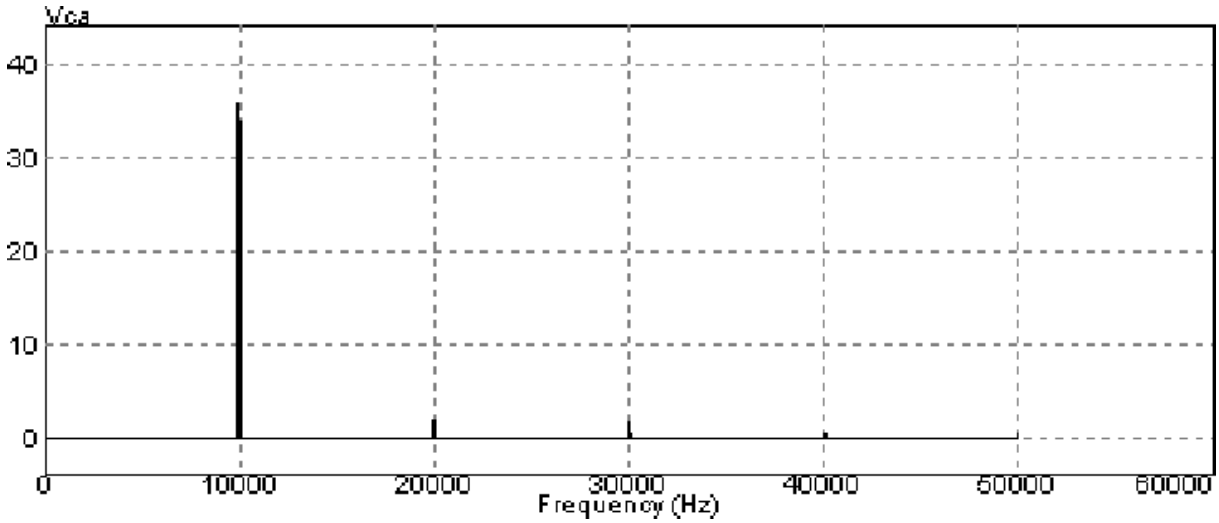

Figure 4.24: FFT of Output Voltage for V_{ca}

4.9 Conclusions

In this chapter an induction dielectric heating device with high frequency transformer structure has been described. Comparison of proposed circuit has been carried out both by mathematical analysis and by simulation. The result shows that value of power factor obtained is unity. Flexibility aspects of switching transformer leads to several advantages such as unity power factor without using any reactive element, symmetric loading from utility point of view, isolation of working coil, compact dimensions and almost uniform sinusoidal output.

Additionally, this topology can provide any voltage level conversion ability, which leads to desired power even at low input voltage levels. Furthermore, proposed topology provides maximum output power and reduced THD utilization. This requires comparatively smaller size of matching filter coil which work suitably with auto tuning switching frequency controller.

Chapter 5

EXPERIMENTAL VERIFICATION

5.1 Introduction

The objective of the conducted experiment is to assess the versatility of IDH technology, which provides heat up of conducting and non-conducting materials.

In this chapter, first the proposed IDH system has been described and the considered the experimental parameter has been defined and follows the experimental results.

5.2 Experimental System

Induction Dielectric Heating takes power from the mains, converts it into frequencies suitable for specific applications, and then uses this power to create controllable heat in any conducting material or non-conducting material.

Power is applied to the work-piece by 3 phase induction coils. An alternating current flowing through a coil; (i) Generates a magnetic field, (ii) Places a work-piece, (iii) Induces eddy current or displacement current within the magnetic field. Heat is produced only after the eddy current or displacement current is induced.

The heating pattern of an object mainly depends on the design of winding or induction coil pattern. However the power and frequency can be obtained by taking suitable converter rating. The depth of heat penetration into the work-piece depends on the frequency; the lower the frequency, the deeper the penetration.

Figure 5.1 demonstrates structure of the 1 phase to 3 phase IDH coil control which can be divided into seven parts as follows:

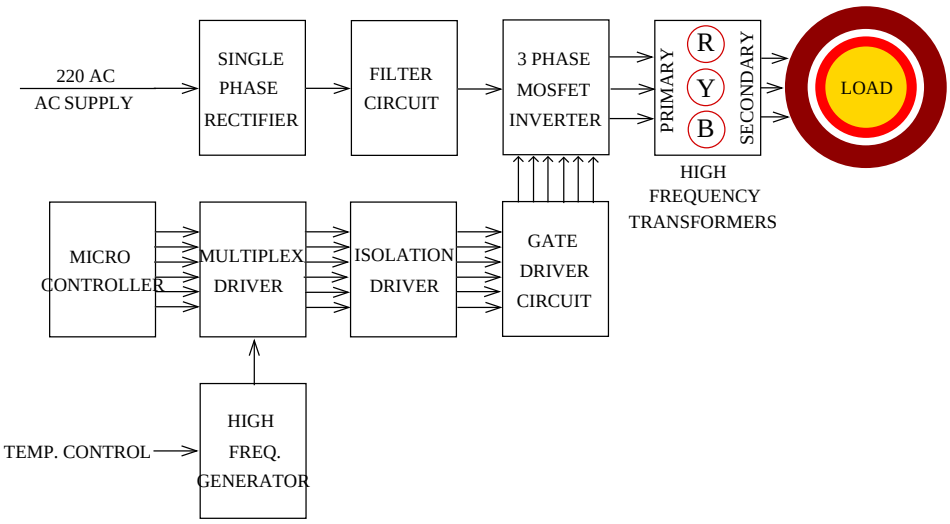

Figure 5.1: The Experimental System of IDH System Control

A. Main control unit

Main control unit consists of micro controller and multiplex driver as shown in Figure 5.1. In the experimental system the main control unit has to do the following tasks:

(i) To determine the SVM signal patterns and the main frequency control values for the SVM signal generator has been described in chapter 2.

(ii) To read in the three phase signals from the encoder.

(iii) To implement the digital control system.

(iv) To calculate the switching actions for the three inverter-legs.

(v) To control all the six timings individually of the SVM signal for firing circuit of the MOSFET devices.

(vi) To send the switching actions to the MOSFET driver card through multiplex driver.

B. High frequency generator unit

To generate the high frequency signal for desired patterns using 4093 IC. The unit has protection circuit for false phase fixing which may damage the MOSFET's three phase inverter.

Figure 5.2: High Frequency Transformer

C. MOSFET gate driver unit

Adjusts the signal derived from the multiplex driver to suitable for the MOSFET gate in the MOSFET inverter unit.

D. Rectifier unit

1 phase or 3 phase AC to DC converter using bridge rectifier unit.

E. MOSFET inverter unit

Frequency value and patterns have been developed by the micro controller and supplying power to primary side of high frequency transformers. The switches used are MOSFETs with a rated current of 25 A. The dead-time is 6 micro second. The maximum switching frequency of the MOSFETs is 20 kHz.

F. High frequency transformer unit

Suppling driving power from the three phase MOSFET inverter to the 3 phase

Figure 5.3: Three Phase Induction Coils

induction coil. High frequency transformer consisting of three, 1 phase transformers designed for specific needs as shown in Figure 5.2.

G. Heating coil unit

Generating high frequency magnetic field at resonance position for distributing heat to the material. Three phase induction coils are shown in Figure 5.3.

The hardware circuit layout for IDH control system is shown in Figure 5.4

5.2.1 Determination of control frequency

The control frequency which is required for heating the work-piece and can be determined by either main control unit or high frequency generating unit depending on type i.e. conducting or non-conducting material.

The main control unit frequency generated by the micro controller [108], [115] can be

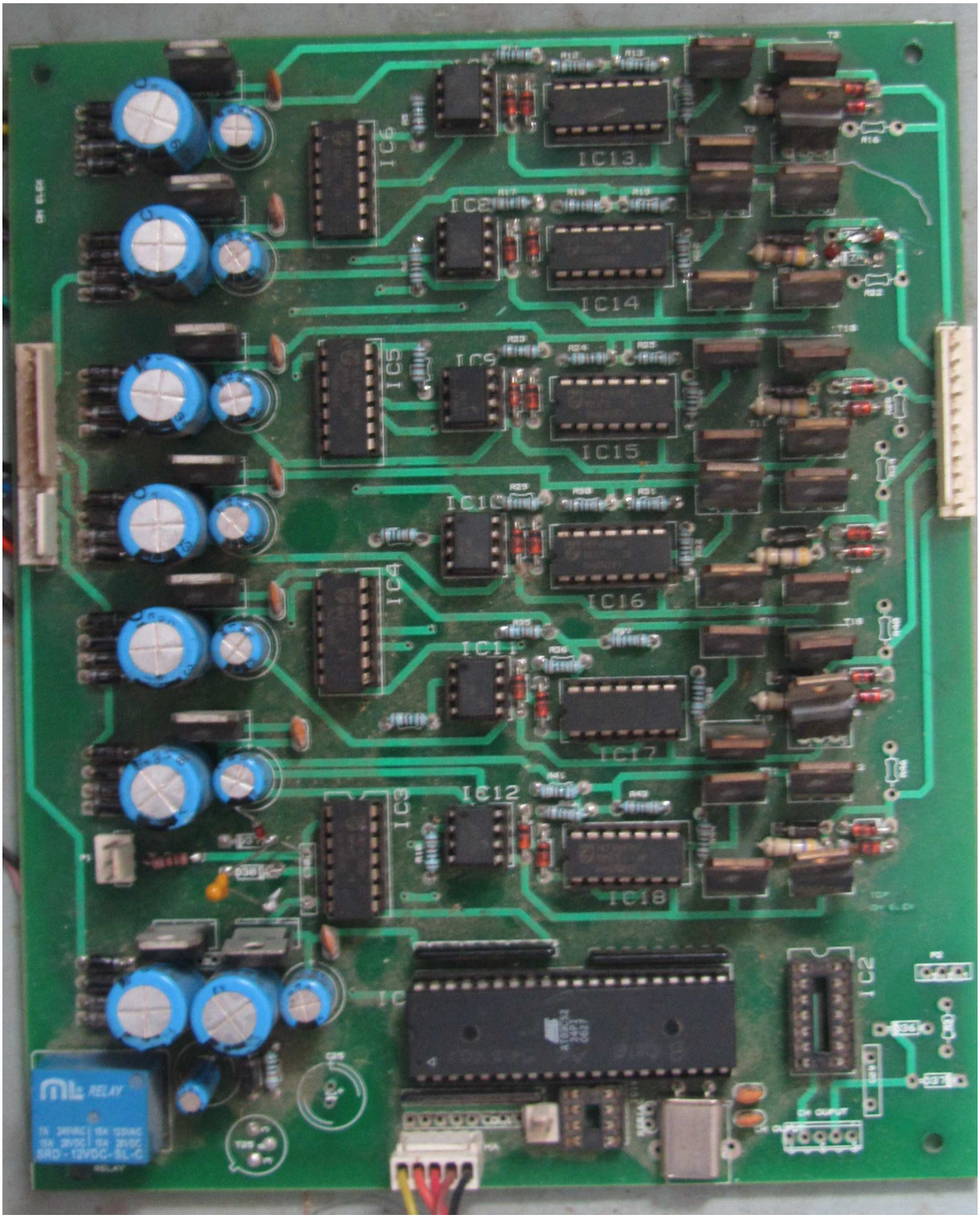

Figure 5.4: Hardware Structure of IDH System Control

Table 5.1: Limits of f_{PWM} and f_H

Range	f_{PWM}	f_H							
		8	7	6	5	4	3	2	1
Max (kHz)	15.69	2007.84	1003.92	501.96	250.98	125.49	62.75	31.37	15.69
Min (kHz)	0.03	3.94	1.97	0.98	0.49	0.25	0.12	0.06	0.03

derived from the following equations:

$$f_{CPU} = \frac{f_{OSC}}{2 \times D_{OCR}} \tag{5.1}$$

Where

f_{CPU} = Main control frequency generated by the micro controller in Hz

f_{OSC} = Micro controller clock signal in Hz

D_{OCR} = Divided frequency value in the micro controller in Hz

PWM frequency is given as follows:

$$f_{PWM} = \frac{f_{CPU}}{256 \times 2} \tag{5.2}$$

Where

f_{PWM} = PWM frequency in the induction coil in Hz

f_{CPU} = Main control frequency generated by the micro controller in Hz

The high frequency generated unit by the IC 4093 can be derived from the following equations:

$$f_H = \frac{1}{1.1RC} \tag{5.3}$$

Where

f_H = High frequency in the IDH coil in Hz

So that, equations of induction coil PWM frequency is obtained as follows:

$$f_{PWM} = \frac{f_{OSC}}{1024 \times D_{OCR}} \tag{5.4}$$

And equations for calculating the divided frequency value in the micro controller is

$$D_{OCR} = \frac{125}{16 \times f_{PWM}} \tag{5.5}$$

Where

f_{OSC} = $11.0592MHz$

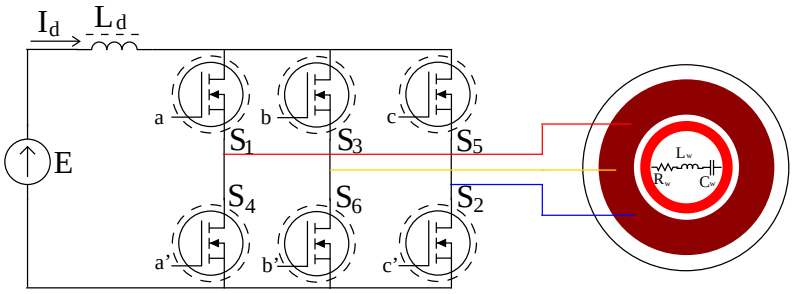

Figure 5.5: Three Phase MOSFET Base Inverter

According to the equation 5.3 and equation 5.4 the frequency generated from f_H and f_{PWM} are shown in Table 5.1. Results from Table shows that by using the PWM principle the frequency has been determined between $0.03 - 15.69\ kHz$ by main control unit. The high frequency generator unit generates the frequency in the range of 0.03 to 2007.84 kHz.

5.3 Protection Considerations

Three phase MOSFET base inverter as shown in Figure 5.5. Protection against over voltages across the power devices is shorting out devices S_1 & S_4 and concurrently forcing the DC current to zero. Over voltages could arise as a result of too large a capacitor voltage. This in turn could take place if the load coil were to become open circuited. The current source inverter has the additional attribute of tolerating fault currents since DC current source is controllable. Consequently the applied current source can be phased back upon detection of a fault current. A fault current would occur if either the coil or a device were to become shorted or if a device had failed to commutate. Additional necessary protection includes the capability of maintaining sufficient turn off time margin for the load commutated devices. This can be accomplished by monitoring the tank voltage and calculating the turn off time available until the succeeding voltage zero crossing. Consequently transient changes in the systems could result in a commutation failure. Hence additional turn off time margin has been typically provided in order to take into account the likelihood of such an event. This type of event mainly occurs for ferrous metal melting where the resonance frequency increases during the melt cycle.

5.4 Component Ratings

The ratings of the components are established by using Fourier analysis techniques. Initially an equivalent circuit model is developed. This model is based on the following simplifying assumptions:

1. The input current of the inverter is constant.
2. The semiconductor switches are ideal.
3. The output transformer is ideal and has a unity turns ratio.
4. The inverter operates in the continuous mode.
5. The effect of the overlap period is neglected.

It is also convenient to define base values for voltages, currents and times for adopting a comparative reference base from which other inverter schemes are to be judged. From a users point of view, it is appropriate to consider the effective coil resistance as a base impedance. Furthermore, it is useful to establish the driving source as base value. This happens to be the current for the case of a current source.

5.5 Advantages

The technical features of induction dielectric heating deliver three key benefits: improved throughput, better and consistent quality and reduced costs.

5.5.1 Throughput

Using induction dielectric heating into the production line improves production efficiency. It can cut lead times and speed up throughput. The IDH heating process itself is faster than open-flame and oven alternatives.

5.5.2 Quality

Quality improves because it can apply pre-set temperatures to pre-set parts of individual work-pieces and because induction coils are special-made for specific work-pieces, in

advance, the delivered heat pattern. Also, precise heat delivery means any adjoining components and/or materials remain unharmed during the heating process.

5.5.3 Costs

Costs go down because of shorter lead times and increased throughput. Integrated in-line induction dielectric heating means lower pre-processing and logistics costs. Swift heat cycles, precise delivery and accurate repeatability minimize waste and scrap. IDH frequency converters are particularly effective at lowering energy costs, as it has a proven higher efficiency and power factor than competing converters.

5.6 Experimental Results

Experimental circuit parameters are given in Table 5.2. The switching frequency generated from encoder is $279H_Z$. Figure 5.6, Figure 5.7 and Figure 5.8 show waveform of encoder, respectively. Figure 5.9, Figure 5.10, Figure 5.11, Figure 5.12, Figure 5.13 and Figure 5.14 show waveform of gate pulse applied to power devices using main control unit, respectively. High frequency transformer input and output voltages are shown in Figure 5.15, Figure 5.16, Figure 5.17, Figure 5.18, Figure 5.19 and Figure 5.20, respectively for conducting material. Figure 5.21, Figure 5.22 and Figure 5.23 show FFT of three phase inverter output voltage waveform, respectively. FFT of three phase IDH (Load) waveforms are shown in Figure 5.24, Figure 5.25 and Figure 5.26, respectively for conducting material.

Figure 5.27 shows high frequency generator unit waveform. Figure 5.28, Figure 5.29, Figure 5.30, Figure 5.31, Figure 5.32 and Figure 5.33 show waveform of gate pulse applied to power devices using high frequency generator unit, respectively. High frequency transformer input voltages are shown in Figure 5.34, Figure 5.35, Figure 5.36, respectively for non-conducting material. Figure 5.37, Figure 5.38 and Figure 5.39 show FFT of three phase inverter output voltage waveform, respectively for lemon. Experimental verification summaries are given in Table 5.3. Experimental sample results are shown in Figure 5.40 and Figure 5.41 respectively.

Table 5.2: Circuit Parameters

Parameter	**Value**	**Parameter**	**Value**
Utility	220V/50H$_Z$	N_1/N_2	50
V_{ref}	300V	L_F	$200\mu H$
L_P	$10\mu H$	C_P	26.96μF
R_o	50mΩ	L_M	20mH

Table 5.3: Experimental Verification Summaries

Parameter	**Value**	**Parameter**	**Value**
V_{ab}	1.272 V	I1	122 A
V_{bc}	1.285 V	I2	132 A
V_{ca}	1.269 V	I3	118 A
PF	0.9999	THD(V_O)	0.7%
F_s	279H$_Z$	Pout	100.61W

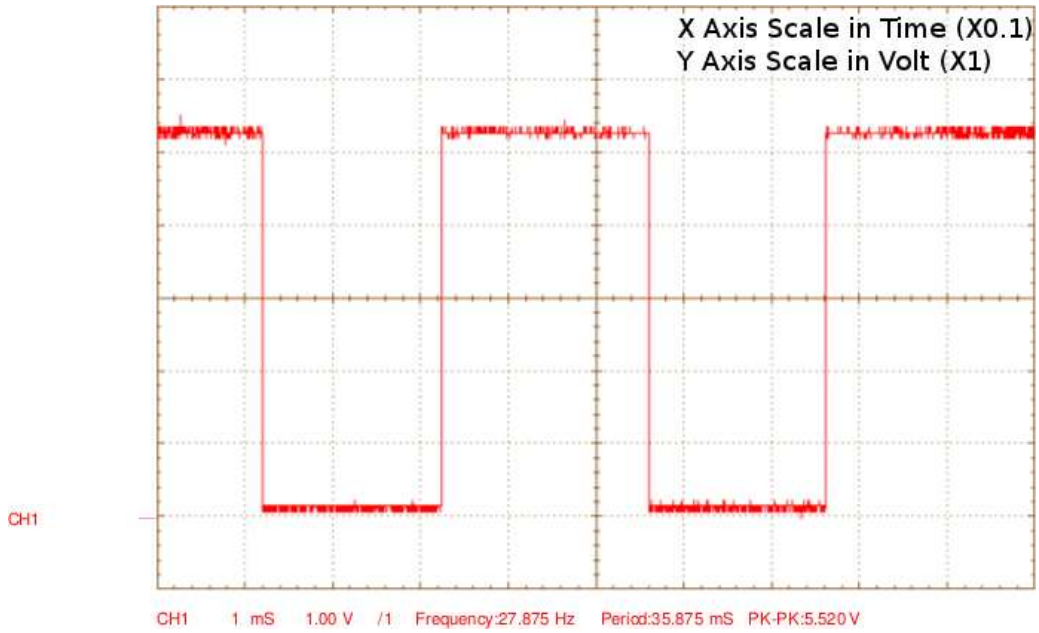

Figure 5.6: Encoder 1

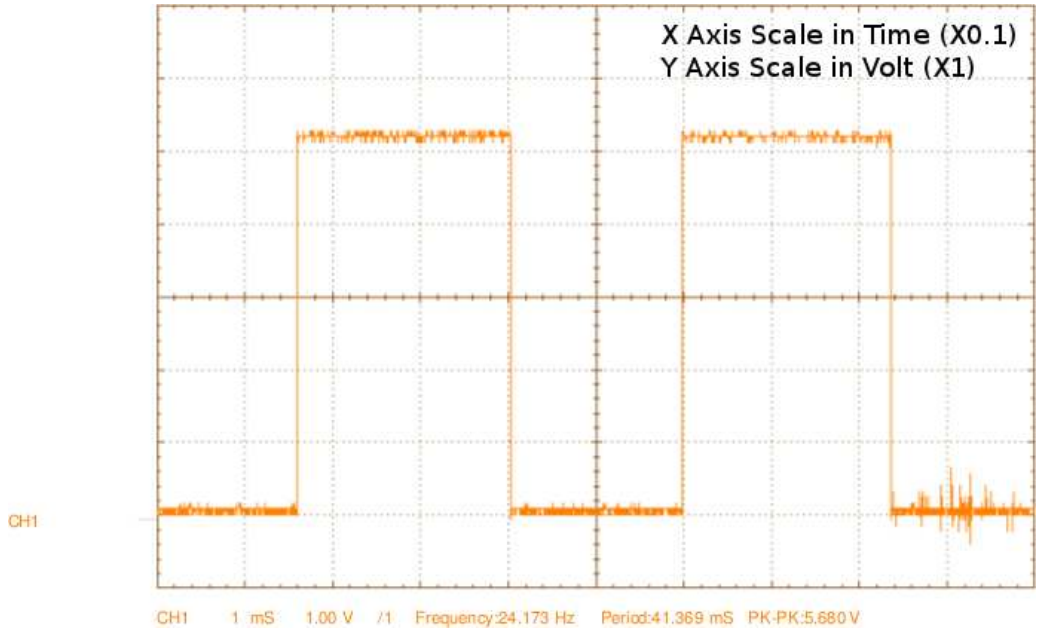

Figure 5.7: Encoder 2

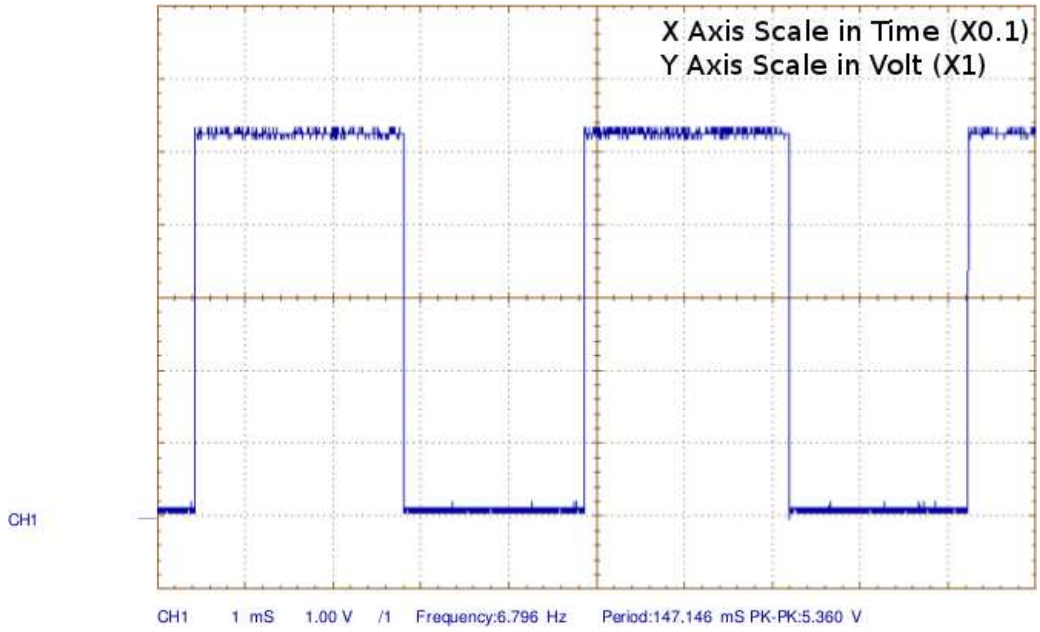

Figure 5.8: Encoder 3

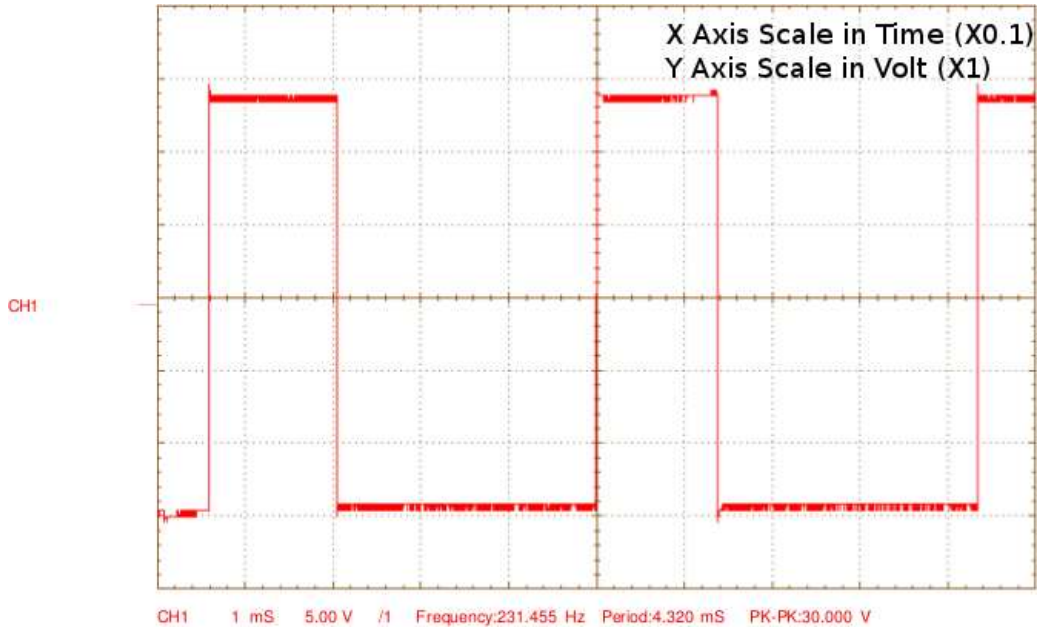

Figure 5.9: Gate Pulse for S_1 Using Main Control Unit

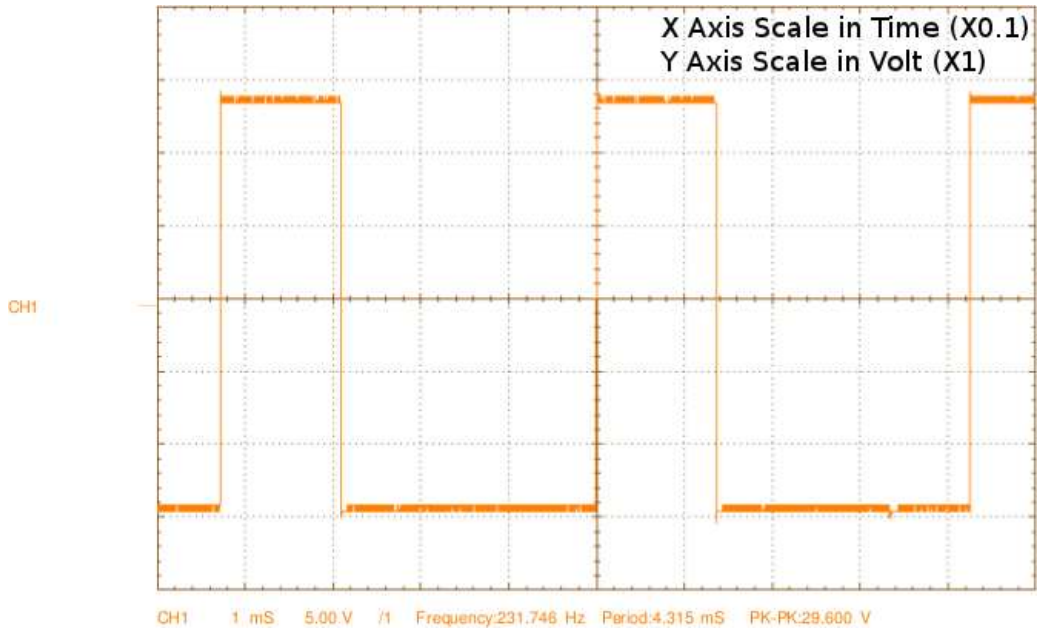

Figure 5.10: Gate Pulse for S_3 Using Main Control Unit

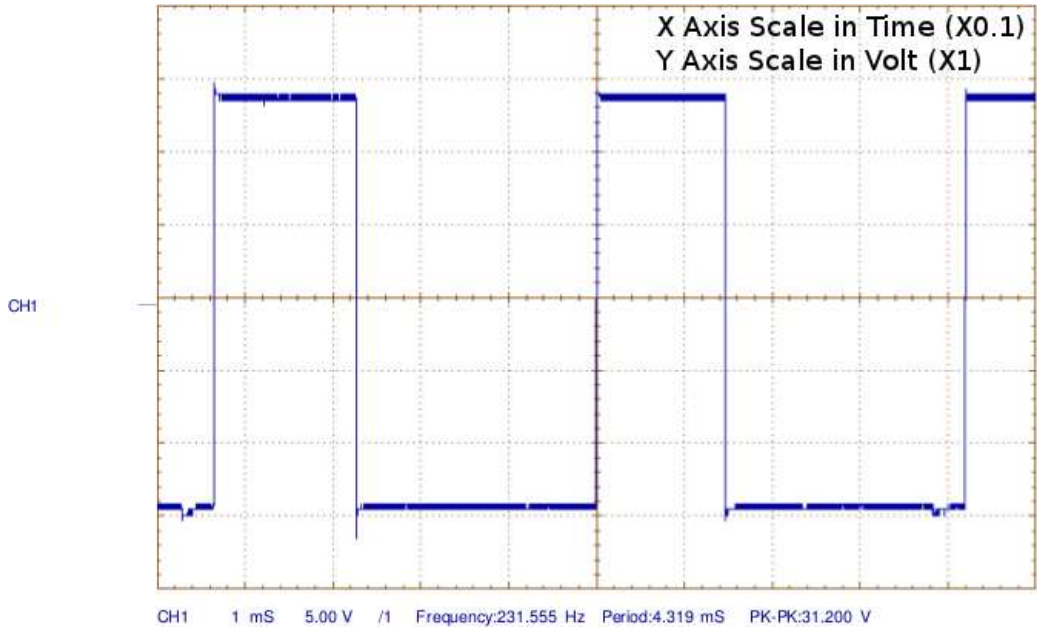

Figure 5.11: Gate Pulse for S_5 Using Main Control Unit

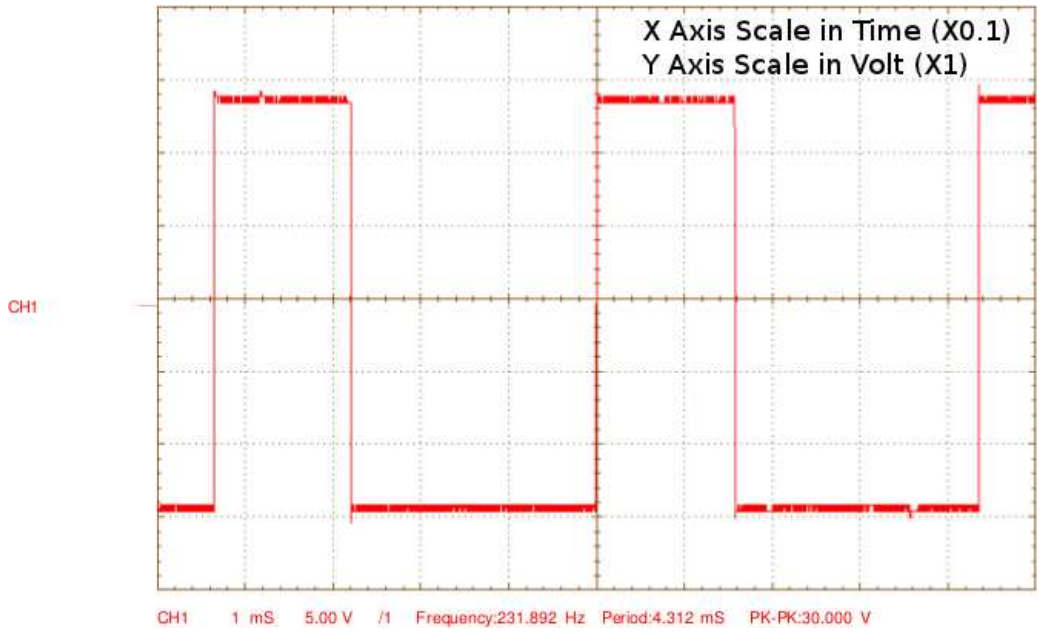

Figure 5.12: Gate Pulse for S_4 Using Main Control Unit

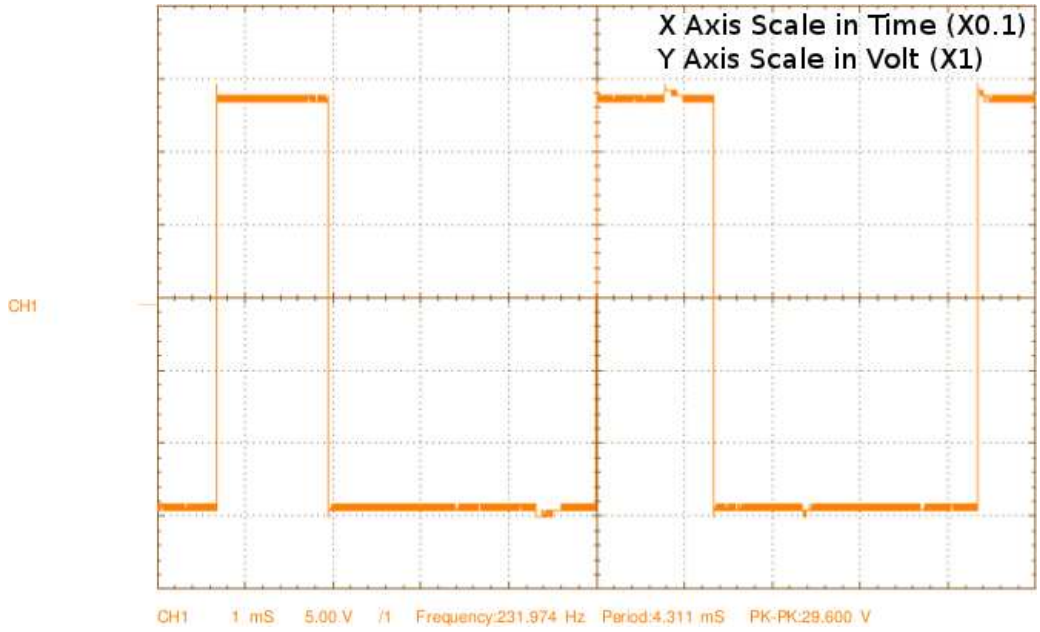

Figure 5.13: Gate Pulse for S_6 Using Main Control Unit

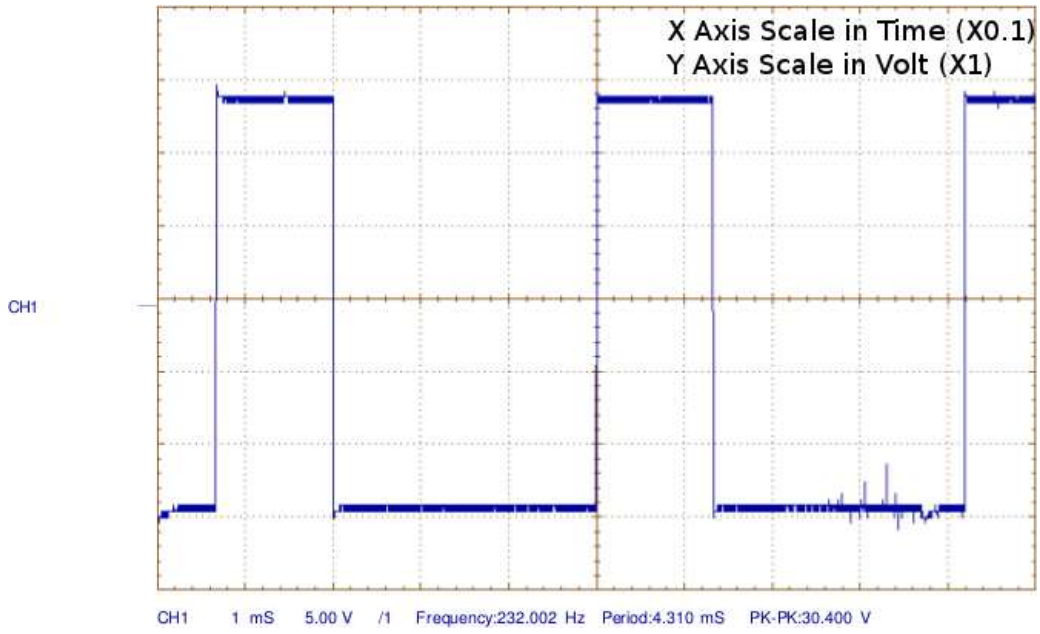

Figure 5.14: Gate Pulse for S_2 Using Main Control Unit

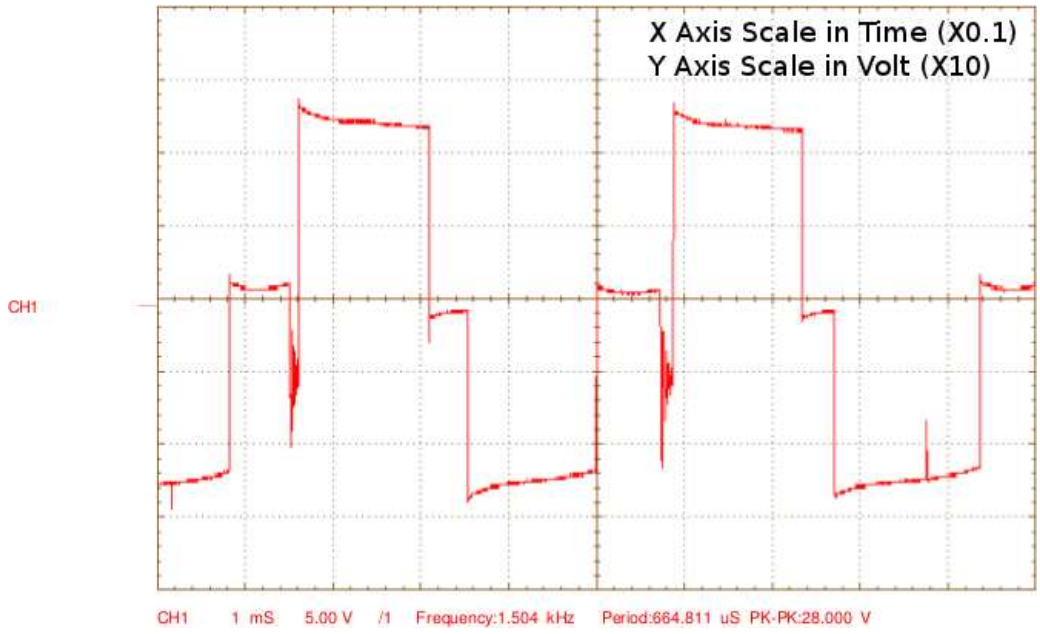

Figure 5.15: High Frequency Transformer Input Voltage Waveform (V_{iRY})

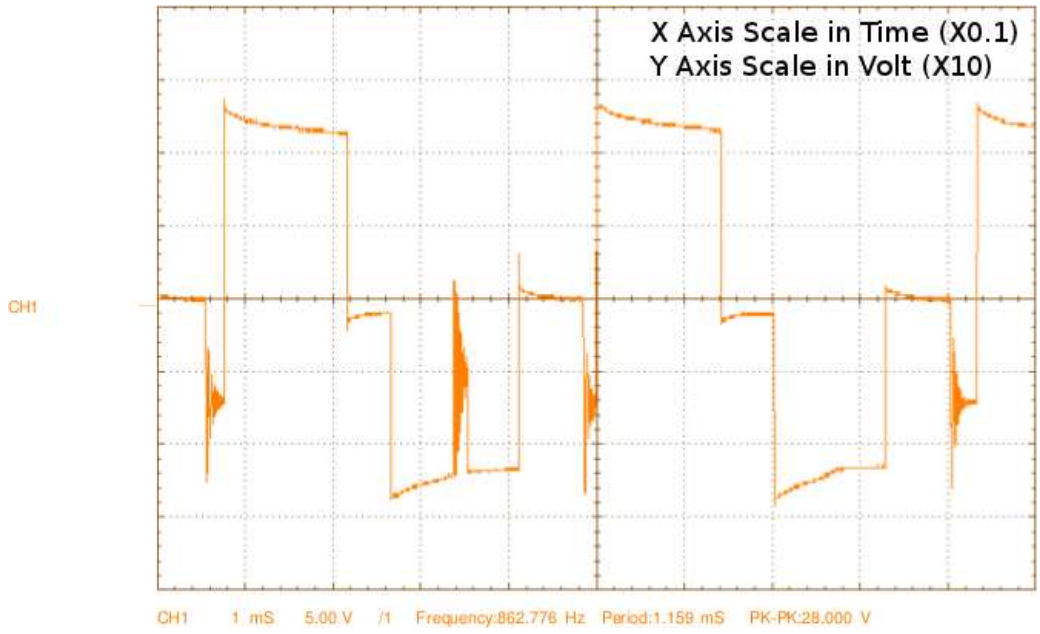

Figure 5.16: High Frequency Transformer Input Voltage Waveform (V_{iYB})

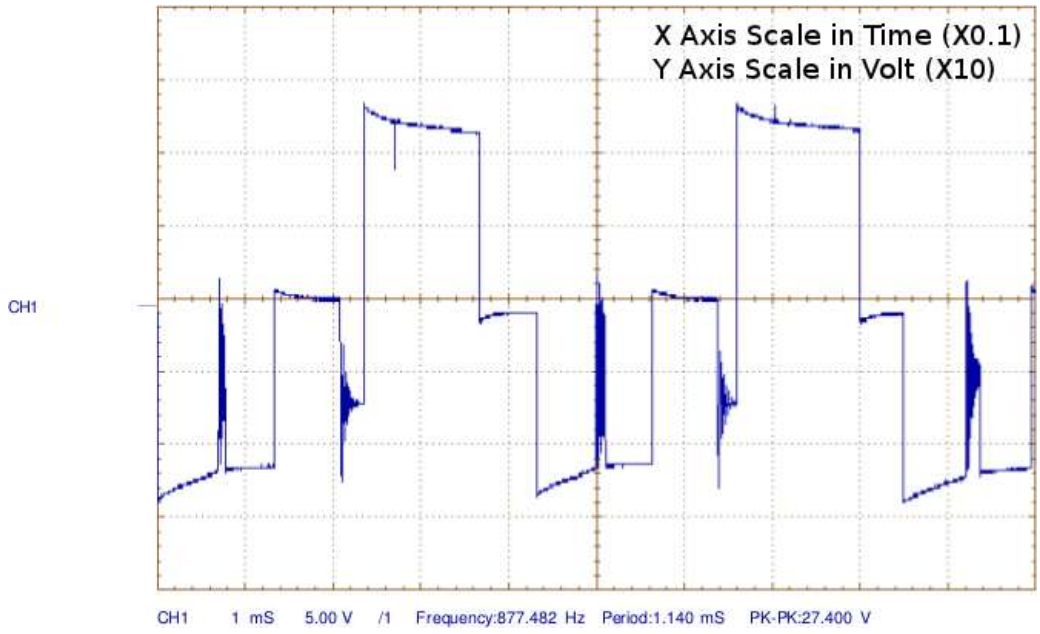

Figure 5.17: High Frequency Transformer Input Voltage Waveform (V_{iBR})

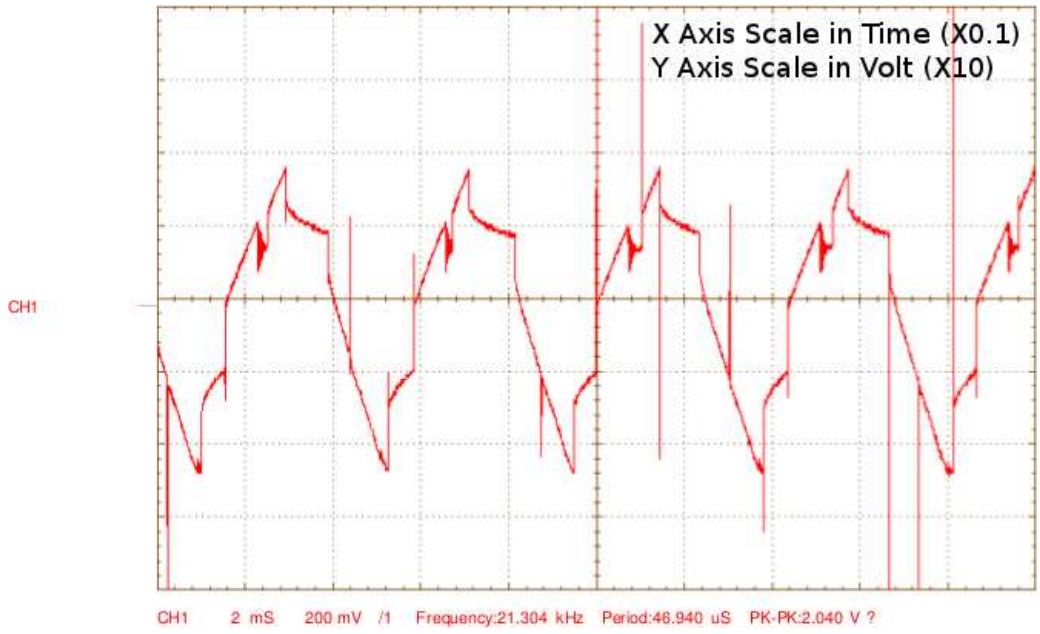

Figure 5.18: High Frequency Transformer Output Voltage Waveform (V_{oRY})

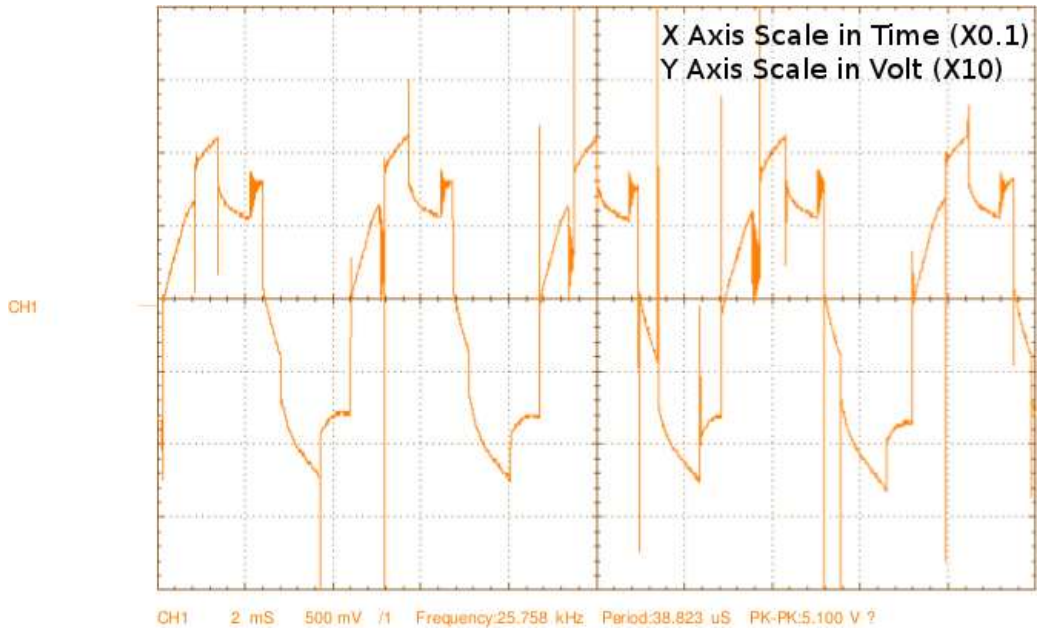

Figure 5.19: High Frequency Transformer Output Voltage Waveform (V_{oYB})

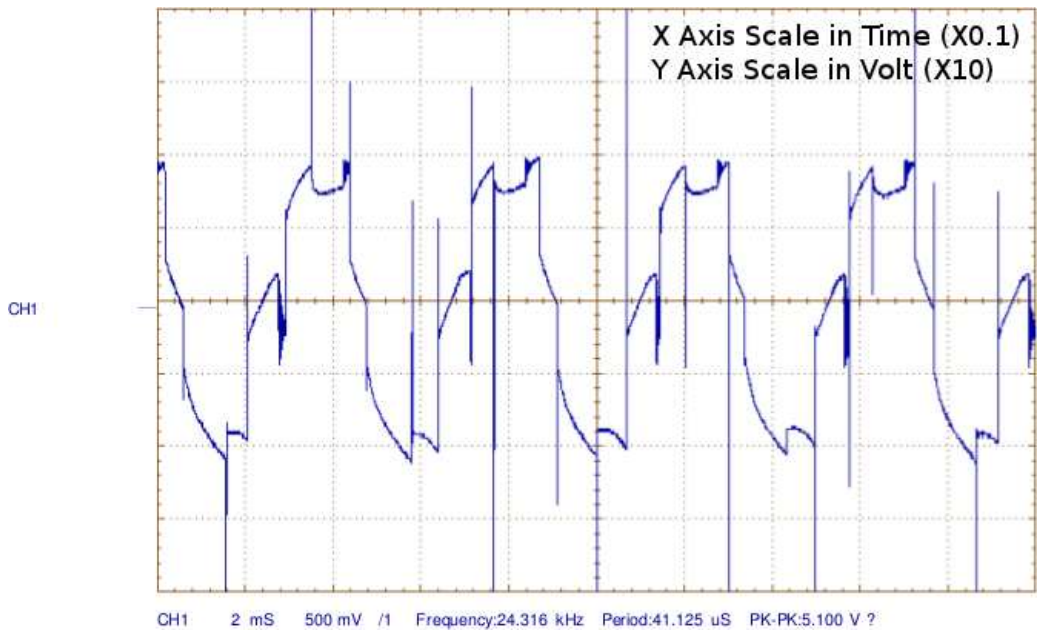

Figure 5.20: High Frequency Transformer Output Voltage Waveform (V_{oBR})

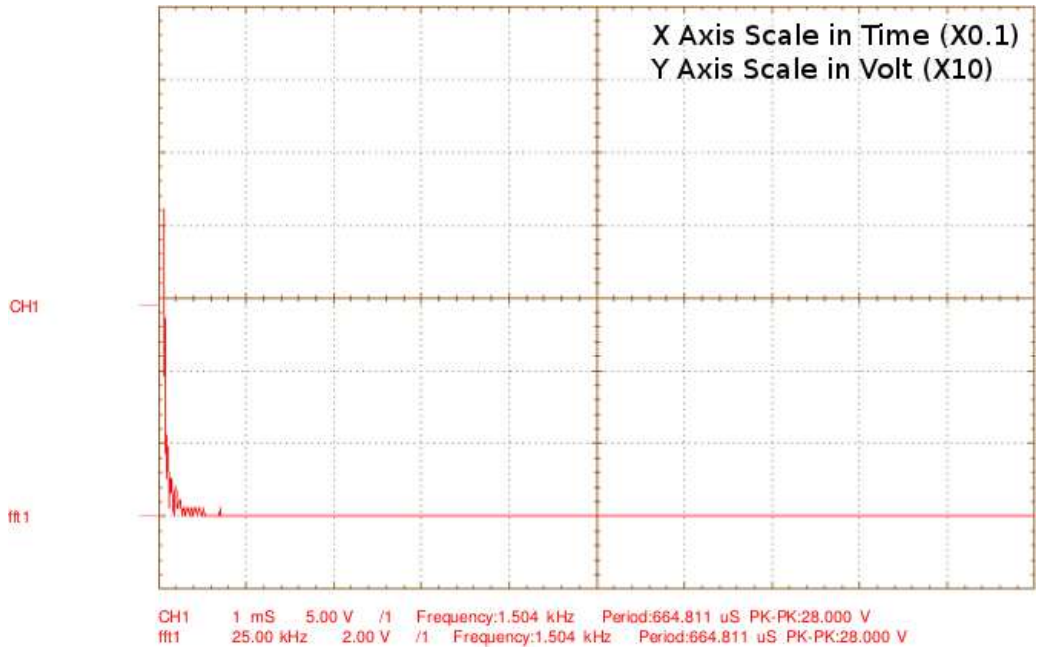

Figure 5.21: FFT of Three Phase Inverter Output Voltage Waveform (V_{iRY})

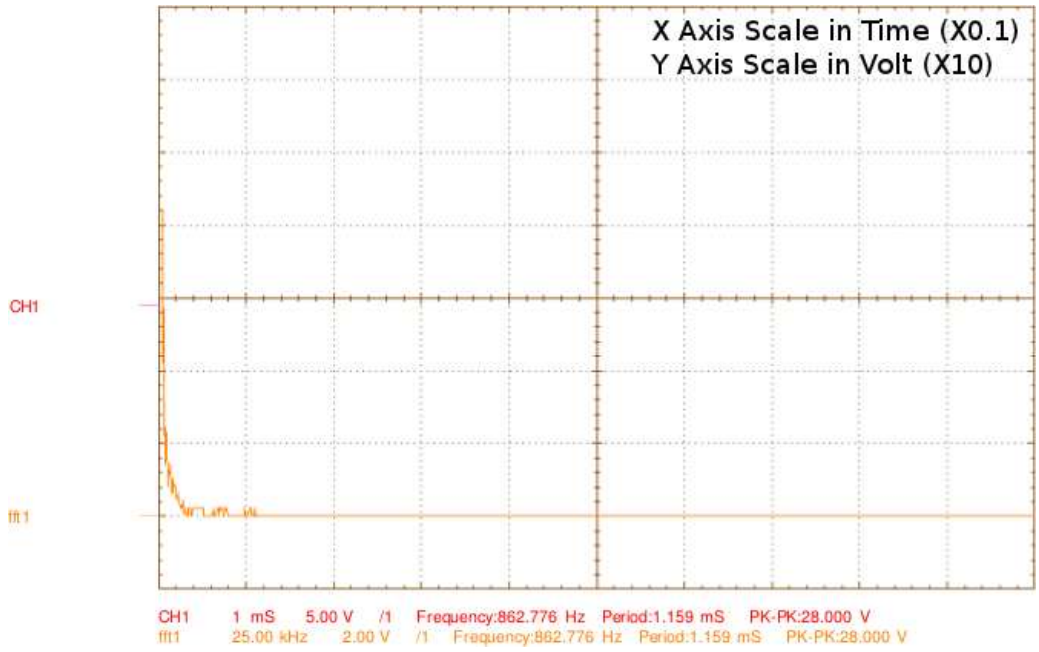

Figure 5.22: FFT of Three Phase Inverter Output Voltage Waveform (V_{iYB})

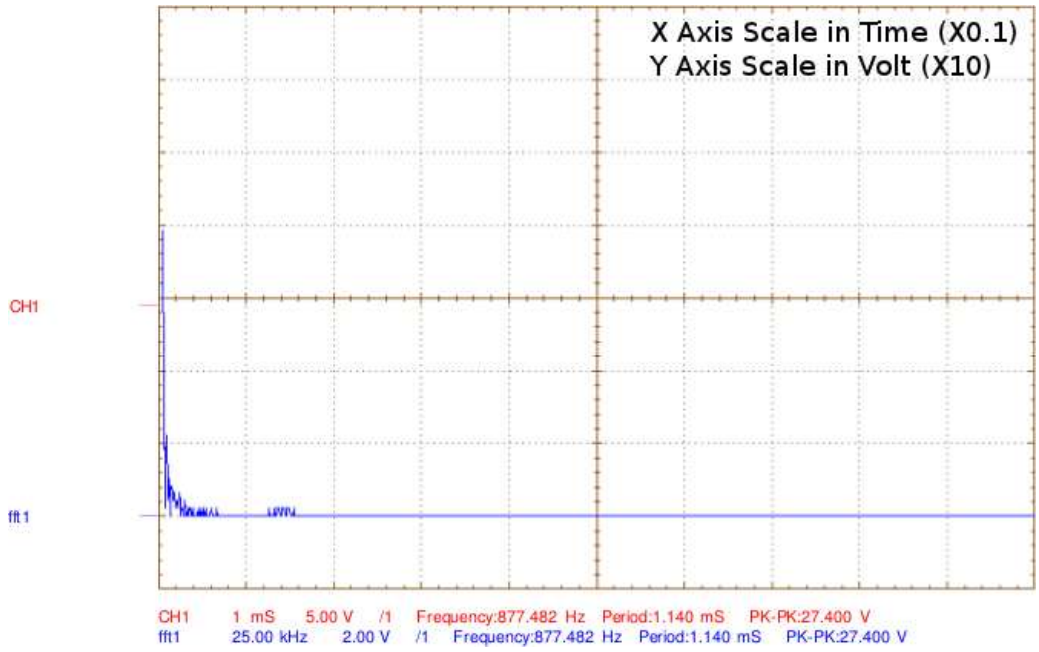

Figure 5.23: FFT of Three Phase Inverter Output Voltage Waveform (V_{iBR})

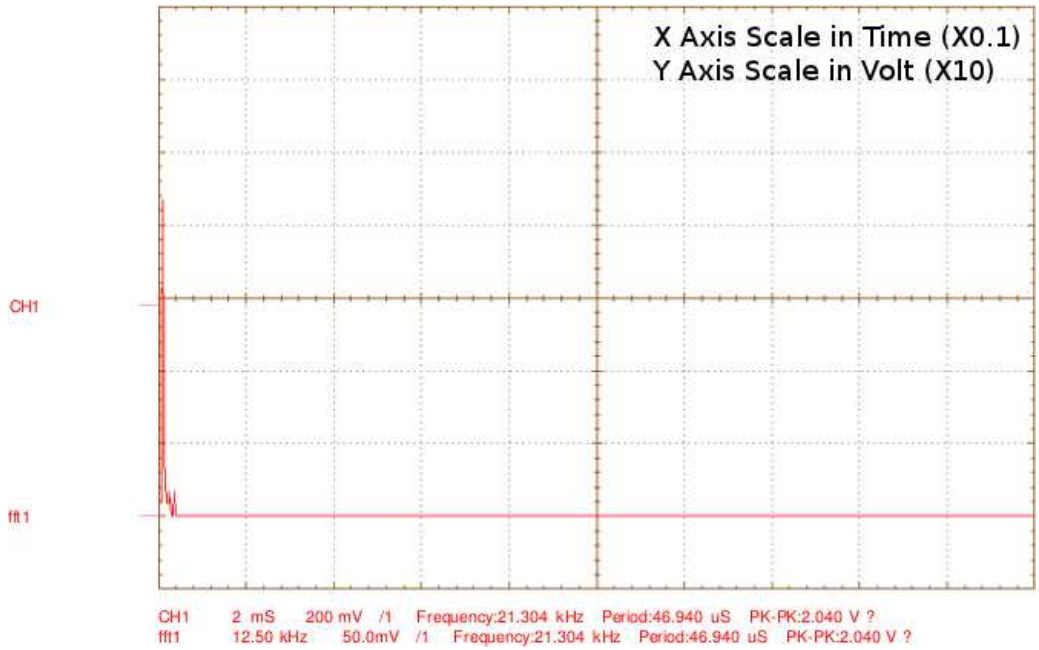

Figure 5.24: FFT of Three Phase IDH (V_{oRY})

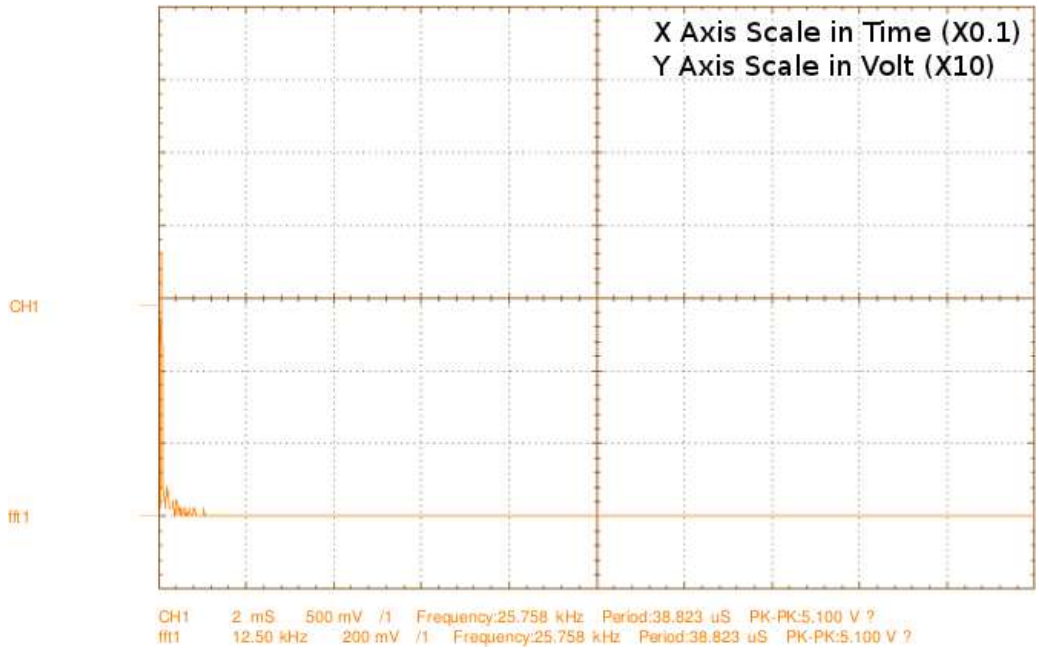

Figure 5.25: FFT of Three Phase IDH (V_{oYB})

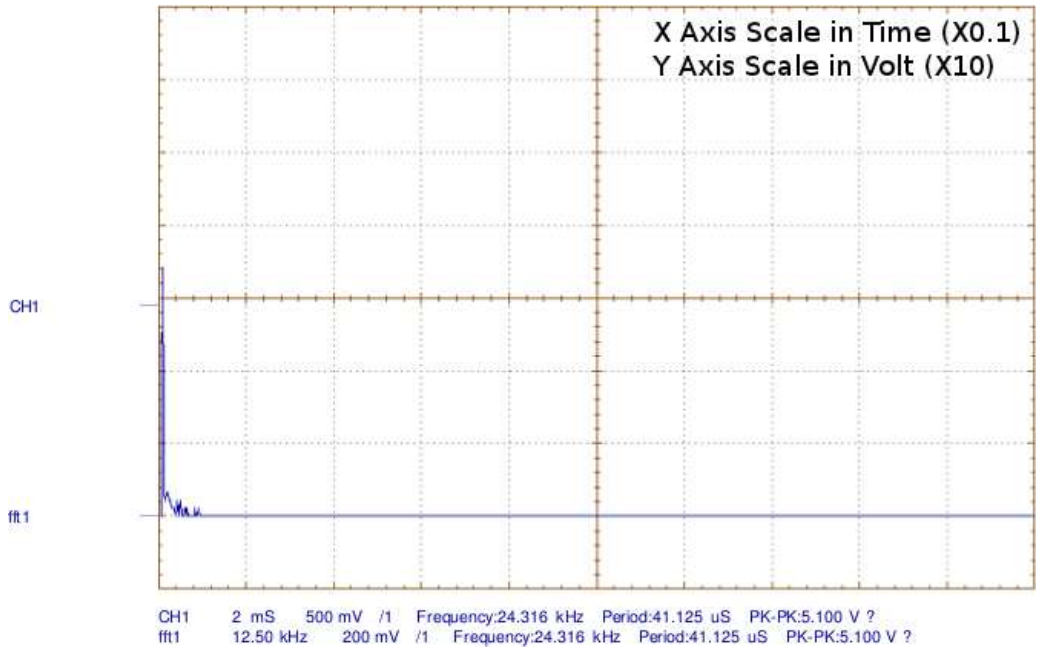

Figure 5.26: FFT of Three Phase IDH (V_{oBR})

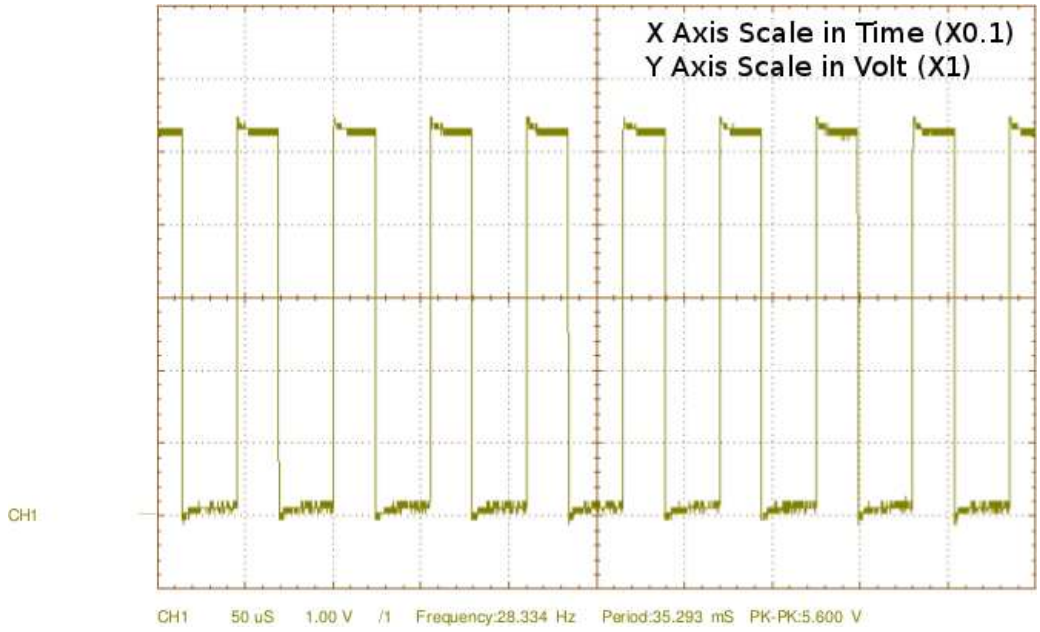

Figure 5.27: High Frequency Generator Unit

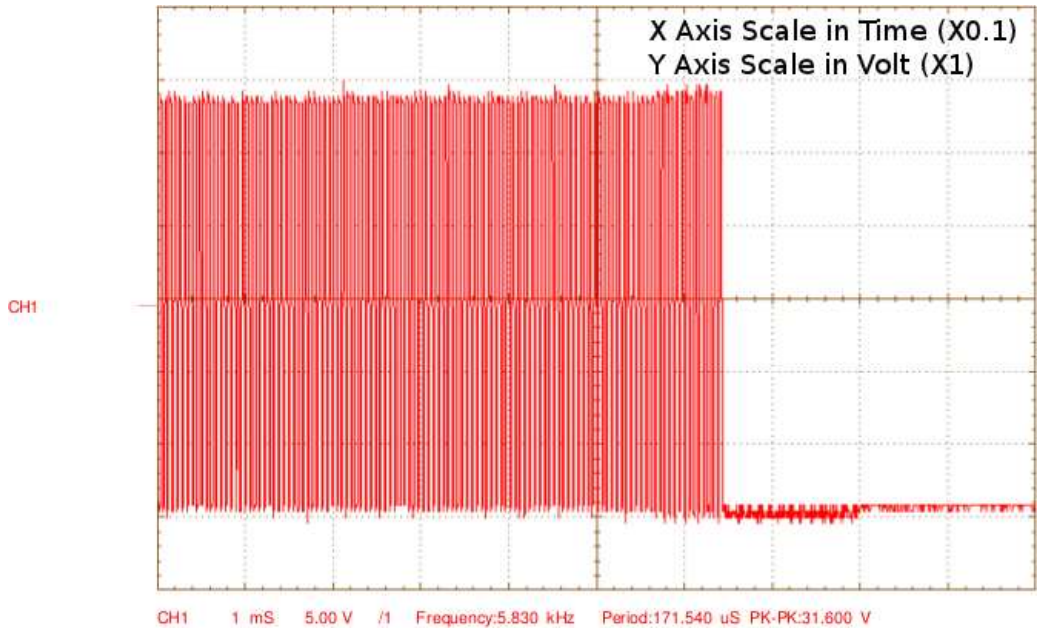

Figure 5.28: Gate Pulse for S_1 Using High Frequency Generator Unit

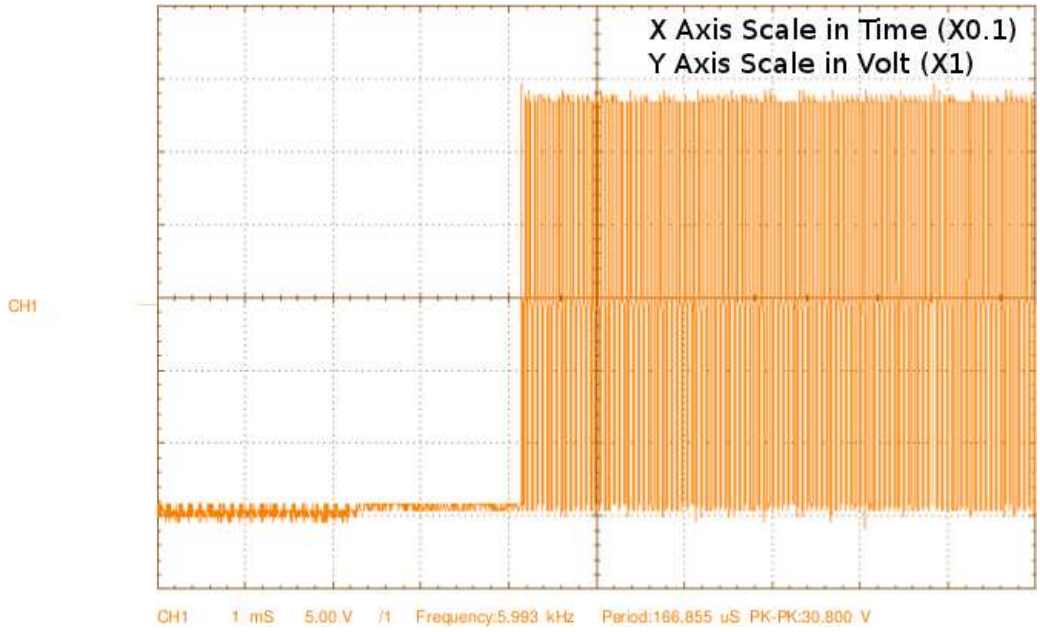

Figure 5.29: Gate Pulse for S_3 Using High Frequency Generator Unit

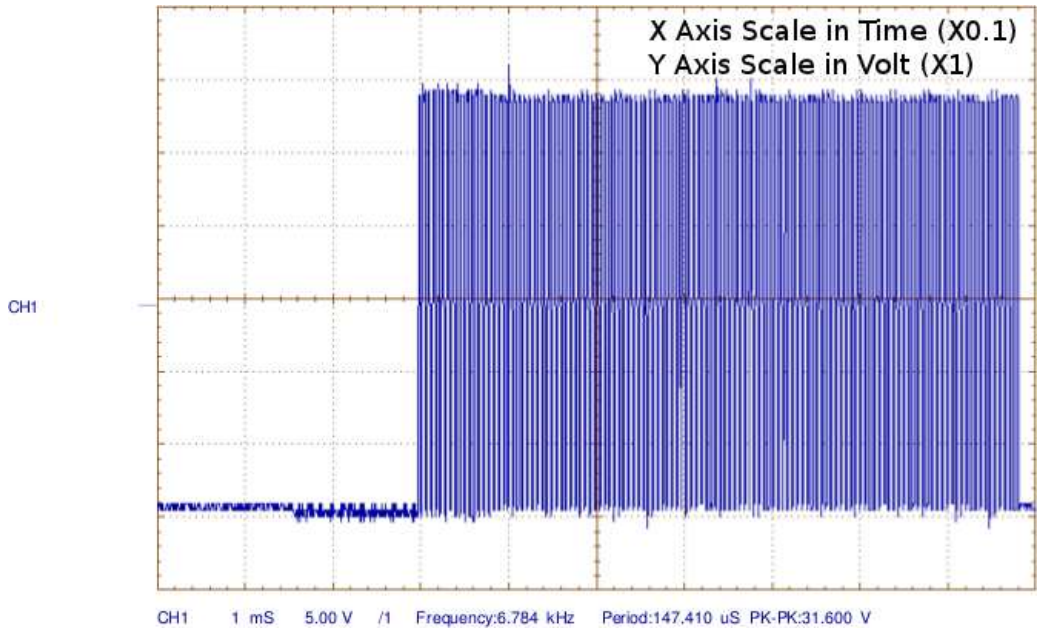

Figure 5.30: Gate Pulse for S_5 Using High Frequency Generator Unit

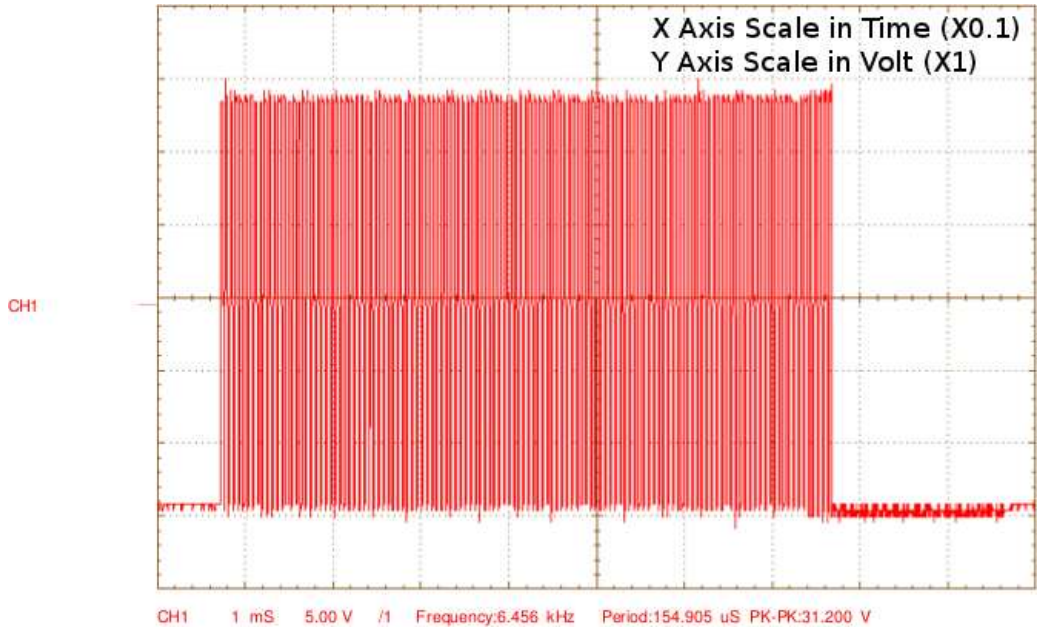

Figure 5.31: Gate Pulse for S_4 Using High Frequency Generator Unit

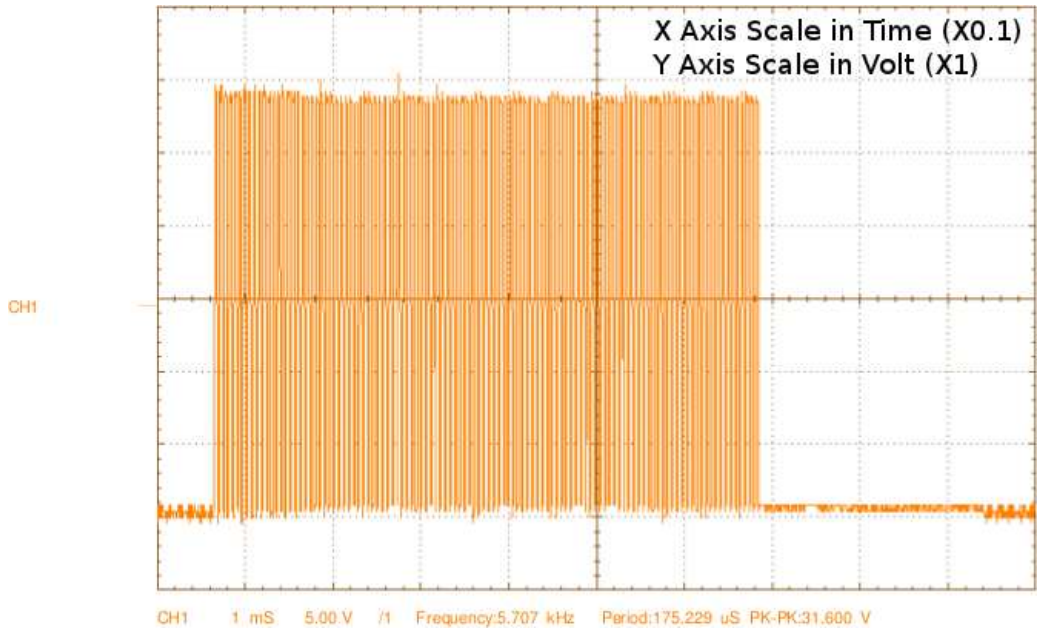

Figure 5.32: Gate Pulse for S_6 Using High Frequency Generator Unit

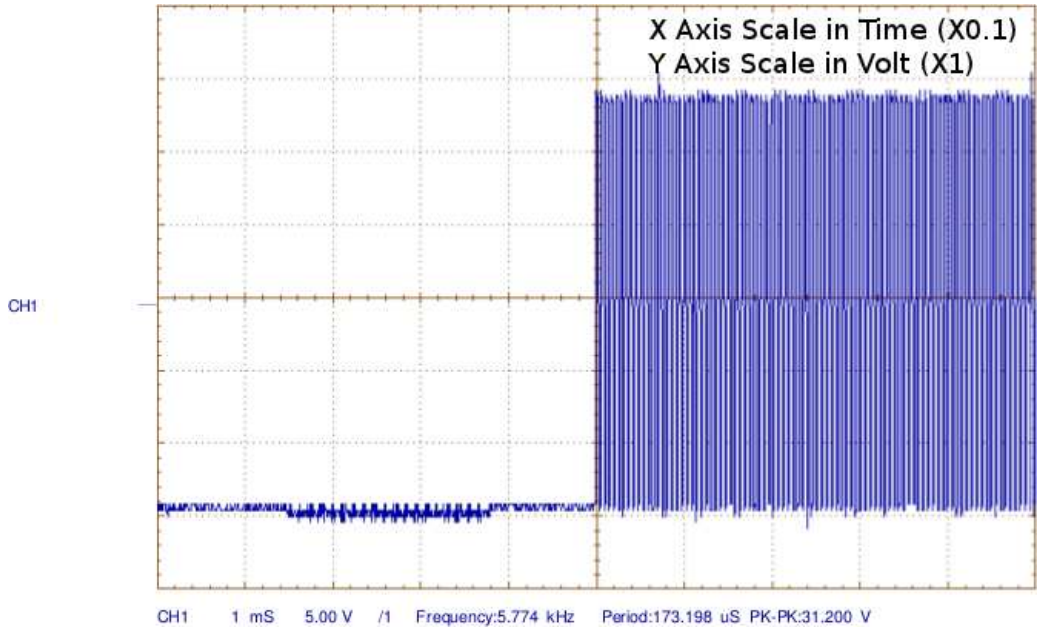

Figure 5.33: Gate Pulse for S_2 Using High Frequency Generator Unit

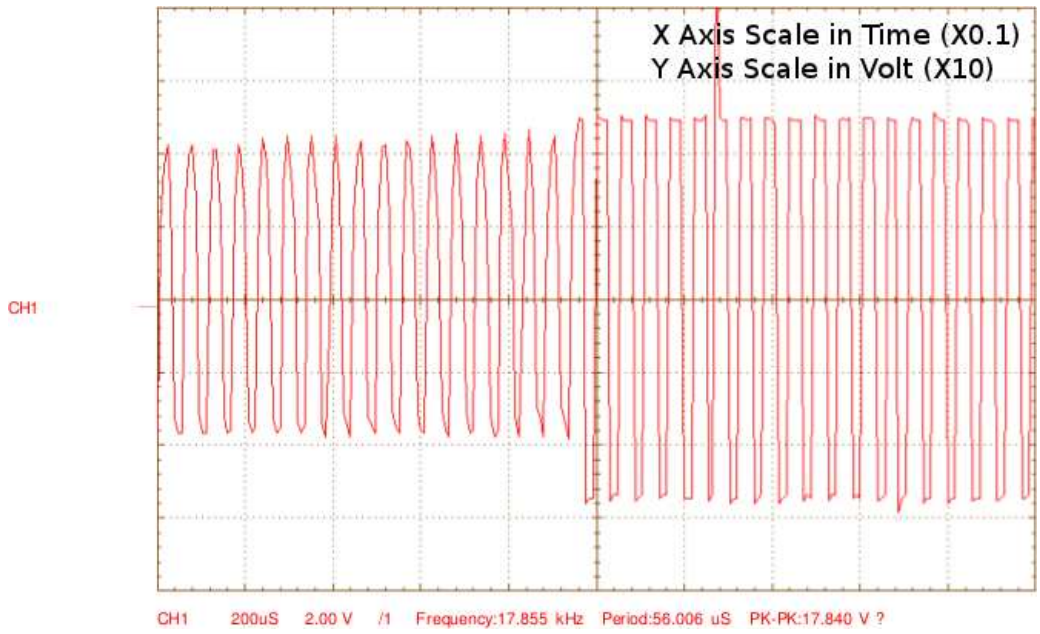

Figure 5.34: High Frequency Transformer Input Voltage Waveform (V_{iRY})

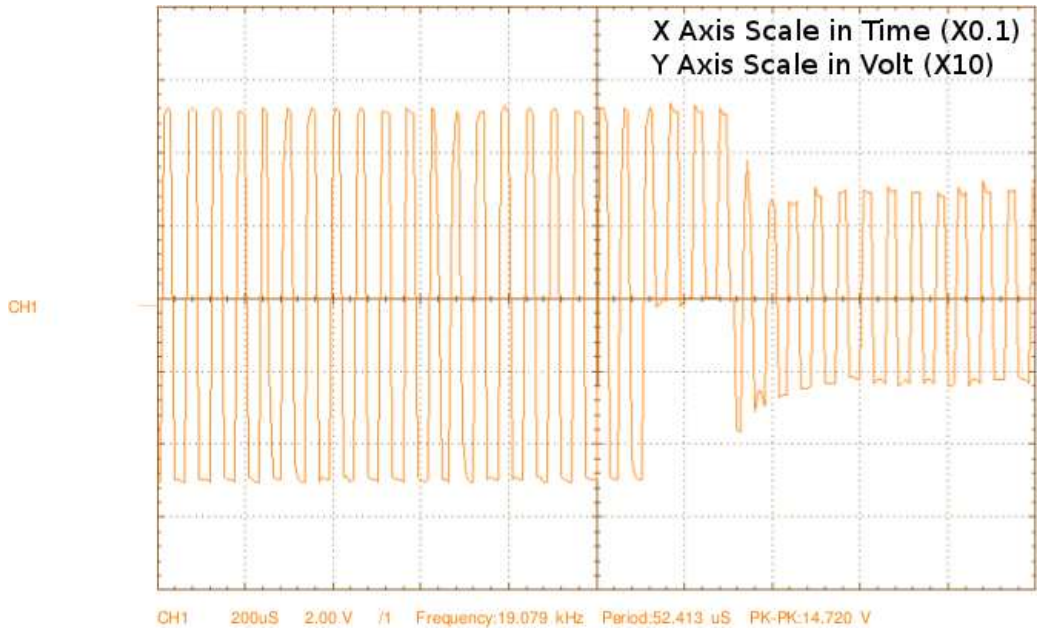

Figure 5.35: High Frequency Transformer Input Voltage Waveform (V_{iYB})

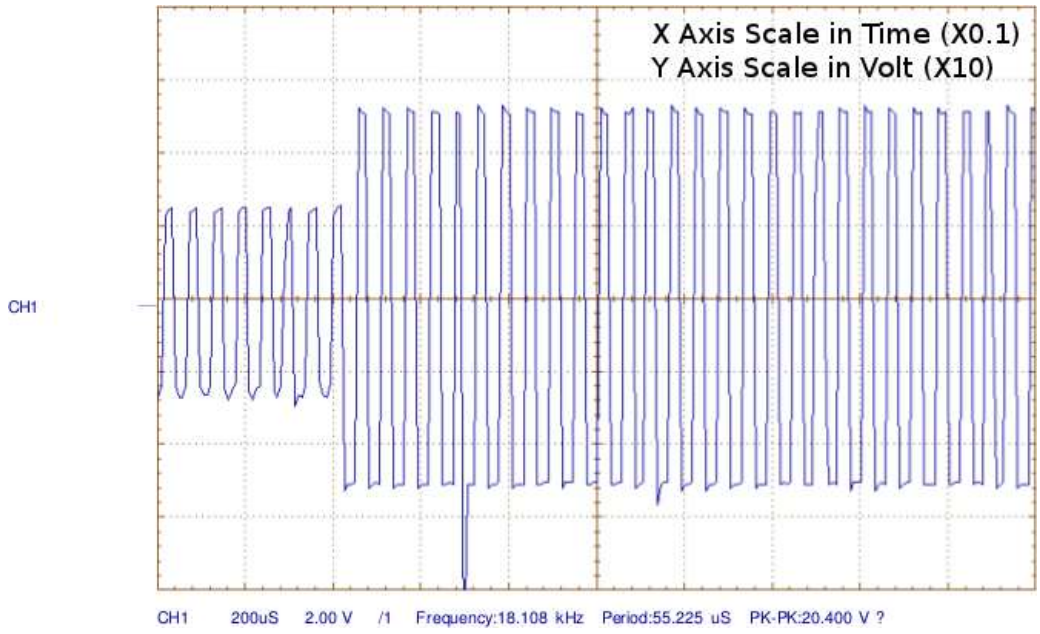

Figure 5.36: High Frequency Transformer Input Voltage Waveform (V_{iBR})

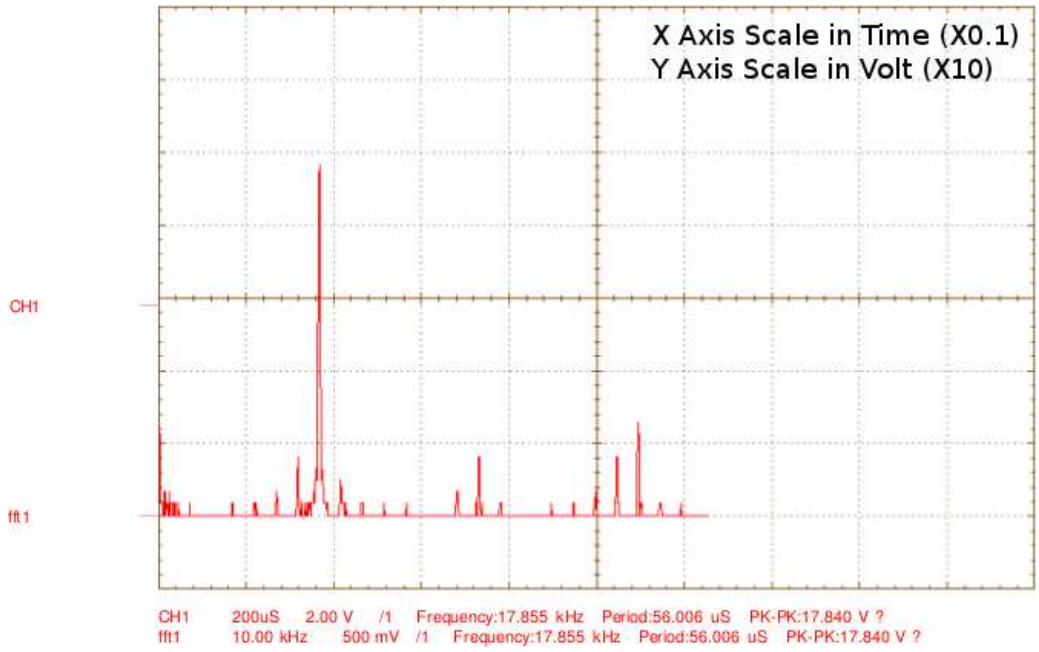

Figure 5.37: FFT of Three Phase Inverter Output Voltage Waveform (V_{iRY})

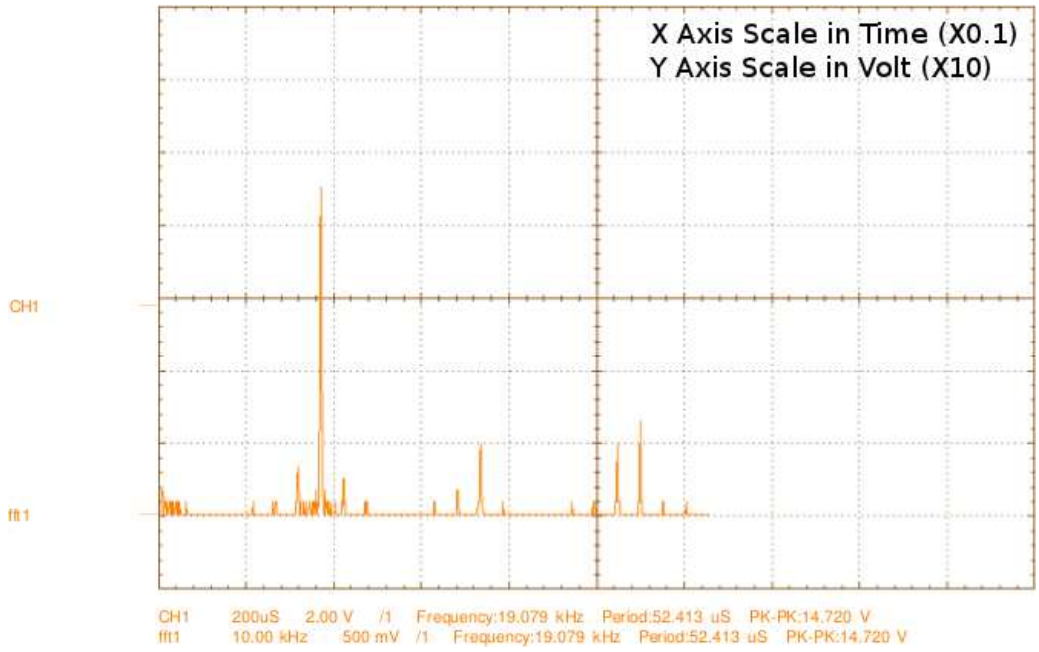

Figure 5.38: FFT of Three Phase Inverter Output Voltage Waveform (V_{iYB})

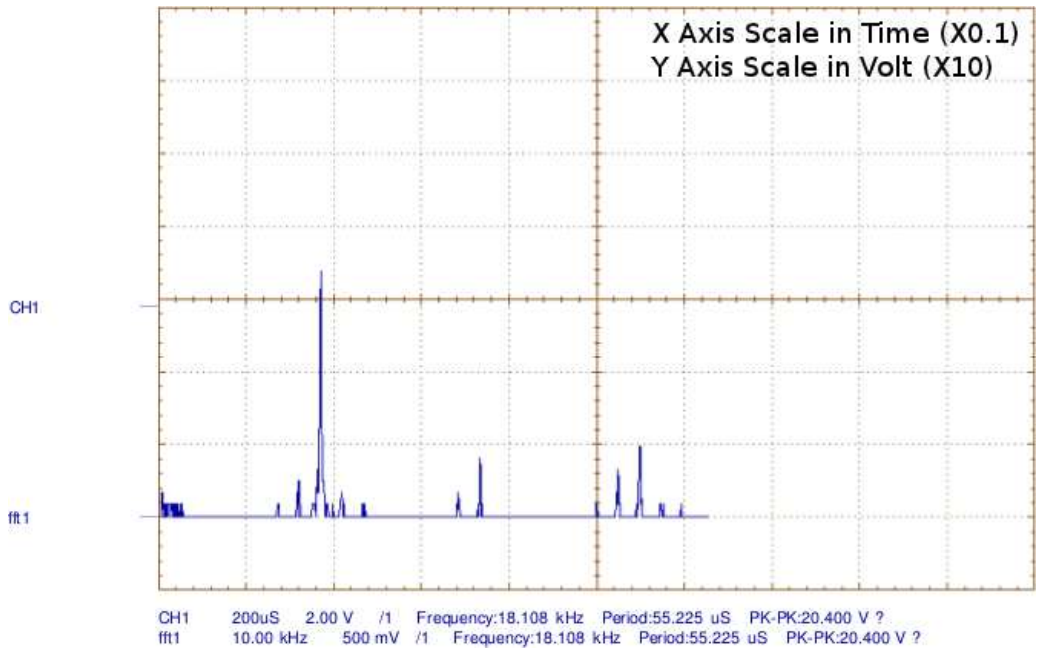

Figure 5.39: FFT of Three Phase Inverter Output Voltage Waveform (V_{iBR})

Figure 5.40: Sample Result 1

Figure 5.41: Sample Result 2

5.7 Conclusions

This chapter has described an induction dielectric heating experimental control structure and reveals the following findings:

1. This experiment demonstrated the ability of voltage level conversion ability, which leads to desired power even at low input voltage levels.
2. As frequency increases, the current becomes concentrated along the outer surface of the object.
3. The frequency of load can be varied by encoder.
4. The proposed algorithm is flexible and suitable for advanced vector control.
5. The strategy of the switching minimizes the distortion of load current as well as loss due to minimization commutations in the inverter.
6. Experimental technique of Induction Dielectric Heating (IDH) has been developed using micro controller.
7. The effectiveness of the SVM in the contribution in the switching power losses reduction has been demonstrated by performing an experiment.
8. SVM is one of the best solutions to achieve good voltage transfer.
9. It also provides excellent output performance optimized efficiency and high reliability compared to similar three phase inverter with conventional pulse width modulations.
10. Flexibility aspects of switching transformer leads to several advantages such as nearly unity power factor without using any reactive elements, symmetric loading from utility point of view, isolation of working coil, compact dimensions and almost uniform output voltage and temperature. It is proved by experimental setup.

Chapter 6

CONCLUSIONS

6.1 General

This thesis has addressed modulation techniques for IDH system, mathematical model of heating for conducting and non-conducting material, simulation results and experimental verification for induction dielectric heating system. The main contribution of the thesis includes the development of,

- A symmetrical space vector modulation pattern, to reduce Total Harmonic Distortion (THD) without increasing the switching losses. The design and implementations of a 3 phase PWM inverter for 3 phase IDH to control temperature using space vector modulation (SVM) as described in Chapter 2,
- A mathematical model of IDH for obtaining a reflection coefficient, transmission coefficient and electromagnetic wave properties for the work-piece, as descried in Chapter 3,
- An induction dielectric heating device with high frequency transformer structure has been developed. Comparison of results of proposed circuit has been carried out both by mathematical analysis and simulation and is described in Chapter 4 and
- An induction dielectric heating experimental control structure has been developed. The IDH concepts and their advantages are discussed in Chapter 5.

The Objective of this concluding chapter is to highlight the main finding of the work carried out in this thesis and provide suggestions for further research work in this area.

Some of the main findings are given below.

6.2 Summary of Important Findings

In chapter 2 design and implementation of a 3-phase pulse width modulation for three phase induction dielectric heating has been described. The system has been used to control temperature using symmetrical space vector modulation and the effect on temperature of frequency. The mathematical model has been developed and it has been simulated using Matlab.

The main finding of this chapter reveals following:

1. Space vector modulation requires only a reference space vector to generate three phase sine wave.

2. The amplitude and frequency of load voltage can be varied by controlling the reference space vector.

3. The algorithm proposed is flexible and suitable for advanced vector control.

4. The strategy of the switching minimizes the distortion of load current as well as loss due to optimum number of commutations in the inverter.

5. The effectiveness of the SVM to reduce the switching power losses reduction has been proved.

6. SVM is among one of the best solutions to achieve good voltage transfer and reduce harmonic distortion in the output of three phase inverter for IDH.

7. SVM provides excellent output performance, optimized efficiency and high reliability compared to similar three phase inverter with conventional pulse width modulations.

Chapter 3 has been devoted to mathematical model for obtaining a reflection coefficient, transmission coefficient and electromagnetic wave properties for the work-piece contribution to the impedance of a given IDH system. This is intended to assess how work-piece is linked to the excitation loop and to find out conditions where the eddy current or displacement current occurrence is enhanced. Empirical rules already known by IDH practitioners have been proved and the finding can be extrapolated to design

new possibilities. The proposed approach has been validated using MATLAB and FEM software.

The main finding of this chapter reveals following:

1. As frequency increases, the current becomes concentrated along the outer surface of the object.

2. The electromagnetic shield may be necessary to prevent waves from radiating out of the shielded volume or to prevent waves from penetrating into the shielded volume.

3. Attenuation constant, phase constant and propagation constant increases with increase in frequency in conducting material and non-conducting material.

4. Intrinsic impedance increases with increase in frequency in conducting material and is remaining constant with increase in frequency for non-conducting material.

5. Velocity of propagation and intrinsic impedance of conducting material exponentially increases with increase in frequency and reactive component of conducting material remains constant at 45^0.

6. Velocity of propagation and intrinsic impedance of non-conducting material remains constant with increase in frequency and reactive component of non-conducting material is small.

In chapter 4 an induction dielectric heating device with high frequency transformer structure has been described. Comparison of proposed circuit has been carried out both by mathematical analysis and by simulation. The result shows that value of power factor obtained is unity. Flexibility aspects of switching transformer leads to several advantages such as unity power factor without using any reactive element, symmetric loading from utility point of view, isolation of working coil, compact dimensions and almost uniform sinusoidal output.

Additionally, this topology can provide any voltage level conversion ability, which leads to desired power even at low input voltage levels. Furthermore, proposed topology provides maximum output power and reduced THD utilization. This requires comparatively smaller size of matching filter coil which work suitably with auto tuning switching frequency controller.

An induction dielectric heating experimental control structure has been described in chapter 5.

The main finding of this chapter reveals following:

1. This experiment demonstrated the ability of voltage level conversion ability, which leads to desired power even at low input voltage levels.

2. As frequency increases, the current becomes concentrated along the outer surface of the object.

3. The frequency of load can be varied by encoder.

4. The proposed algorithm is flexible and suitable for advanced vector control.

5. The strategy of the switching minimizes the distortion of load current as well as loss due to minimization commutations in the inverter.

6. Experimental technique of Induction Dielectric Heating (IDH) has been developed using micro controller.

7. The effectiveness of the SVM in the contribution in the switching power losses reduction has been demonstrated by performing an experiment.

8. SVM is one of the best solutions to achieve good voltage transfer.

9. It also provides excellent output performance optimized efficiency and high reliability compared to similar three phase inverter with conventional pulse width modulations.

10. Flexibility aspects of switching transformer leads to several advantages such as nearly unity power factor without using any reactive elements, symmetric loading from utility point of view, isolation of working coil, compact dimensions and almost uniform output voltage and temperature. It is proved by experimental setup.

6.3 Scope for Further Research

Consequent to investigations carried out in thesis, the following aspects are being suggested as future work to be carried out.

1. By using different modulation techniques, the effect on performance like efficiency, rate of heating and most efficient production equipment can be made.
2. With the use of IDH method adopted, the characteristic behaviour of metal or food on rate of heating can be analyzed.
3. Three phase induction dielectric melting can be investigated.
4. In chapter 5, an open loop approach was used for IDH system. It can be extended for a close loop approach.
5. The feasibility of use of IDH in place of microwave oven can be investigated.

Bibliography

[1] Jin-Woo Jung, *Space Vector PWM Inverter*, Ph.d Student, Ohio State University.

[2] Bierwirth R. A., and Hoyler C. N., *Radio Frequency Heating Applied to Wood Gluing*, Processing of the I.R.E., pp. 529-537, Oct. 1943.

[3] E.R. Laithwaite, *Linear induction motors*, The Institution of Electrical Engineers, pp. 461-470, Dec. 1957.

[4] Simpson P. G., *Induction heating coil and system design*, McGraw Hill book company, London, 1960.

[5] Bengtsson N. E., *Radio Frequency heating application in the European Food Industry*, Microwave Energy Application Newsletter , Vol. 2, No. 4, pp. 3, 1969.

[6] Leatherman, A. F. and D. E. Stutz, *Induction Heating Advances*, National Aeronautics and Space Administration, 1969.

[7] Nils E. Bengtsson, and Thomas Ohlsson, *Microwave Heating in the Food Industry*, Procceeding of the IEEE, Vol. 62, No.1, Jan. 1974

[8] S.R.Bowes, *New sinusoidal pulse width modulation inverter*, Proceedings International Electronic Engineering, Vol. 122, pp.1279-1285, 1975.

[9] G. Buja and G. Indri, *Improvement of pulse width modulation techniques*, Archiv jiir Electro technik, Vol.57, pp.281-289, 1975.

[10] Depenbrock M., *Pulse width control of a 3-phase inverter with non sinusoidal phase voltages*, in Proc. IEEE-IAS Int. Semiconductor Power Conversion Conference, Orlando, FL, pp. 389-398, 1975 .

[11] I. G. Harvey, *A method of improving the energy transfer in induction heating processes and its application in a 1 MW billet heater*, IEEE conference publication, 149: Electricity for Materials processing and conservation, pp. 16-20, 1977.

[12] E. Davies, *Induction heaters*, British Patent No. 1 513242, June 1978.

[13] J. Davies, P. Simpson, *Induction Heating Handbook*, McGraw-Hill Company, UK, ch.2, pp. 43-48, 1979.

[14] Alesina A., Venturini M. G. B., *Solid state power conversion: a Fourier analysis approach to generalized transformer synthesis*, IEEE Transactions on Circuit and Systems, Vol. CAS-28, No. 4, pp.319-330, April 1981.

[15] A.L. Bowden, E.J. Davies, *Travelling wave induction heaters: design consideration*, BNCE-UIE Electroheat for Metals Conference, Cambridge, England, N.5.2, 21-23 September 1982.

[16] E. Bercovich, G. Ivensky, U. Matchak, and V. Morgun, *Medium frequency converters for electric industrial devices*, Energoatomizdat, Leningrand, pp.30, 1983.

[17] P. Bhagwat and V. Stefanovi c., *Generalized Structure of a Multilevel PWM Inverter*, IEEE Transaction on Industry Applications, Vol.IA-19,Issue 6 pp. 1057–1069, Nov. 1983.

[18] Bose B. K. and Sutherland H. A., *A high performance pulse width modulator for an inverter-fed drive system using a microcomputer*, IEEE Translation Industrial Application., Vol. 19, pp. 235-243, Mar./Apr. 1983.

[19] Murai,Y., Sugimoto S., Iwasaki, H., Tsunehiro Y. *Analysis of PWM Inverter Fed Inductions Motors for Microprocessors*, Proceedings IEEE/IECON, pp.58-63, 1983.

[20] Y.Murai, Y.Tsunehiro, *Improved PWM Method for Induction Motor Drive Inverters*, IPEC, Tokyo, pp.407-417, 1983.

[21] Hale G.E. and Nutting J., *Overheating of Low Alloy Steels*, International Metals Reviews, Vol. 29, 1984.

[22] Decareau R.V., *Microwaves in the Food Processing Industry*, Academic Press, Inc., New York, 1985.

[23] S. R. Elowes and A. Midoum, *Suboptimal switching strategies for microprocessor-controlled PWM inverter drives*,Electric Power Applications, IEE Proceedings B, Vol.132,Issue 3, pp. 133-148, May 1985.

[24] S. Hinchliffe and L. Hobson, *Review of Solid State Devices and Circuit for HF Electric Process Heating Application*, International Journal of Electronics, Vol.61, No.2, pp. 143-167, 1986.

[25] H. Van der Broeck, H. Skudelny, and G. Stanke, *Analysis and realization of a pulse width modulator based on voltage space vectors*, in Proceedings IEEE Ind. Applications Conference, pp.244-251,1986.

[26] *Direct and Encased Resistance Heating*, Published by the Center for Metals Fabrication, Vol. 3. No. 8. 1986.

[27] P.L. Jones, *Radio frequency processing in Europe*, Journal of Microwave Power Electromagnetic Energy, Vol.22, No.3, pp.143-153, 1987.

[28] P.P. Yannopoulos, J.A. Tegopoulos, *Three dimensional eddy current distribution in cylinders due to rotating magnetic fields*, IEEE Transactions on Magnetics, Vol.23, Issue 5, pp. 3056- 3058, Sept. 1987.

[29] Zinn, S. and S. L. Semiatin, *Elements of Induction Heating: Design, Control and Applications*, ASM International, Dec. 1987.

[30] H. W. Van Der Broeck, H. C. Skudenly, G. V. Stanke, *Analysis and Realization of a Pulse Width Modulator Based on Voltage Space Vectors*, IEEE Transaction on Industry Applications, Vol.24, No.1, pp.142-150, Feb. 1988,.

[31] Leonard Harrison W. *Electric Power for Industrial processes using Dielectric Heating*, Power Engineering Journal, pp. 105-113, March 1988.

[32] Alesina A., Venturini M. G. B., *Analysis and design of optimum amplitude nine switch direct AC-AC converters*, IEEE Transactions on Power Electronics, Vol. 4, No. 1, pp. 101-112, Jan. 1989.

[33] Jin Yuan Chen, and Om P. Gandhi, *Electomagnetic Deposition in an Anatomically Based Model of Man for Leakage Fields of a Parallel Plate Dielectric Heater*, IEEE Transactions on Microwave theory and techniques, Vol.37, No.1, Jan. 1989.

[34] Granado, J., Harley, R.G., Diana G., *Understanding and Designing a Space Vector Pulse-Width-Modulator to Control a Three Phase Inverter*, Transaction of the SAIEE, Vol.80, pp.29-37, Sept.-1989.

[35] S. Ogasawara, H. Akagi, and A. Nabae, *A novel PWM scheme of voltage source inverters based on space vector theory*, in Proceedings of EPE'89, Aachen, Germany, pp.1197-1202, 1989.

[36] Davies E. J., *Conduction and Induction Heating*, London: Peregrinus, 1990.

[37] F.P.Dawson and P.Jain, *System for Induction heating and Melting applications a comparison of load commutated Inverter*, Power Electronics Specialists Conference, 1990. PESC '90 Record., 21st Annual IEEE ,pp.281 - 290, 11-14 June 1990.

[38] Fukuda, S., Iwaji, Y., Hasegawa H., *PWM Technique for Inverter with Sinusoidal Output Current*, IEEE Transaction on Power Electronics, Vol. 5, Issue:5, pp.54-61,Jan 1990.

[39] Dawson, F.P., and Jain, P.*A Comparison of Load Commutated Inverter Systems for Induction Heating and Melting Applications*, IEEE Transaction on Power Electronic,Vol. 6,Issue:3, pp. 430-441, July-1991.

[40] R. Ducharme, F. Scarfe, P. Kapadaia and J. Dowden, , *The Induction Heating in Glass*, Journal of Physics-D, Vol. 24, No.5, pp. 658-663, 1991.

[41] Lawrence R. E. and Edward P. F., *A Computer Simulation of an Induction Heating System*, IEEE Transaction on Magnetic , Vol. 27, No. 5, pp. 4343-4354,Sep. 1991.

[42] T. Kunie, et al., *A novel PWM technique to decrease lower harmonics*, in Proceedings of EPE'91, Vol. 3, pp.223-227, 1991.

[43] *Dielectric Heating* working group, Dielectric Heating for Industrial Processes, U.I.E. Paris, 1992.

[44] J.Holtz, *Pulse width Modulation - A Survey*, IEEE Transaction on IE, Vol.39, No.5, pp.410-420, Dec.-1992.

[45] J. Holtz, W. Lotzkat, A. Khambadkone, *On Continuous Control of PWM Inverters in the Over modulation Range Including the Six-Step Mode*, Proceedings of the 1992 International Conference on Industrial Electronics, Control, Instrumentation, and Automation, Power Electronics and Motion Control.,Vol. 1, pp.307-312, 9-13 Nov. 1992.

[46] V. R. Stefanovic and S. N. Vukosavic, *Space-vector PWM voltage control with optimized switching strategy*,Industry Applications Society Annual Meeting, Conference Record of the 1992 IEEE ,Vol.1, pp.1025-1033, 4-9 Oct. 1992 .

[47] D.Casadei,G.Grandi,G.Serra and A Tani, *Space vector control of matrix converters with unity input power factor and sinusoidal input/output waveforms*, European power electronics association, 1993.

[48] F.Dughiero, S.Lupi, P.Siega, Analytical Calculation of Traveling Wave Induction Heating Systems, International Symposium on Electromagnetic Fields in Electrical Engineering 1993, Warsaw-Poland, pp. 207-210, 16-18 September 1993.

[49] Fisher, G., Doht, H.C., and Hemmer, B. *Operation Modes of Series Inverter 400kHz for Induction Heating*. Conference ERE, Proceedings European power electronics, London, UK, pp. 322–327, 1993.

[50] Grajales, L., Sabate, J.A., Wang, K.R., Tabisz, W.A., and Lee, F.C.*Design of a 10kW, 500 kHz phase-shift controlled series-resonant inverter for induction heating*. Proceedings Industry applications society annual meeting, Toronto, Oat., Canada, pp. 843–849, 1993.

[51] T.G.Habelter,*A sapce vector based rectifier regulator for AC/DC/AC converter*, IEEE Transaction on Power Electronics,Vol.8, No.1, pp.30-36, 1993.

[52] L.Serrano, Iribarnegaray, *The Modern Space Vector Theory, Part I: Its Coherent Formulation and Its Advantages for Transient Analysis o Converter-Fed AC Machines*, ETEP, Vol.3, No.2, March/April-1993.

[53] Dughiero F., Lupi S., Nemkov V., Siega P., *Traveling wave Inductors for the continuous Induction heating of metal strips*, Electro Technical Conference, Proceedings., 7th Mediterranean, Vol.3, pp.1154-1157, April 1994.

[54] J. Holtz, *Pulse width modulation for electronics power conversion* , Proceedings IEEE, Vol.82, pp.1194-1214, Aug-1994.

[55] A. Quarteroni and A. Vialli, *Numerical Approximation of Partial Differential Equation* , Springer Series in Computational Mathematics 23. Bertine Springer Verlag, 1994.

[56] *Indirect Resistance Heating*, Published by the EPRl Center for Materials Fabrication, Vol. 3, No. 7 Revised 1994.

[57] Dughiero F. , Lupi S, and Siega P., *Calculation of forces in travelling wave induction heating systems*, IEEE Transactions on Magnetics, Vol. 31, No. 6, Nov. 1995.

[58] Lucanu, M., Neacsu, D., *Optimal V/f Control for Space Vector PWM Three-Phase Inverters*, European Transactions on Electrical Power Engineering, Vol.5, No.2, pp.115-120, March/April-1995.

[59] V. Bukanin, V. Nemkov, F. Dughiero, M. Forzan, S. Lupi, *Induction heating of flat metal bodies*, Proc. of BNCE-VIE International Congress on Electricity Applications, Birmingham, UK, Vol. 1, pp.3-17, 16-20 June 1996.

[60] M.Kamli, S.Yamamoto, and M. Abe, *A 50-150 kHz Half-Bridge Inverter for induction heating application*, IEEE Transactions on Industrial Electronics, Vol. 43, pp. 163-172, Feb. 1996.

[61] A. C. Metaxes, *Foundations of Electro heat*, Chichester, U.K., Wiley,ISBN 0-471-95644-9, 1996

[62] Ying-yu Tzou, Hau-Jean Hsu, Tien-Sung Kuo. *FPGA based SVPWM control IC for 3-phase PWM inverters*, Industrial Electronics, Control and Instrumentation, Proceedings of the IEEE IECON 22nd International Conference, Vol.1, pp.138-143, 5-10 Aug. 1996.

[63] Chaboudez C., Clain S., Glardon R. Mari D. Rappaz J., and Swierkosz *Numerical Modealing in Induction Heating for Axisymmetric Geometries*, IEEE Transaction on Magnetic, Vol. 33, No. 1, pp. 739-745, Jan. 1997.

[64] Z. Yu, A. Mohammed, and I. Panahi, *A review of three pwm techniques*, in Proceedings Amer. Control Conference, pp. 257-261, 1997.

[65] *Saving Energy with Electric Resistance Heating*, Energy Efficiency and Renewable Energy, U.S., DOE/GO-10097-381, FS 230, Oct.1997.

[66] S.M. Bradshaw, E.J. van Wyk, and J.B. de Swardt, *Microwave heating principles and the application to the regeneration of granular activated carbon*, The Journal of The South African Institute of Mining and Metallurgy, pp. 201-212, July/Aug. 1998.

[67] D. W. Chung, J. S. Kim, and S. K. Sul, *Unified voltage modulation technique for real time three phase power conversion*, IEEE transactions industrial application , Vol.34, pp.374-380, Mar./April-1998.

[68] Davies P. G. , *State of art of the transverse flux induction heatings*, Proc. of UIE Induction Heating Seminar, Padua, pp.105-109, 13-15 May 1998.

[69] Hava A. M., Kerkman R., and Lipo T. A., *Carrier-based PWM-VSI over modulation strategies: Analysis, comparison, and design*, IEEE Trans. Power Electron., vol. 13, pp. 674-689, July 1998.

[70] J. M. Ho and F. C. Juang, *4 Practical PWM Inverter Control Circuitry for Induction Heating and Studying of the Performance under Load Variations*, Proceedings IEEE Conference, International Symposium on Industrial Electronics, Vol.1, pp. 294-299, July-1998.

[71] I. Khan, J. Tapson and I. de Vries, *An Induction Furnace Employing a 100kHz MOSFET Full Bridge Current Source Load Resonant Inverter* , Proceedings IEEE Conference International Symposium on Industrial Electronics, Vol.2, pp. 530-534, July-1998.

[72] Dieckerhoff,S,Ruan, M.J,De Doncker, R.W., *Design of an IGBT-based LCL-Resonant Inverter for High-Frequency Induction Heating* , IEEE Conference on Industry Applications, Vol. 3, pp. 2039-2045, 3-7 Oct.1999.

[73] Lupi S., Dughiero F., and Forzan M., *Comparison of Edge-Effects of Transverse Flux and Travelling Wave Induction Heating Inductors*, IEEE Transactions on Magnetics, Vol. 35, No. 5. Sep. 1999.

[74] Kwon, Y.-S., Yoo, S.-B., and Hyun, D.-S. *Half-bridge series resonant inverter for induction heating applications with load-adaptive PFM control strategy.* Proceedings Applied power electronics Conference, Dalias, TX, USA, pp. 575–581, 1999.

[75] Do-Hyun Jang, and Duck-Yong Yoon, *Space-vector PWM techniques for two phase inverter fed two phase induction motor*, IEEE Conference, 1999.

[76] Peter Vas, *Artificial Intelligence based electrical machines and drives*, Oxford university, 1999.

[77] P. Dorland. and J. D. Van Diyck, *On the influence of coil design and electromagnetic configuration on the efficiency of an induction melting furnace*, IEEE transactions on Industry applications, Vol. 36, No.4, pp. 946-957, 2000.

[78] Sewell, H.I., Stone, D.A., and Bingham, C.M.*Novel, Three-Phase, Unity Power Factor Modular Induction Heater*, IEEE Proceedings, Power Electronic Application, Vol.147, pp.371-378, Sep. 2000.

[79] J. Klima, *Analytical model for the time and frequency domain analysis of space-vector PWM inverter fed induction motor based on the Laplace transform of space-vectors*, in Proceedings Power Conversion Conference, Osaka, Japan, pp. 1334-1339, 2002.

[80] G. Narayanan and V.T. Ranganathan, *Extension of operation of space vector PWM strategies with low switching frequencies using different over modulation algorithms*, IEEE Transaction Power Electronic, Vol.17, pp.788 -789, Sep. 2002.

[81] Chen R.Y. and Yeun W.Y.D., *Review of the High-Temperature Oxidation of Iron and Carbon Steels in Air or Oxygen*, Oxidation of Metals, Vol. 59, pp. 433-468, 2003.

[82] Christopher J., Cottee and Stephen R. Duncan, *Design of Matching Circuit Controllers for Radio Frequency Heating*, IEEE Transactions on Control System Technology, Vol.11, No.1, Jan.2003.

[83] Mondal, S.K., Bose, B.K., Oleschuk, V., Pinto, J.O.P, *Space vector pulse width modulation of three-level inverter extending operation into over modulation region*, IEEE Transactions on Power Electronics Vol.18, Issue 2, pp.604-611, March 2003.

[84] Kelly, J.W. Strangas, E.G. Miller, J.M. *Multiphase Space Vector pulse width modulation*, IEEE Transaction on Energy Conservations, Vol.18, No.2, pp.254-264, June 2003.

[85] Do-Hyun Jang, and Duck-Yong Yoon, *Space-vector PWM techniques for two phase inverter fed two phase induction motor*, IEEE Transaction On industry applications, Vol.39, No.2, pp.542-549, Mar./Apr. 2003.

[86] Rudnev, V., D. Loveles, R. Cook, and M. Black, *Handbook of Induction Heating*, New York, NY, 2003.

[87] Yang Xiaoguang, Wang Youhua, *The Effect of Coil Geometry on the Distributions of Eddy Current and Temperature in Transverse Flux Induction Heating Equipment*, Heat Treatment of Metals, Vol.28, No.7, pp.49-54, 2003.

[88] I.Hirota, H.Yamashita, H.Omori, M.Nakaoka, *Historical review of Electric Household Appliances using Induction-Heating and Future challenging Trends*, IEEE Transactions on Fundamentals and Materials, Vol. 124-A, No.8, pp.713-719 (in Japanese), Aug. 2004.

[89] M.A. Jabbar, Ashwin M. Khambad Kone, and Zhang Yanfeng, *Space-vector modulation in a two phase induction motor drive for constant power operation*, IEEE Transaction on Industrial Electronics, Vol.51, No.5, pp.1081-1088, Oct. 2004.

[90] Tipsuwanporn, V., Intajag, S., Charean, A., Sawaengsinkasikit, W., *Adjustable frequency control using BRM for induction heating*, Power Electronics and Motion Control Conference, IPEMC 2004. The 4th International Conference Proceedings, 2004.

[91] Yang Xiaoguang, Wang Youhua, *New Method for Coupled Field Analysis in Transverse Flux Induction Heating of Continuously Moving Sheet*, Heat Treatment of Metals, Vol.29, No.4, pp.53-57, 2004.

[92] S Behera, S P Das and S R Doradla, *A New SVM Technique for Soft-switched DC-AC Converter*, IE (I) Journal EL, Vol.85, March 2005.

[93] A. Goullieux, J. Pain and S. Da-Wen, *Ohmic heating*, in Emerging Technologies for Food Processing Anonymous London: Academic Press, pp. 469-505, 2005.

[94] M.Huasheng, Z. Bo, Z. Jianchao, L. Xuechao, *Dynamic Characteristics Analysis and Instantaneous Value Control Design for Buck-type Power Electronic Transformer (PET)*, IEEE Annual Conference of Industrial Electronic Society IECON, pp.1043-1047, Nov.2005.

[95] Anderson Arhtur Rabello, Elson Jose Silva, Rodney Rezende Saldanha, Christian Vollaire, and Alain Nicoals, *Adaptive Time Stepping Analysis of Nonlinear Microwave Heating Problems*, IEEE Transactions on Magnetics, Vol. 41, No. 5, May 2005.

[96] L. Franquelo, M. Prats, R. Portillo, J. Galvan, M. Perales, J. Carrasco, E. Diez, and J. Jimenez, *Three-dimensional space-vector modulation algorithm for four-leg multilevel converters using abc coordinates*, IEEE Transaction Industrial Electronic, Vol.53, No.2, pp. 459-466, Apr.2006

[97] Nabil A. Ahmed, T. Iwani, H Omori,H .W. Lee and m. Nakaoka *A novel Auxiliary Edge Resonant Snubber -Assisted Soft Switching PWM High Frequency Inverter with Series capacitor Compensated Resonant Load for Consumer Induction Heating*, KIPE. Power Electronics, Vol.6, No.2, pp.95-103, April 2006.

[98] H.Sadakata, T.Kitaizumi, K.Yasui, T.Okude, H.Omori, *Advanced Soft- Switching High Frequency Power Supply with Charge-up Function for IH Cooking Heater*, JIPE-32-9 (in Japanese), pp. 1146, June 2006.

[99] Tomita H., Sekine T., Obata S., *Induction heating using traveling magnetic field and three-phase high frequency inverter*, Power Electronics and Applications , 2005 European Conference,6 pp-P.6, Aug.2006.

[100] E. Dominguez-Tortajada, J. Monzo-Cabrera, and Al. Diaz-Morcillo, *Uniform electric field distribution in microwave heating applicators by means of genetic algorithms optimization of dielectric multilayer structures*, IEEE Trans. Microwave Theory, Vol. 55, pp. 8591, Jan. 2007.

[101] Nam-Ju P., Dong-Yun L., and Dong-Seok H., *A Power Control Scheme with Constant Switching Frequency in Class-D Inverter for Induction Heating Jar Application*, IEEE Transactions Industrial Electronics, Vol. 41, No. 3, June 2007.

[102] Jan Spannhake, Andreas Helwig, Alois Friedberger, Gerhard Mller, and Wolfgang Hellmich, *Resistance Heating*, Wiley Encyclopedia of Electrical and Electronics Engineering, 15 June 2007.

[103] Yausi K., Mihara M. Omari H. and Nakaoka M., *Latest Developments of Soft Switching Pulse Modulated High Frequency Conversion Systems for Consumer Induction Heating Power Appliances*, Power Conversion Conference - Nagoya, PCC '07, pp. 1139 - 1146 , 2-5 April 2007.

[104] Bosquets Monge. S, Bordonau. J., Rocabert. J, *A virtual vector pulse width modulation for a four level diode clamped DC-AC converter*, Power Electronics, IEEE Transaction, Vol.23, pp.1964 -1972, July 2008.

[105] Camelia Petrescu, and Lavinia Ferariu, *Modeling of Dielectric Heating in Radio-Frequency Applicator Optimized for Uniform Temperature by Means of Genetic Algorithms*, World Academy of Science, Engineering and Technology,Vol.47, pp. 129-134, 2008.

[106] Carrillo, E. . *Optimization of Electromagnetic Coupling in Induction Heating Systems Excited by Solenoidal and Axial Windings*, International Journal of Applied Electro magnetics and Mechanics, Vol. 28(3),pp. 395-412, 2008.

[107] A.Iqbal, *Analysis of space vector pulse width modulation for a five phase voltage source inverter*,IE (I)journal-EL, Vol.89, Issue 3, pp.8-15, Sep. 2008.

[108] Mazidi M. A., Mazidi J. G. and Mckinaly R. D.., *The 8051 microcontroller & embedded systems*, Person education, India, 2008.

[109] Nabil A. Ahmed, *Three phase high frequency AC conversion circuit with dual mode PWM/PDM control strategy for high power IH application*, Proceedings of world academy of science, Engineering & Technology, Vol.35, Nov. 2008.

[110] Wang Youhua, Wang Junhnua, Li Jiangui, Li Haohuna, *Analysis of Induction Heating Eddy Current Distribution Based On 3D FEM*, IEEE region 8 Sibircon, 2008.

[111] Wenxi Yao, Haibung Hu, Zhengyu Lu, *Comparison of space vector modulation and carrier based modulation of multilevel inverter*, IEEE Transaction, Power Electronics, Vol.23, pp.4551, Jan. 2008.

[112] Wikipedia contributors, *Joule's laws*, pp.1, 2008.

[113] R.Arumaozhiyal and K.Baskaran, *Space vector pulse width modulation based speed control of induction motor using fuzzy PI controller*, International Journal of Computer and Electrical Engineering, Vol.1, No.1, pp. 1793-8198, April 2009.

[114] Chudjuarjeen S., Sangswang A., and Koompai C., *LLC Resonant Inverter for Induction Heating with Asymmetrical Voltage Cancellation Control, Circuit and Systems*, ISCAS 2009, IEEE International Symposium, pp. 2874-2877, 2009.

[115] Alya K. J. and Grade D. V., *The 8051 microcontroller & embedded systems using assembly and C*, Cengage learning, India, 2010.

[116] Namadmalan A. R., Abdi B., and Moghani J. S., *Current Fed Parallel Resonant Push Pull Inverter with Coil Flux control for Induction Heating Application*, 1^{ST} Power Electronic & Drive Systems & Technologies conference, pp. 186-190, 2010.

[117] Ahmed N.A, *High-Frequency Soft-Switching AC Conversion Circuit With Dual-Mode PWM/PDM Control Strategy for High-Power IH Applications*, Industrial Electronics, IEEE Transactions, Vol.58, Issue:4, pp. 1440-1448, March 2011.

[118] Youhua Wang, Junhua Wang, Lingling Pang, S. L. Ho, and W. N. Fun, *An advanced double-layer combined windings transverse flux system for thin strip induction heating*, Journal of Applied Physics, Vol. 109, Issue 7, April 2011.

Curriculum-Vitae

Yagnesh B. Shukla

Associate Professor

Department of Electronics and Communication Engineering

Sardar Vallabhbhai Patel Institute of Technology (SVIT)

Vasad-388306

GUJARAT, INDIA

Educational Qualifications

Sr. No.	Examination passed	University	Years of passing	% of marks	Main Subjects
1	B.E.	N.M. Unvi., Jalgoan	1998	66.13%	Electronic Engg.
2	M.E.	M.S. Unvi., Baroda	2004	73.78%	Electrical Engg.

List of Publications

[1] Y.B.Shukla, and S.K.Joshi, *Three phase induction heating system using bi directional switching transformer*, The International Journal of Electrical Engineering, Vol.11, Edition 1, pp.185-190, 2011. ISSN1582-4594

[2] Y.B.Shukla, and S.K. Joshi, *Induction heating system using self oscillating driver*, The International Journal of Electrical Engineering, Vol.11, Edition 2 ,pp.107-112, 2011. ISSN1582-4594

[3] Y.B.Shukla, S.K.Joshi, R.J.Makwana and A.A.Daiya, *AC to AC Voltage controller using PWM Technique without DC link*, The National Conference on recent trands in engineering and technology, NCRTET-2011, BVM Engineering College, V.V.Nagar, 13-14 May 2011, ISBN978-81-921358-3-0

[4] Y.B.Shukla, and S.K. Joshi, *Modulation Techniques for Three Phase IDH*, Journal of Power Electronics, accepted.

[5] Y.B.Shukla, and S.K. Joshi, *Configuration Proposals for an Optimal Electromagnetic Coupling in IDH System for conducting Material*, IET Power Electronics, under review.